

学位論文

Kinematics of halo stars  
and the formation history of the Milky Way

(ハロー星の運動と銀河系形成史)

平成 25 年 12 月博士（理学）申請

東京大学大学院理学系研究科

天文学専攻

服部 公平



# **Kinematics of halo stars and the formation history of the Milky Way**



東京大学 大学院  
理学系研究科・理学部  
SCHOOL OF SCIENCE, THE UNIVERSITY OF TOKYO

**Kohei Hattori**

Institute of Astronomy

University of Tokyo

A thesis submitted for the degree of

*Doctor of Philosophy*

## Acknowledgements

It was 4th September, 2008, when I entered the room 1042 of Building 1 of School of Science, University of Tokyo. The interview was just nothing, literally nothing more than exchanging some words with academic staffs in the room, until one of the professors there asked me a single question.

‘There is a possibility that you might not be able to enter *my* laboratory, which you wish to enter. What do you want to do in that case?’

My reply:

‘All I want my supervisor to do is to give me the signature or seal when needed.’

The room 1042 was filled with laughter.

Five years after the interview, here I acknowledge *that* professor, Prof. Yuzuru Yoshii, for not only giving me his signature or seal when needed, but also providing me with a lot of ideas, strategies, time of discussions, travel budget, and some opportunities to work abroad by introducing me to researchers in other countries.

Also, I really acknowledge Prof. Timothy C. Beers, Dr. Daniela Carollo, and Dr. Young Sun Lee, for fruitful and constructive comments and discussions.

I am also grateful to many people in the astronomical community. Especially I thank Prof. Toshikazu Shigeyama, Prof. Masashi Chiba, Prof. Kazuyuki Omukai, Dr. Takuji Tsujimoto, Dr. Kentaro Motohara, Dr. Masaomi Tanaka, Dr. Takuma Suda, Takafumi Sonoi, and Akimasa Kataoka for helpful comments and discussions on the topics presented in Chapter 2; Prof. Masashi Chiba, Dr. Naoto Kobayashi, Dr. Kentaro Motohara, Dr. Shigeki Inoue, Dr. Tsuyoshi Sakamoto, and Nobuyuki Sakai, for helpful comments and discussions on the topics presented in Chapter 3; Prof.

Gerry Gilmore, Prof. Naoteru Gouda, Prof. Mareki Honma, Dr. Shigeki Inoue, Dr. Georges Kordopatis, Kouhei Hayashi, and Nobuyuki Sakai, for helpful comments and discussions on the studies which are not presented in this thesis; Takayuki Hayashi for providing some gadgets to communicate with astronomy guys; Soh Ikarashi for teaching me how to combine PDF files; Mei Sasaki for introducing GSL, Dr. Shigeki Inoue and Akimasa Kataoka for introducing nice seminars at NAOJ, and Dr. Takeo Minezaki, Dr. Yu Sakata, Takayuki Kakehata, Hirokazu Fujii, Takanori Shimizu, Mitsuru Kokubo, and Kei Sano, for daily funny activities at Institute of Astronomy. Some people appear more than once, by the way.

It is sometimes very difficult to conduct my research at full throttle. Without chat with my family, the host family at Cambridge, and my friends with various backgrounds, I could not have accomplished any of my research. I really thank them all, and I really wish them to enjoy their lives.

Also, I thank Mac, Skype, and lpc10.

## Abstract

Stellar halo is the oldest component of the Milky Way, and the kinematics and chemical abundances of halo stars have long been studied to infer the formation history of the Milky Way. The basic starting points of these studies are two assumptions that the motion of halo stars observed today reflect the motion of the progenitor systems in which they formed; and that the chemical abundance of heavy elements of halo stars observed today reflect the chemical abundance of the gas from which they formed. Among these two assumptions, the first one has been validated by theoretical considerations and numerical simulations. However, the latter assumption has not been fully validated yet, although there has been a theoretical proposal that accretion of metal-enriched material onto stellar surface might enhance the surface metal content.

In the first half of this thesis, we present a purely observational test on the significance of metal accretion. The underlying idea of our method is that if both of the above-mentioned assumptions are valid, we expect identical chemo-dynamical correlations for G- and K-type main-sequence stars, since these long-lived stars reflect the same mass-assembly and star-formation histories. We make use of the kinematical information and surface metallicity data of G/K-type dwarfs taken from data release 8 of Sloan Digital Sky Survey (SDSS DR8) and calculate the correlation between rotational velocity  $V_\phi$  and stellar surface metallicity  $[\text{Fe}/\text{H}]$ . As a result, we find a statistically significant offset in  $[\text{Fe}/\text{H}]$  between the correlations of G- and K-type dwarfs in such a way that G-type dwarfs have systematically higher  $[\text{Fe}/\text{H}]$  than K-type dwarfs do at a fixed rotational velocity. This result is consistent with the prediction from metal accretion, since G-type dwarfs are more sensitive to metal accretion due to their shallower surface convective envelope. We also find that similar offset can be found for those stars with large vertical motion, but not for those stars with small vertical motion.

Taking into account that halo stars with larger vertical motions are more likely to belong to outer halo component – which originate from disrupted stellar systems (such as dwarf galaxies) –, our result suggests that outer halo stars are more likely to have experienced metal accretion before their progenitor systems were tidally disrupted, but metal accretion may not have been effective for inner-halo stars, which formed in the main progenitor of the Milky Way. Our results indicate that some previous studies of formation history of the Milky Way might need modification if metal accretion onto their sample stars can not be neglected. Moreover, since our results indicate the existence of metal accretion, there is a possibility that some low-mass Population III stars with primordial metal abundance might be disguising themselves as ordinary Population II stars due to metal accretion.

In the last half of this thesis, we derive the kinematical properties of distant blue horizontal-branch (BHB) stars and investigate their  $[\text{Fe}/\text{H}]$ -dependence, assuming that BHB stars are not significantly affected by metal accretion. There, we present a model-independent analysis of the line-of-sight velocities and spatial distribution of 1865 halo BHB stars within 30 kpc of the Galactic center taken from SDSS DR8. First, we find that the mean rotational velocity of the very metal-poor ( $[\text{Fe}/\text{H}] < -2.0$ ) BHB stars significantly lags behind that of the relatively more metal-rich ( $[\text{Fe}/\text{H}] > -2.0$ ) BHB stars in the Galactocentric distance range of  $13 \text{ kpc} < r < 23 \text{ kpc}$ . This result is the first, purely observational evidence for the existence of the rotational shear of halo stars outside the Solar neighborhood. Secondly, we derive the 3-dimensional velocity dispersion of BHB stars as a function of  $r$  and find that the relatively more metal-rich BHB stars are dominated by stars with eccentric orbits at  $12 \text{ kpc} < r < 15 \text{ kpc}$ , while the very metal-poor BHB stars are dominated by stars on round, low-eccentricity orbits at  $13 \text{ kpc} < r < 18 \text{ kpc}$ . This result for the very metal-poor halo stars contradicts recent galaxy formation simulations in which it is predicted that the orbits of halo stars in Milky Way-like galaxies are dominated by radial orbits at any Galactocentric distance. Based on these newly discovered kinematic properties of outer halo, we propose that those metal-poor outer halo stars with round orbits formed in gas-rich systems (similar to high-velocity clouds) whose orbits had been circularised due to inelastic interaction with other gas-rich systems.

# Contents

Contents	v
<b>1 General introduction</b>	<b>1</b>
1.1 Formation of structure in the Universe . . . . .	1
1.2 Formation of stars and galaxies . . . . .	2
1.3 A brief overview of the structure of the Milky Way . . . . .	3
1.4 Kinematics of the halo stars . . . . .	4
1.4.1 The position and velocity of the Sun . . . . .	4
1.4.2 Orbital properties of halo stars and the formation history of the Milky Way . . . . .	5
1.4.3 Accurate kinematics of stars in the Solar neighborhood . . . . .	6
1.4.4 Substructure in the phase space distribution of halo stars . . . . .	8
1.4.5 Dwarf galaxies around the Milky Way . . . . .	11
1.4.6 Dual structure of the Milky Way stellar halo . . . . .	15
1.5 The aim of this thesis . . . . .	17
1.5.1 The aim of Chapter 2 of this thesis . . . . .	17
1.5.2 The aim of Chapter 3 of this thesis . . . . .	18
1.6 Some basic concepts relevant to this thesis . . . . .	25
1.6.1 Metallicity . . . . .	25
1.6.2 Initial mass function . . . . .	26
<b>2 Evidence of Metal Accretion onto Main-Sequence Halo Stars</b>	<b>27</b>
2.1 Abstract of this chapter . . . . .	27
2.2 Introduction . . . . .	28
2.3 Sample . . . . .	30
2.3.1 Target selection . . . . .	30



2.3.2	Selection of G/K-type dwarfs with reliable stellar parameters and kinematics . . . . .	31
2.3.3	Construction of a volume-limited sample . . . . .	31
2.3.4	Caveats on a metallicity selection bias . . . . .	32
2.4	Median velocity as a function of metallicity . . . . .	32
2.4.1	Kinematical information . . . . .	32
2.4.2	Median rotational velocity behavior with [Fe/H] . . . . .	33
2.4.2.1	Use of full sample . . . . .	33
2.4.2.2	Use of $z_{\max}$ -limited subsamples . . . . .	34
2.5	Plausibility of our results . . . . .	34
2.5.1	Selection bias in SDSS . . . . .	34
2.5.2	Observational errors . . . . .	35
2.5.2.1	Systematic errors in SSPP metallicity estimates . . . . .	35
2.5.2.2	Random errors in proper motion . . . . .	35
2.5.2.3	Systematic errors in SSPP distance estimates . . . . .	36
2.5.2.4	Mock data analysis . . . . .	36
2.6	Discussion . . . . .	37
2.6.1	Evidence of metal accretion onto main-sequence halo stars . . . . .	38
2.6.2	Where did the metal accretion take place? . . . . .	39
2.6.3	Impact on the metallicity distribution function in the stellar halo system . . . . .	40
2.6.4	On the case of $\omega$ Centauri . . . . .	42
2.6.5	Implication for the first stars . . . . .	42
2.7	Summary . . . . .	43
<b>3</b>	<b>Negative Beta Problem</b> . . . . .	<b>55</b>
3.1	Abstract of this chapter . . . . .	55
3.2	Introduction . . . . .	56
3.3	Sample selection . . . . .	57
3.4	Analysis method . . . . .	57
3.4.1	Derivation of rotational velocity . . . . .	57
3.4.2	Derivation of 3-D velocity dispersion . . . . .	59
3.4.3	Testing the reliability of our method . . . . .	59
3.5	Application of our methodology – derivation of rotation velocities, velocity dispersions, and velocity anisotropy parameters . . . . .	60
3.6	Discussion and conclusions . . . . .	61

<b>4 Summary and conclusions</b>	<b>67</b>
<b>Appendix A</b>	<b>71</b>
A Mock catalogs of G/K-type dwarfs . . . . .	71
A.1 Construction of mock catalogs . . . . .	71
A.2 Mock observations of mock catalogs . . . . .	75
<b>References</b>	<b>81</b>



# Chapter 1

## General introduction

The Universe is illuminated by countless numbers of galaxies, and each of these galaxies contain  $10^{10} - 10^{12}$  stars. Since galaxies are ubiquitous building blocks of the Universe, understanding their formation history is an important step toward unravelling the history of the whole Universe. In this respect, studying the formation history of the Milky Way (or the Galaxy) – in which we live – has a special meaning. This is simply because the Milky Way is the ‘nearest’ galaxy and therefore detailed observations of constituent stars or gas are possible.

### 1.1 Formation of structure in the Universe

Recent high-precision measurements of cosmic microwave background are in good agreement with theoretical prediction from the standard  $\Lambda$  cold dark matter ( $\Lambda$ CDM) model so that very strict constraints on the model parameters are available nowadays. For example, the latest data release by *Planck* suggests that dark matter accounts for 84% of the total matter density in the Universe, while baryon accounts for only 16%. These accurate cosmological parameters have enabled us to picture the formation and evolution of structure in the Universe with the help of numerical simulations.

In the currently accepted standard model, the structure in the Universe is believed to be initiated from tiny fluctuations of the matter density (baryon and dark matter) just after the Big Bang. As the Universe expands, so does the matter in the Universe, until the gravitational force of the over-dense regions overwhelms the expansion and starts gravitational collapse to form clumps of matter. These clumps are the first structure to be formed in the Universe, and the standard  $\Lambda$ CDM model predicts that small clumps (called sub-halos) form first, and larger systems (halos) form as a result

---

of subsequent aggregation of smaller clumps.

Recent numerical simulations well reproduce the statistical properties of observed large scale structure in the Universe. This is not only due to the machine power that enables small spatial resolution in the calculations, but also due to the simple physics behind: Formation of the large-scale structure is governed exclusively by the gravitational interaction. Unfortunately, this is not the case for smaller-scale structure such as galaxies, where baryon plays an important role.

## 1.2 Formation of stars and galaxies

As the Universe expands after the Big Bang, baryonic matter continues to cool down to form light elements. About a few minutes after the Big Bang, the baryon in the Universe mainly consists of hydrogen (H) and helium (He). The only other element is lithium (Li), but its contribution to the total baryonic mass is less than  $10^{-7}$ . The early history of galaxy formation is therefore driven by the hydrodynamics and thermodynamics of H/He gas as well as the gravitational interaction of dark matter and baryon.

The gravitational collapse of over-dense regions cause baryonic matter inside – mainly consists of atomic hydrogen – to be adiabatically compressed and thus be heated, until it attains density of  $n \sim 1 \text{ cm}^{-3}$  and temperature of  $T \simeq 10^3 \text{ K}$ . At this point,  $\text{H}_2$ -cooling becomes important, and the later evolution of baryonic matter – including molecular hydrogen – is determined by the balance between various heating (e.g., adiabatic compression or formation of  $\text{H}_2$  molecule) and cooling processes (e.g.,  $\text{H}_2$  cooling or dissociation of  $\text{H}_2$  molecule). When the gas density becomes high enough, the first stars (Population III stars) in the Universe are formed in gas clouds. The ultra-violet (UV) emission from first stars ionize the surrounding gas, and form  $\text{H}_{\text{II}}$  regions around them. The inter stellar gas outside  $\text{H}_{\text{II}}$  regions is also compressed due to radiation, and such compressed gaseous material may ignite further star formation. At least some portion of first stars end their lives as supernovae, dispersing large amount of metals (those elements heavier than helium) in the system. The second generation of stars are formed out of metal-enriched gas clouds and some portion of these stars disperse metals at the end of their lives, and so do any subsequent generations of stars.

While formation of new generations of stars continues within each sub-halo, hierarchical merging of these sub-halos continues to form larger stellar systems. In general, gas clouds easily alter their motion in the course of merger due to inelastic collision with other gas clouds. On the other hand, the motion of stars is drastically altered only when they experience major merger (when two merging systems have comparable

---

mass – mass ratio up to  $\sim 1 : 3$ ); and the stellar orbits after minor mergers more or less trace their initial orbits.

Since stars and gas have different efficiency in retaining their initial kinematic information, kinematical or morphological properties of the galaxies are determined by the mass assembly history and the star formation activity within their progenitor systems. For example, elliptical galaxies have no significant gas components and their constituent stars show no net rotation with their orbital planes isotropically distributed. These properties may suggest that elliptical galaxies are formed through dry major merger (major merger of two systems lacking in gaseous components) of systems at the last stage of their formation. As another example, disk galaxies (such as the Milky Way) have an eminent gas disk and stellar disk(s). Taking into account that major merger would destroy the spatial structure of the disk, disk galaxies may not have experienced recent major mergers, at least after the formation of disk.

In recent cosmological simulations of galaxy formation, many efforts have been made in order to reproduce the observations. However, we do not fully understand the physics of star formation, so that they have to assume some empirical star formation prescription when they convert ‘gas particles’ into ‘star particles’ in their simulations. An immediate outcome of our incomplete understanding of star formation theory is that we cannot precisely predict orbital structure of the galaxies, since the dynamical reaction of stars and gas clouds to merger events are different. Numerical simulation is still in progress, and the simulated galaxies are not yet ready for rigorous comparison with observations. (The plausibility of the prediction from  $\Lambda$ CDM simulations is a part of this thesis, as presented in Chapter 3.) In the following section, we will describe the current status of observations of the Milky Way.

### 1.3 A brief overview of the structure of the Milky Way

Observations of the Milky Way have revealed that the structure of the Milky Way is very complex. It consists of billions of stars and planets, interstellar gas, and dust. Most of the stars, gas and dust are distributed in a flat, nearly axisymmetric disk structure, moving in nearly circular orbits in the same direction. The disk extends out to  $\sim 15$  kpc away from the Galactic center, and the mass of the disk is  $\sim 10^{11} M_{\odot}$ , comprising of  $\sim 90\%$  of the total baryonic mass of the Milky Way. Recent observations suggest that the stellar disk of the Milky Way consists of two components, namely thin and thick disks, with different kinematics, age, chemical composition, and formation mechanism. At the central part of the disk, there is an old stellar component called bulge, which

---

mostly consists of old stars and shows less flattened, triaxial shape. The bulge, stellar and gaseous disks are surrounded by stellar halo with a mass of  $\sim 10^9 M_\odot$ , which consists of isolated (field) stars, globular clusters, and dwarf galaxies. The stellar halo shows a spheroidal distribution, and extends out to  $\sim 100$  kpc away from the Galactic center. Stars in the stellar halo are much less metal-enhanced than disk stars, indicating that these stars were formed in the early stage of the formation of the Milky Way. The kinematics of the above-mentioned visible stars and gas indicates that they are embedded in a massive halo of dark matter, whose mass is estimated to be  $\sim 10^{12} M_\odot$ .

## 1.4 Kinematics of the halo stars

Stellar halo of the Milky Way consists of  $N \simeq 10^9$  stars, and therefore its relaxation time

$$t_{\text{relax}} \simeq \frac{0.1N}{\ln N} t_{\text{cross}} \quad (1.1)$$

is much larger than the age of the Universe ( $\sim 10$  Gyr), where  $t_{\text{cross}} \simeq 100$  Myr denotes the crossing time [Binney and Tremaine, 2008]. It follows that the stellar halo is well approximated as a collisionless system. This means that the orbital properties of the halo stars as observed today reflect those when they were formed at the early phase of the formation of the Milky Way. With this regard, kinematics of the halo stars provides precious information on the formation history of the Milky Way.

### 1.4.1 The position and velocity of the Sun

Since we are stick to the Solar System, we can only measure the motion of stars or gas clouds with respect to the Sun. Therefore, estimating the motion of the Sun with respect to the rest frame of the Milky Way as well as the position of the Sun is an important task.

The distance between the Sun and the Galactic center and the velocity of the Local Standard of Rest (LSR) are estimated to be around  $R_\odot = 7.5 - 9.0$  kpc and  $V_{\text{LSR}} = 210 - 240$  km s $^{-1}$ , but we adopt (more or less) well accepted set of  $(R_\odot, V_{\text{LSR}}) = (8.5$  kpc, 220 km s $^{-1})$  throughout this thesis [Kerr and Lynden-Bell, 1986].

As for the peculiar velocity of the Sun with respect to the LSR, we adopt  $(U_\odot, V_\odot, W_\odot) = (10.0, 5.3, 7.2)$  km s $^{-1}$  [Dehnen and Binney, 1998], although these values are also not conclusive, except for  $W_\odot$ .

---

### 1.4.2 Orbital properties of halo stars and the formation history of the Milky Way

Our Sun is located at  $\sim 8.5$  kpc away from the Galactic center, and moving around it at  $\sim 220 \text{ km s}^{-1}$  in a nearly circular orbit. The motion of other disk stars in the Solar neighborhood move in a similar fashion, so that the relative velocity of nearby stars with respect to the Sun is of the order of the velocity dispersion of disk stars, which is  $\sim 40 \text{ km s}^{-1}$ . On the other hand, halo stars do not show systematic motion, and their velocity distribution is more or less random, with velocity dispersion of  $\sim 200 \text{ km s}^{-1}$ . Therefore, the relative velocity of the halo stars with respect to the Sun is typically very large.

This is why, historically, halo stars were first identified as ‘high-velocity stars’ [Oort, 1922]. Later studies reveal that these high-velocity stars tend to have high UV excess and thus they are metal-poor, seemingly old stars [Roman, 1955]. Eggen et al. [1962] investigate the orbital motion of 221 nearby stars by adopting a simple, two-dimensional gravitational potential model of the Milky Way, and seek for a correlation between the orbital eccentricity  $e$  and UV excess (Figure 1.1, top panel). They find that there are no metal-poor ( $\delta(U - B) > 0.15$ ) stars with low-eccentricity ( $0 < e < 0.3$ ) orbits in their sample. Based on this finding, they propose that the Milky Way form out of a rapidly collapsing gas cloud, whose timescale is of the order of the free-fall time ( $\sim 0.1$  Gyr). In their ‘monolithic collapse’ scenario, the early generations of stars form within the radially collapsing gas cloud, and they can be observed today as high-velocity stars with large eccentricity or high inclination with respect to the disk plane. Also, the collapse of gas cloud is stopped to some point and the thin gas disk is formed due to the non-zero total angular momentum of the collapsing gas cloud. Later generations of stars form in this gas cloud, so that their orbital eccentricity is small.

Many authors investigated the kinematics of nearby stars, following the study of Eggen et al. [1962]. The first clear counter argument against Eggen et al. [1962] was presented by Yoshii and Saio [1979], who enlarged the sample of stars and improved the kinematical analysis. Their sample includes 220 stars in Eggen et al. [1962] sample, as well as 532 low-velocity (disk) stars and 114 RR Lyrae stars from other catalogs. They calculate the 3-dimensional orbital motion of their sample stars, by adopting a more sophisticated gravitational potential model. They demonstrate that there are indeed some fraction of stars which have low-metal content and low-eccentricity (Figure 1.1, middle panel), contrary to the statement of Eggen et al. [1962]. By calculating the orbital evolution of stars under time-dependent gravitational potential models, they



---

conclude that the Milky Way formed out of slow contraction of gaseous medium, whose timescale is  $\sim 3$  Gyr. Another argument was proposed by [Searle and Zinn \[1978\]](#), who studied the metal abundance of globular clusters in the outer part of the halo. They find that the metal abundance distribution is nearly independent of the Galactocentric distance. They interpret this finding as the evidence that the Milky Way form as a result of ‘chaotic merger’ of smaller sub-systems. This ‘chaotic merger’ scenario also goes against the rapid formation of halo, similar to the ‘slow contraction’ scenario proposed by [Yoshii and Saio \[1979\]](#).

Later, [Chiba and Beers \[2000\]](#) present an analysis of orbital parameters based on kinematically unbiased sample of  $\sim 1200$  nearby stars. As can be seen on the bottom panel of Figure 1.1, there are indeed finite fraction of low-eccentricity stars even at  $[\text{Fe}/\text{H}] < -1.5$ , where halo stars start to dominate. It turns out that the lack of such stars in the [Eggen et al. \[1962\]](#) sample is due to the kinematic bias, since those stars with large proper motions are preferentially selected in high-velocity star catalogs and low-eccentricity stars are less likely to be selected. The emergence of accurate, kinematically-unbiased sample like that in [Chiba and Beers \[2000\]](#) has enabled us to probe more detailed formation scenario of the Milky Way.

### 1.4.3 Accurate kinematics of stars in the Solar neighborhood

In this section, we summarize the observed kinematics of nearby halo and disk stars, as revealed by astrometric *Hipparcos* satellite.

[Chiba and Yoshii \[1998\]](#) analyse the kinematics of nearby giants and RR Lyrae stars within 2 kpc away from the Sun, by using the accurate proper motion data taken from *Hipparcos* as well as line-of-sight velocity and photometric metallicity  $[\text{Fe}/\text{H}]$  taken from ground-based telescope. The derived velocity distribution as a function of  $[\text{Fe}/\text{H}]$  shown in Figure 1.2 clearly demonstrates the transition from halo-dominated region at  $[\text{Fe}/\text{H}] \lesssim -1.5$  to disk-dominated region at  $[\text{Fe}/\text{H}] \gtrsim -1.0$ .

They find that the mean velocity with respect to the LSR for stars with  $[\text{Fe}/\text{H}] < -1.6$  ( $N = 124$  stars) is

$$(\langle U \rangle, \langle V \rangle, \langle W \rangle) = (-16 \pm 18, -217 \pm 21, -10 \pm 12) \text{ km s}^{-1}. \quad (1.2)$$

Taking into account that the mean rotational velocity with respect to the Galactic rest frame corresponds to  $V_{\text{LSR}} + \langle V \rangle$ , their finding suggests that the halo shows essentially no net rotation. They also derive the 3-dimensional velocity dispersion at  $[\text{Fe}/\text{H}] < -1.6$

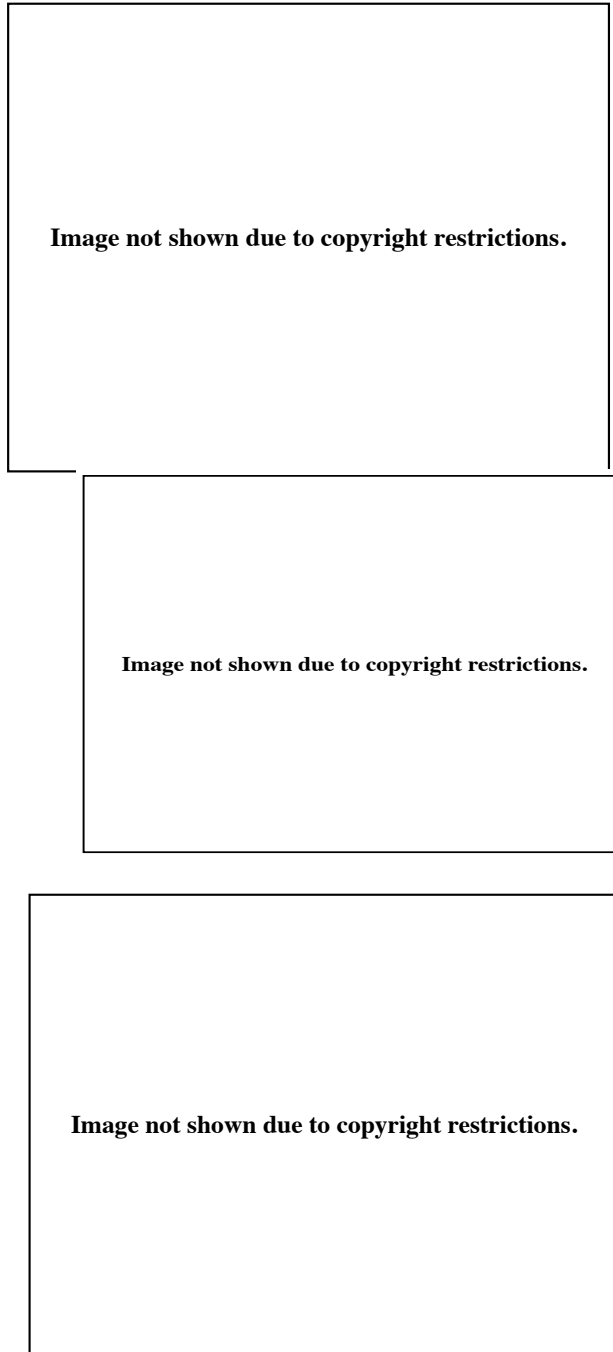


Figure 1.1: Distribution of nearby stars in a phase space spanned by orbital eccentricity (horizontal axis) and metal indicator (vertical axis). (Top) The ultra-violet excess  $\delta(U-B)$  is adopted as the metal indicator [more metal-poor stars show larger  $\delta(U-B)$ ]. Taken from Figure 4 of *Eggen et al. [1962]*. (Middle) The ultra-violet excess  $\delta(0.6)$  is adopted as the metal indicator [more metal-poor stars show larger  $\delta(0.6)$ ]. Taken from Figure 6(a) of *Yoshii and Saio [1979]*. (Bottom) Taken from Figure 6(a) of *Chiba and Beers [2000]*.

---

to be

$$(\sigma_U, \sigma_V, \sigma_W) = (161 \pm 10, 115 \pm 7, 108 \pm 7) \text{ km s}^{-1}. \quad (1.3)$$

This suggests that the velocity ellipsoid for Solar-neighbor halo stars is radially elongated and that these halo stars are dominated by radial orbits.

Although their sample contains only  $N = 4$  stars with  $-0.4 < [\text{Fe}/\text{H}] < +0.1$ , their velocity distribution is very different from that of halo stars. In this (thin-) disk dominated region, they find that the mean velocity and velocity dispersion are

$$\langle \langle U \rangle, \langle V \rangle, \langle W \rangle \rangle = (-14 \pm 7, -21 \pm 8, 9 \pm 9) \text{ km s}^{-1} \quad (1.4)$$

and

$$(\sigma_U, \sigma_V, \sigma_W) = (40 \pm 16, 23 \pm 10, 31 \pm 13) \text{ km s}^{-1}, \quad (1.5)$$

respectively. The small negative value of  $\langle V \rangle$  suggests that disk stars in the Solar neighborhood rotates very fast, but they slightly lag behind the LSR velocity. (This phenomena is referred to as ‘asymmetric drift.’)

The transition from halo-dominated to disk-dominated  $[\text{Fe}/\text{H}]$ -range can be clearly seen in Figure 1.3. The top panel of this figure shows that the mean rotational velocity  $\langle V_\phi \rangle$  is near zero at  $[\text{Fe}/\text{H}] < -1.5$ , and it gradually increases as a function of  $[\text{Fe}/\text{H}]$ , until it reaches  $\langle V_\phi \rangle \sim V_{\text{LSR}}$  at  $[\text{Fe}/\text{H}] \simeq 0$ . As can be seen on the middle panel, velocity dispersion in the azimuthal direction  $\sigma_\phi$  decreases as a function of  $[\text{Fe}/\text{H}]$ , from  $\simeq 100 \text{ km s}^{-1}$  at  $[\text{Fe}/\text{H}] < -1.5$  to  $\simeq 20 \text{ km s}^{-1}$  at  $[\text{Fe}/\text{H}] \simeq 0$ . These information suggests that the halo is a dynamical system supported by random motion (with small  $\langle V_\phi \rangle / \sigma_\phi$ ), while disk is a rotationally supported system (with large  $\langle V_\phi \rangle / \sigma_\phi$ ).

#### 1.4.4 Substructure in the phase space distribution of halo stars

With the accurate kinematical data provided by *Hipparcos*, it has become possible not only to grasp the overall (smoothed-out) distribution of nearby halo stars in the velocity space or integral of motion (e.g., energy or angular momentum) space, but also detect the over density (substructure) in the distribution.

[Helmi et al. \[1999\]](#) investigate the velocity and angular momentum distribution of a subset of nearby stars examined in [Chiba and Yoshii \[1998\]](#) and identify a phase-space region in which density of stars is higher than that expected from a smooth distribution, from statistical points of view (see Figure 1.4). They interpret the substructure in the angular momentum space as the relic of a disrupted stellar system, such as a dwarf galaxy, and propose it as an evidence of hierarchical merging process to form the Milky

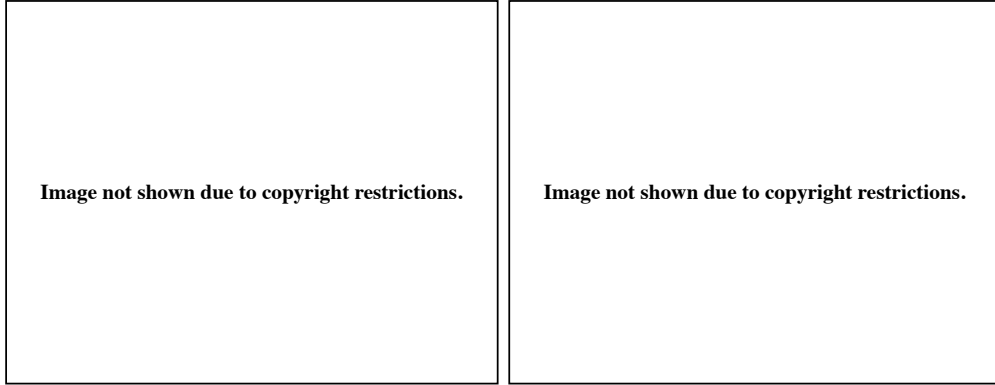


Figure 1.2: 3-dimensional velocity distribution of nearby stars plotted against metallicity  $[\text{Fe}/\text{H}]$ . (Left) Taken from Figure 4 of *Chiba and Yoshii [1998]*. (Right) Taken from Figure 1 of *Chiba and Beers [2000]*.

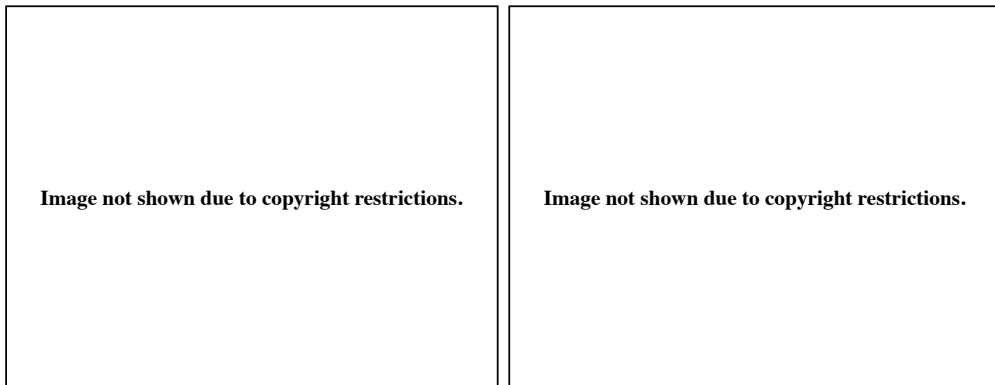


Figure 1.3: Rotational behaviour of nearby stars as a function of metallicity  $[\text{Fe}/\text{H}]$ . (Left) Taken from Figure 5 of *Chiba and Yoshii [1998]*. (Right) Taken from Figure 3(a) of *Chiba and Beers [2000]*.

---

Way halo.

[Chiba and Beers \[2000\]](#) confirm the substructure found by [Helmi et al. \[1999\]](#) by using a different sample. They also find a possible trail of substructure which may connect the detected substructure and the high-angular momentum part of the main distribution.

Their findings of the substructure in the phase space, as well as the discovery of the being disrupted Sagittarius dwarf galaxy [[Ibata et al., 1995](#)], strongly support for the hierarchical merging scenario of the Milky Way formation, which was originally proposed by [Searle and Zinn \[1978\]](#). Following these studies, many authors have performed numerical simulations to reproduce Milky Way-like galaxies. One such attempt is provided by [Helmi and de Zeeuw \[2000\]](#), in which Milky Way-like galaxy is formed via accretion of many dwarf galaxies. [Figure 1.6](#) show the initial (top panels) and final (bottom panels) distribution of simulated star particles in the phase space spanned by energy and angular momentum. On these panels, different colours indicate different dwarf galaxies. From this figure, we see that the coherence in the phase space distribution is not completely erased by the later disruption of the progenitor system.

Although currently available, accurate 6-dimensional data of the position and velocity of halo stars are confined within a few kpc away from the Sun at most, the situation will be greatly improved with the forthcoming astrometric satellite *Gaia*, which will enable us to measure the position and velocity of stars within  $\simeq 10$  kpc with similar accuracy to that of *Hipparcos*.

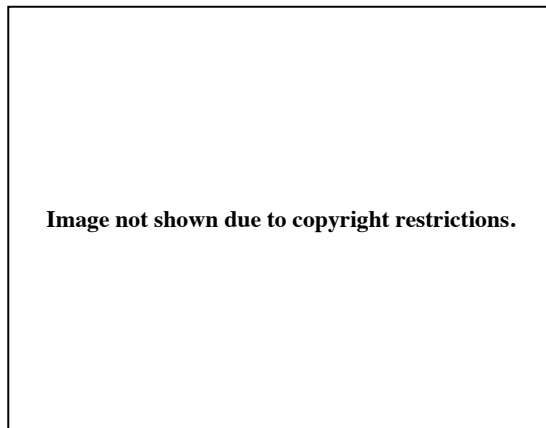



Figure 1.4: The distribution of nearby stars in the velocity space (top panels) and angular momentum space (bottom panel). The substructure is more clearly seen in the angular momentum space. Taken from [Figure 2 of Helmi et al. \[1999\]](#).

---



**Image not shown due to copyright restrictions.**

Figure 1.5: The distribution of nearby stars in the angular momentum space. The solid-line square corresponds to the substructure found by [Helmi et al. \[1999\]](#). The broken-line square is a newly detected over-dense region, which may be considered as trail of the [Helmi et al. \[1999\]](#) substructure. Taken from Figure 15 of [Chiba and Beers \[2000\]](#).

#### 1.4.5 Dwarf galaxies around the Milky Way

The discovery of substructures in the phase-space distribution of nearby stars indicates that at least some fraction of stellar halo consist of remnants of disrupted stellar systems. There are many dwarf galaxies with total mass  $10^9$ - $10^6 M_{\odot}$  or less, and stars in these dwarf galaxies have been investigated in comparison with field halo stars.

[Kirby et al. \[2008\]](#) investigate the metal abundances of dwarf galaxies orbiting around the Milky Way and find an apparent correlation between the total luminosity (which is a good measure of stellar mass) and average metallicity of constituent stars (Figure 1.7). This correlation indicates that those systems with larger stellar luminosity have experienced more intense star formation activity, and therefore their metal abundances are higher. Their results as well as other studies suggest that the metallicities of stars in dwarf galaxies are distributed at around  $-3 \lesssim [\text{Fe}/\text{H}] \lesssim -1$ , similar to nearby halo stars (see Figure 1.2).

However, detailed observations by large telescopes equipped with high-resolution spectrographs have revealed that the chemical compositions of stars in luminous dwarf galaxies (which are often called ‘classical dwarf galaxies’ for historical reasons) are different from those of most halo stars in the Solar neighborhood. Figure 1.8 shows the distribution in the  $[\alpha/\text{Fe}]$ - $[\text{Fe}/\text{H}]$  space of the stars in luminous dwarf galaxies and nearby halo stars. Due to the internal chemical evolution of dwarf galaxies, constituent



Figure 1.6: The angular momentum distribution of halo stars in a simulated galaxy formed via merger of dwarf galaxies. The stars in different dwarf galaxies are shown with different colours. The top panels show the initial condition and the bottom panels show the final condition with observational errors added. *Taken from Figures 3 and 4 of Helmi and de Zeeuw [2000].*

---

stars of these systems show some spread in  $[\text{Fe}/\text{H}]$ , and each dwarf galaxy shows a characteristic narrow sequence in the  $[\alpha/\text{Fe}]-[\text{Fe}/\text{H}]$  space. For example, stars in the Sculptor dwarf galaxy show a flat profile of  $[\text{Ca}/\text{Fe}] \sim 0.3$  at  $[\text{Fe}/\text{H}] \lesssim -1.8$ , and their  $[\text{Ca}/\text{Fe}]$  profile decreases as a function of  $[\text{Fe}/\text{H}]$  at  $[\text{Fe}/\text{H}] \gtrsim -1.8$ . As can be seen in Figure 1.8, other dwarf galaxies show similar sequences, too, although the positions of the ‘knee’ in the sequence ( $[\text{Fe}/\text{H}] \simeq -1.8$  for the case of Sculptor) for these dwarf galaxies are different from each other.

Theoretical studies have shown that the earliest phase of chemical evolution of a given dwarf galaxy is led by Type II supernovae (SNe), whose progenitors are short-lived massive stars, until Type Ia SNe begin to pollute the gas. Before the emergence of Type Ia SNe, the metallicity  $[\text{Fe}/\text{H}]$  of the gas in the system increases as a function of time due to the remnants of Type II SNe, while the abundance ratio  $[\alpha/\text{Fe}]$  remains nearly constant, since the yield of Type II SNe is a weak function of the metallicity of the progenitor star. Since it takes  $\sim 1$  Gyr for a progenitor binary system of a Type Ia SN to explode, the metal abundance of the gas in the system begins to be affected by Type Ia SNe as well, after  $\sim 1$  Gyr of the first episode of star formation in the dwarf galaxy. After this epoch,  $[\alpha/\text{Fe}]$  of the system decreases as a function of time, since the value of  $[\alpha/\text{Fe}]$  of a SN remnant is smaller for Type Ia than Type II. The different positions of the knee in the sequence in  $[\alpha/\text{Fe}]-[\text{Fe}/\text{H}]$  plane therefore correspond to the different star formation activities in dwarf galaxies, such that those dwarf galaxies with longer star formation timescale show higher values of  $[\text{Fe}/\text{H}]$  at the knee.

The fact that the distribution in the  $[\alpha/\text{Fe}]-[\text{Fe}/\text{H}]$  plane of the stars in luminous dwarf galaxies is different from that of the halo stars in the Solar neighborhood indicates that the physical properties of typical progenitor systems of the stellar halo are different from those of luminous dwarf galaxies. In particular, the larger value of  $[\text{Fe}/\text{H}]$  at the knee for the halo stars suggests that most of the progenitor systems that contribute the halo stars in the Solar neighborhood have experienced star formation activities with longer timescale. Indeed, there is a possibility that dwarf galaxies like classical dwarf galaxies are not the typical dwarf galaxies that contribute to the stellar halo in the Solar neighborhood. This is because classical dwarfs are the most luminous class of dwarf galaxies, and recent observations of much less luminous dwarf galaxies (some of which are called ‘ultra faint dwarf galaxies’) suggest that there are much larger number of less luminous dwarf galaxies than have been detected so far. Also, there is a possibility that dwarf galaxies similar to those shown in Figure 1.8 do not contribute the stellar halo in the Solar neighborhood, but contribute to other parts of stellar halo. We will discuss this issue in the following section.



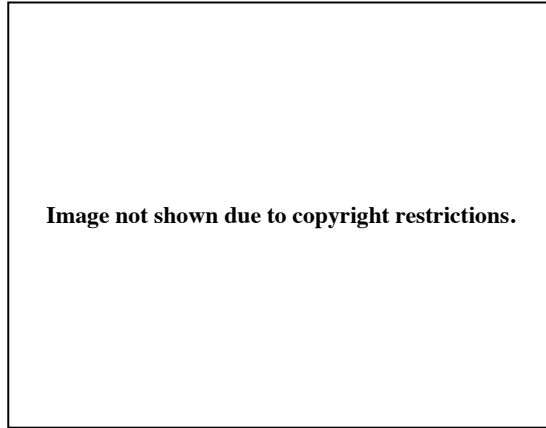


Figure 1.7: The relation between the mean metallicity and the total luminosity of dwarf galaxies. There is an apparent correlation between these two quantities. *Taken from Figure 5 of Kirby et al. [2008].*

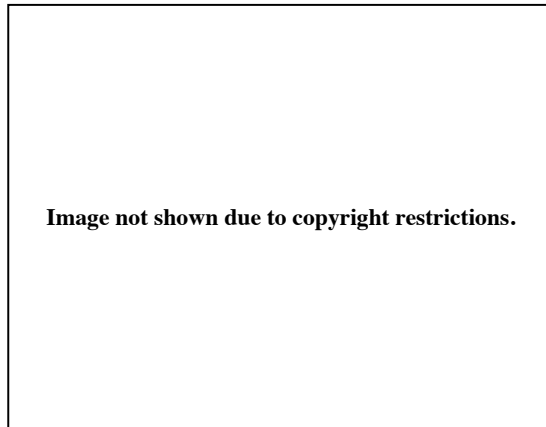


Figure 1.8: The distribution of stars in the  $[\alpha/\text{Fe}]-[\text{Fe}/\text{H}]$  space. The black dots correspond to halo and disk stars of the Milky Way in the Solar neighborhood, while coloured dots correspond to stars in luminous dwarf galaxies. *Taken from Figure 11 of Tolstoy et al. [2009].*

---

### 1.4.6 Dual structure of the Milky Way stellar halo

The discovered relics of merger history of the Milky Way stellar halo suggest that at least some portion of the stellar halo consist of disrupted stellar systems like dwarf galaxies. Then, the next question to be answered is what is the fraction of the halo stars which originate from accreted stellar systems.

[Carollo et al. \[2007\]](#) investigate the orbital and chemical properties of stars in the extended Solar neighborhood ( $d < 4$  kpc) taken from Sloan Digital Sky Survey (SDSS). They show that the metallicity distribution function (MDF) of stars with retrograde rotations – which well trace the halo population – peaks at  $[\text{Fe}/\text{H}] \simeq -1.5$  (see the bottom panel in the left-hand column of [Figure 1.9](#)), which is consistent with previous studies. However, they also discover that there is a tendency that the fraction of very metal-poor stars with  $[\text{Fe}/\text{H}] < -2.0$  is larger for stars with highly retrograde orbits than those with mildly retrograde orbits, as can be seen in the middle column of [Figure 1.9](#). In addition, this tendency becomes more prominent if we further select those stars with larger  $z_{\text{max}}$ , where  $z_{\text{max}}$  is the maximum distance above the disk plane that a given star can reach along its orbit (see right-hand column of [Figure 1.9](#)). They also estimate the spatial distribution of stellar halo as a function of  $[\text{Fe}/\text{H}]$  based on the reconstruction method proposed by [Sommer-Larsen and Zhen \[1990\]](#). The reconstructed density distribution suggests that more metal-poor stars show more spherical distribution, while relatively metal-rich stars show more flattened distribution, as shown in [Figure 1.10](#).

Based on these findings, they propose that the stellar halo consists of two components, inner and outer halo with different kinematical and chemical properties. They claim that inner halo stars have metallicity around  $[\text{Fe}/\text{H}] \simeq -1.6$  with essentially no net rotation, while outer halo stars show  $[\text{Fe}/\text{H}] \sim -2.2$  with highly retrograde rotation and typically have larger  $z_{\text{max}}$  than inner halo stars do.

In the subsequent paper of [Carollo et al. \[2010\]](#) using extended sample, they show that the velocity distribution of nearby stars is different from the conventional view of single halo. In the conventional view of the stellar halo, it is believed that the velocity distribution can be well described by Gaussian distribution. However, the distribution of rotational velocity  $V_\phi$  is not symmetric around  $V_\phi = 0$  km s<sup>-1</sup>, especially at low metallicity range ( $[\text{Fe}/\text{H}] \simeq -2.0$ ), as can be seen in the middle column of [Figure 1.11](#). They also find the observed distribution of orbital eccentricity depends on  $[\text{Fe}/\text{H}]$ . As shown in [Figure 1.12](#), the fraction of halo stars with highly eccentric orbits (large eccentricity) is smaller at  $[\text{Fe}/\text{H}] < -2.0$  than at  $-2.0 < [\text{Fe}/\text{H}] < -1.5$ , which is not

---

expected if there is only one single component in the stellar halo. They perform a decomposition of the observed  $V_\phi$ -distribution as shown in Figure 1.13, and conclude that the observed distribution of stars in velocity and metallicity space favors dual structure of stellar halo from a statistical points of view. Based on their decomposition analysis, they estimate the mean rotational velocity of inner halo to be  $\langle V_\phi \rangle = 7 \pm 4 \text{ km s}^{-1}$  (consistent with zero net rotation) and that of outer halo to be  $\langle V_\phi \rangle = -80 \pm 13 \text{ km s}^{-1}$  (highly retrograde rotation).

In addition, they construct MDFs as a function of  $|z|$ , by using stars outside the Solar neighborhood as well as local sample. Figure 1.14 shows that the MDF of halo stars gradually changes as a function of  $|z|$ . At  $3 \text{ kpc} < |z| < 4 \text{ kpc}$ , the peak metallicity of the derived MDF is at  $[\text{Fe}/\text{H}] \simeq -1.6$  (which corresponds to the inner-halo metallicity), while it gradually decreases as a function of  $|z|$ , until it reaches at  $[\text{Fe}/\text{H}] \simeq -2.2$  (which corresponds to the outer-halo metallicity) at  $|z| > 9 \text{ kpc}$ .

The difference in the kinematical and chemical properties of the inner and outer halo suggest that these stellar components have different origins. The proposed scenario of Carollo et al. [2007, 2010] is as follows. The hierarchical mergers of proto-Galactic clumps give rise to a few large clumps with comparable masses. These large clumps experience a head-on merger, which erases the initial kinematical information of the colliding systems, and the resultant large system corresponds to the inner halo of the Milky Way. Due to the nearly radial merger of the progenitor systems, stars of inner halo component typically show highly eccentric orbits. The dissipative contraction of the system flatten the spatial structure of the inner halo, while concentrated gas in the inner part of the system give rise to the stellar disk. During the course of the formation history of the Milky Way, small dwarf galaxies continuously accrete onto the Milky Way from every direction and are disrupted by tidal interaction, thereby providing outer halo stars whose spatial distribution is more or less spherical. Since stellar metallicity of member stars is typically larger for large stellar systems (see Figure 1.7), the inner halo stars typically show higher  $[\text{Fe}/\text{H}]$  than outer halo stars. The retrograde motion of outer halo stars might be explained by dynamical friction, since orbital decay of those dwarf galaxies with prograde orbits (with respect to disk rotation) is faster than those with retrograde orbits.

The idea of dual stellar halo with different origins have recently been confirmed by numerical simulations [Font et al., 2011; Tissera et al., 2013]. Detailed comparison of simulated galaxies and the Milky Way stellar halo is also discussed in Section 3.

We note here that there is a counter argument against the dual structure of the stellar halo. Schönrich et al. [2011] point out that the photometric distance adopted in

---

[Carollo et al. \[2010\]](#) is inadequate, and that the apparent asymmetric distribution of  $V_\phi$  of halo stars is only an artefact. They claim that by adopting a new distance estimate, the  $V_\phi$  distribution of nearby stars can be well understood as a superposition of disk and halo stars, without any need for an additional halo component. However, there is a rebuttal paper of [Beers et al. \[2012\]](#), in which they point out the criticism by [Schönrich et al. \[2011\]](#) is partially incorrect, and their adopted photometric distance is based on invalid assumption. They state that the dual nature of stellar halo of the Milky Way can be also confirmed when they correctly take into account the modification pointed out by [Schönrich et al. \[2011\]](#).

Also, [Nissen and Schuster \[2010\]](#) investigate the chemical abundance of kinematically selected nearby stars, including both disk and halo stars. Figure 1.15 shows that there are two distinct sequences in the  $[\alpha/\text{Fe}]$ - $[\text{Fe}/\text{H}]$  space, one of which shows lower- $[\alpha/\text{Fe}]$  ratio, while the other shows higher- $[\alpha/\text{Fe}]$  ratio. They also note that the high- $\alpha$  stars tend to have larger velocity, while low- $\alpha$  stars tend to have smaller velocity. The kinematical properties of high- and low- $\alpha$  stars in this sample are similar to those of outer and inner halo populations in [Carollo et al. \[2010\]](#). In addition, the abundance ratios of the low- $\alpha$  stars are similar to those of the constituent stars in dwarf galaxies (see Figure 1.8), which may indicate that the high- $\alpha$  stars originate from dwarf galaxies. Taking into account that [Carollo et al. \[2007, 2010\]](#) suggest that the outer halo stars originate from dwarf galaxy-like systems, the findings of [Nissen and Schuster \[2010\]](#) is in good agreement with those of [Carollo et al. \[2010\]](#). Although similar studies such as [Ishigaki et al. \[2012\]](#) later suggest that the distinction in  $[\alpha/\text{Fe}]$ - $[\text{Fe}/\text{H}]$  space may not be as clear as in Figure 1.15, the findings of [Nissen and Schuster \[2010\]](#) provide some useful insights into the formation history of the complex stellar halo.

## 1.5 The aim of this thesis

### 1.5.1 The aim of Chapter 2 of this thesis

In the previous sections, we have reviewed the recent theoretical and observational studies on the formation history of the Milky Way, with an emphasis on the kinematics of the halo stars. To summarize, the kinematics and chemistry of the Milky Way stellar halo retain a lot of information on the formation history of the Milky Way. All of these previous studies are based on two, widely-accepted assumptions:

- (1) the motion of halo stars observed today reflect the motion of the progenitor systems in which they formed; and

- 
- (2) the chemical abundance of heavy elements of halo stars observed today reflect the chemical abundance of the gas from which they formed.

The assumption (1) is validated not only by theoretical arguments of collisions nature of the stellar halo but also by recent numerical simulations of galaxy formations (see Figure 1.6). On the other hand, the assumption (2) of constancy of stellar surface metal abundances has not been fully validated yet, although there is a possibility that accretion of metal-enriched material onto its surface enhances the surface metal content [Yoshii, 1981].

If the assumption (2) turns out to be invalid, it has a potentially significant impact on the studies of the Milky Way. In particular, theoretical arguments suggest that the surface metal enhancement due to metal accretion is more significant for main-sequence stars, since they have shallower surface convective zones than evolved, post-main-sequence stars. Taking into account that a large fraction of observable stars in the Solar neighborhood consist of main-sequence stars (e.g., Carollo et al. 2007, 2010), observed chemical properties of nearby stars need re-examination if metal accretion cannot be ignored for these stars. A good news is that those observations based on post-main-sequence stars are more reliable than those based on main-sequence stars, so that studies on distant stars (including those in dwarf galaxies) may be reliable. In Chapter 2, we propose a new way to examine the significance of metal accretion, by using chemo-kinematical properties of nearby main-sequence stars with different depth in surface convective envelope.

### 1.5.2 The aim of Chapter 3 of this thesis

One of the currently hot topic on the stellar halo of the Milky Way is whether the proposed duality in the stellar halo is real or not. Although Beers et al. [2012] have claimed that some of the criticism by Schönrich et al. [2011] is incorrect, even the currently most sophisticated methodology is not enough to determine precise distance to main-sequence stars in SDSS sample. Therefore, the dispute over single/dual stellar halo would not be completely resolved until astrometric satellite Gaia will provide accurate kinematical data of halo stars.

With this regard, it is desired to use other sample of stars to test the concept of dual stellar halo. In Chapter 3, we derive the kinematical properties of distant halo by using blue horizontal-branch stars, thereby discuss the plausibility of the dual halo. Since we do not have accurate proper motion data, we need a new formulation to take advantage of the accurate 3-dimensional position and line-of-sight velocity for this sample. Based

---

on this analysis, we also discuss the plausibility of recent galaxy formation simulations.

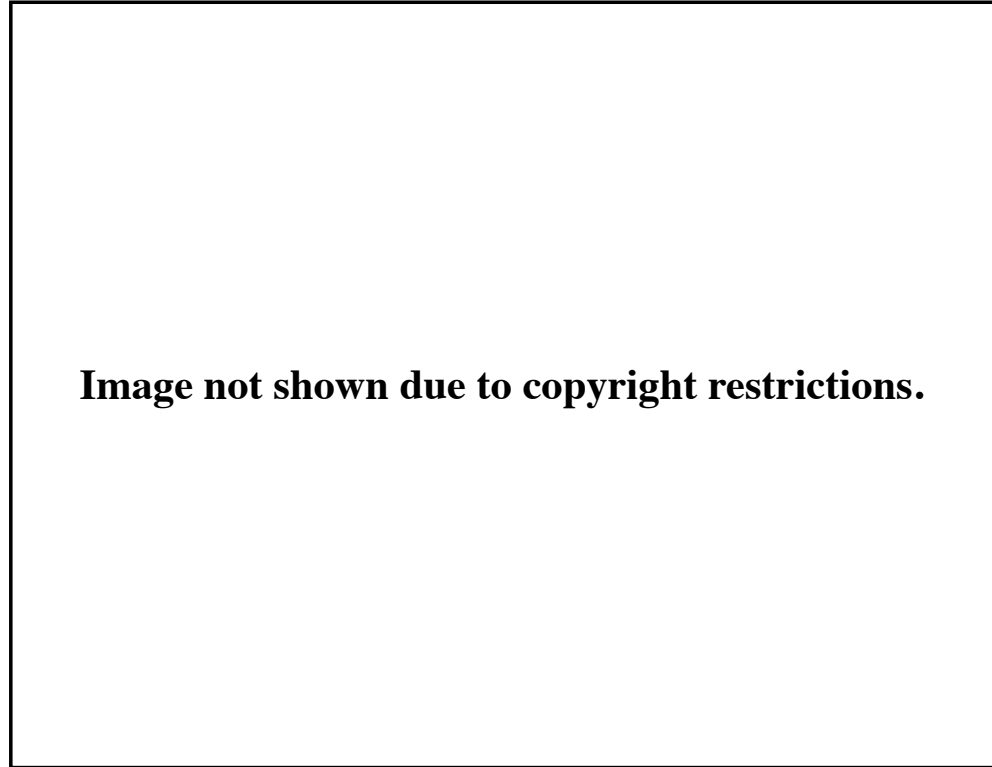
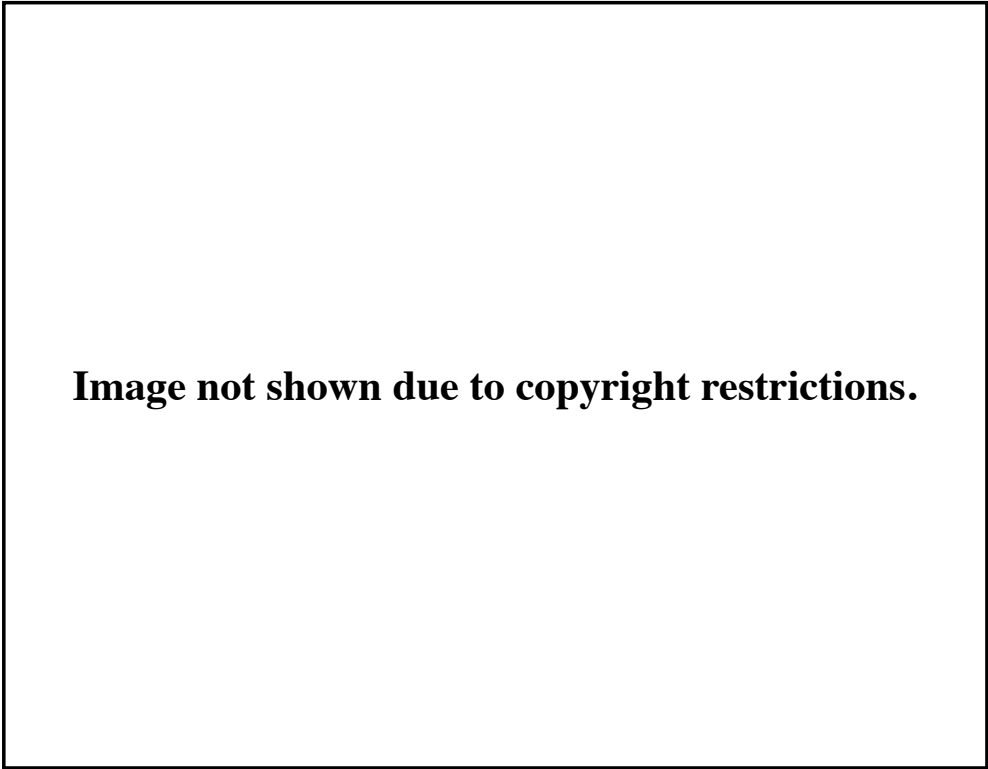


Figure 1.9: The observed metallicity distribution function (MDF) of stars in the Solar neighborhood as a function of  $V$ -velocity relative to the Local Standard of Rest ( $V = -220 \text{ km s}^{-1}$  corresponds to no rotation.). Note that stars with retrograde rotation have peak metallicity at  $[\text{Fe}/\text{H}] = -1.5$  (see the bottom panel in the left-hand column), while stars with highly retrograde rotation show peak metallicity at  $[\text{Fe}/\text{H}] = -2.0$  (see the bottom panel in the middle column). *Taken from Figure 2 of [Carollo et al. \[2007\]](#).*

---



**Image not shown due to copyright restrictions.**

Figure 1.10: The reconstructed density distribution of stars, based on local observation of orbits of nearby stars. Note that more metal-poor halo stars show more spherical distribution, while relatively metal-rich halo stars show more flattened distribution  
*Taken from Figure 5 of [Carollo et al. \[2007\]](#).*

---

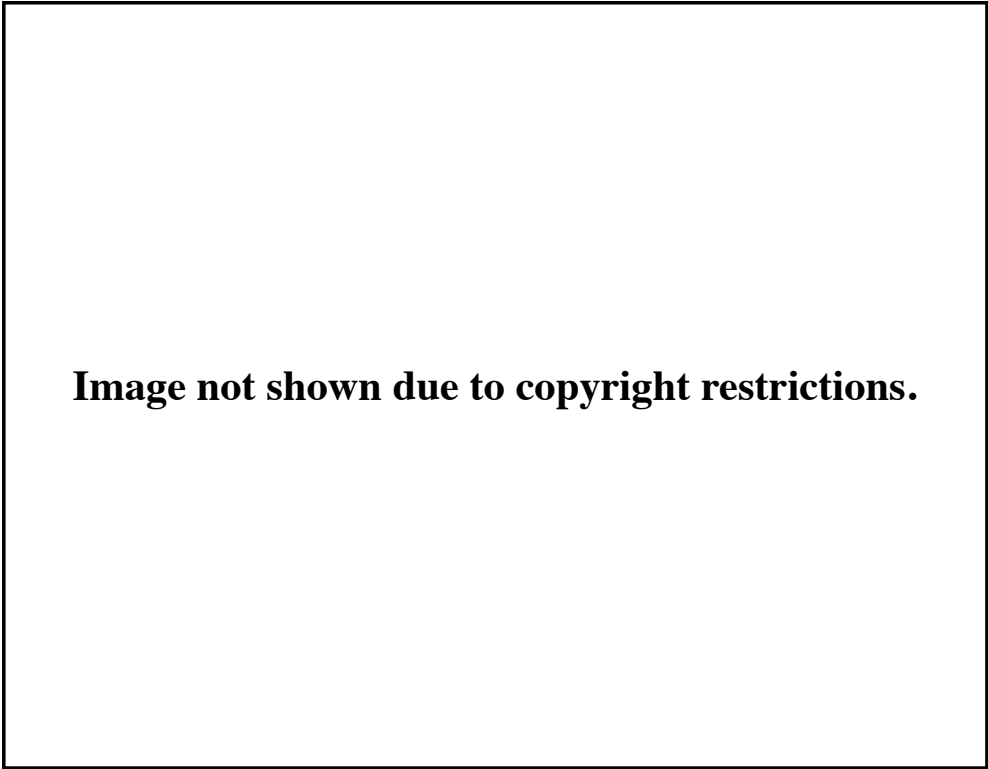


**Image not shown due to copyright restrictions.**

Figure 1.11: The 3-dimensional (3-D) velocity distribution of stars in the Solar neighborhood as a function of metallicity  $[\text{Fe}/\text{H}]$ . Note that the distribution of rotational velocity  $V_\phi$  is not symmetric around  $V_\phi = 0 \text{ km s}^{-1}$  for subsample of stars with  $[\text{Fe}/\text{H}] < -2.2$  (see the bottom panel in the middle column). *Taken from Figure 6 of [Carollo et al. \[2010\]](#).*



---

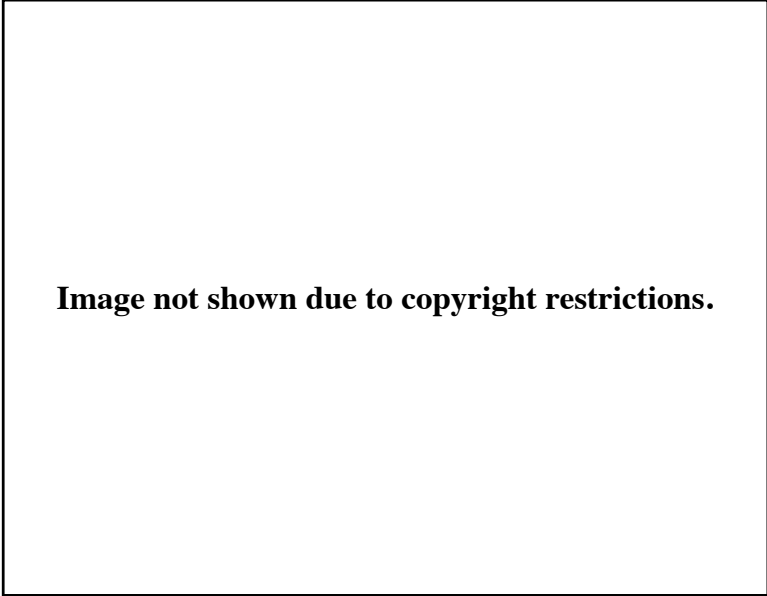


**Image not shown due to copyright restrictions.**

Figure 1.12: The distribution of orbital eccentricity for different ranges in  $|z|$  (vertical distance from the Galactic disk) and metallicity  $[\text{Fe}/\text{H}]$ . Note that the fraction of halo stars with eccentric orbits is smaller at  $[\text{Fe}/\text{H}] < -2.0$  than at  $-2.0 < [\text{Fe}/\text{H}] < -1.5$ . Taken from Figure 5 of *Carollo et al. [2010]*.

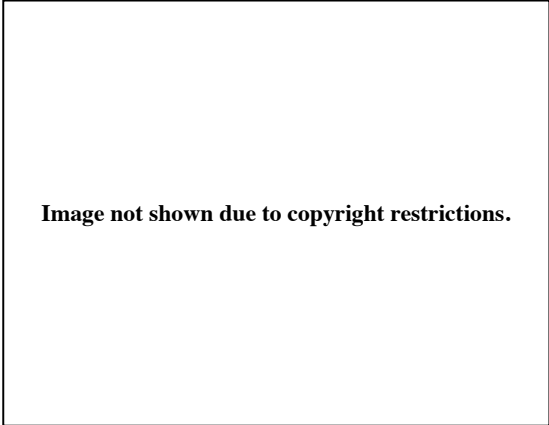


**Image not shown due to copyright restrictions.**

Figure 1.13: The distribution of rotational velocity  $V_\phi$  for stars at  $2-4$  kpc away from the Galactic plane with different  $[\text{Fe}/\text{H}]$  ranges. The results of decomposition method adopted in *Carollo et al. [2010]* is also shown. The  $V_\phi$ -distribution of stars with  $-2.0 < [\text{Fe}/\text{H}] < -1.5$  suggests the existence of a stellar halo component with highly retrograde rotation (see the top panel). Taken from Figure 15 of *Carollo et al. [2010]*.

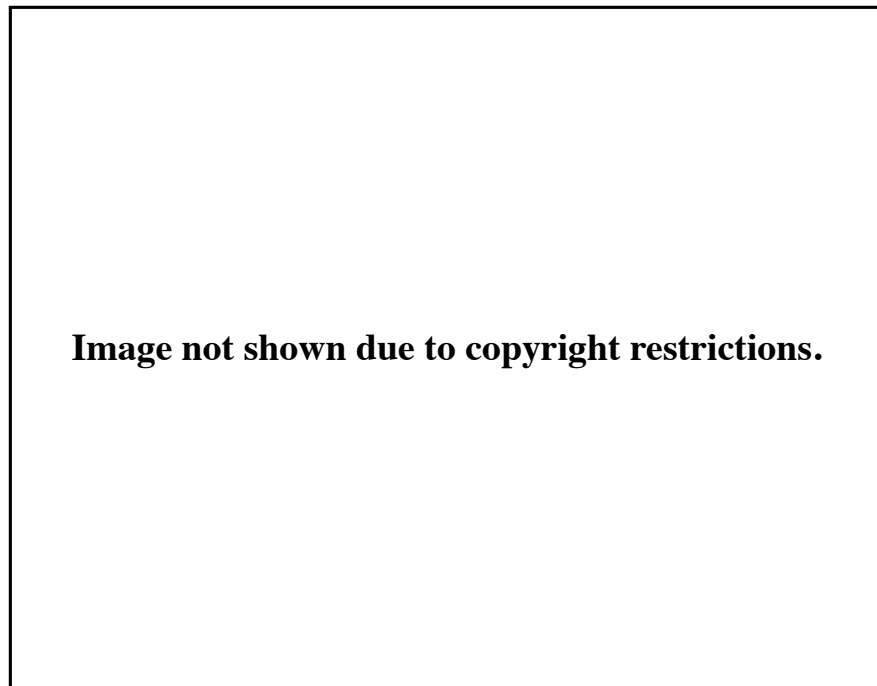


Figure 1.14: The metallicity distribution (MDF) of stars as a function of  $|z|$  (vertical distance from the Galactic disk). Note that the peak metallicity is  $[\text{Fe}/\text{H}] \simeq -1.6$  at  $3 \text{ kpc} < |z| < 4 \text{ kpc}$ , and it gradually decreases to reach  $[\text{Fe}/\text{H}] \simeq -2.2$  at  $|z| > 9 \text{ kpc}$ . Taken from Figure 20 of *Carollo et al. [2010]*.

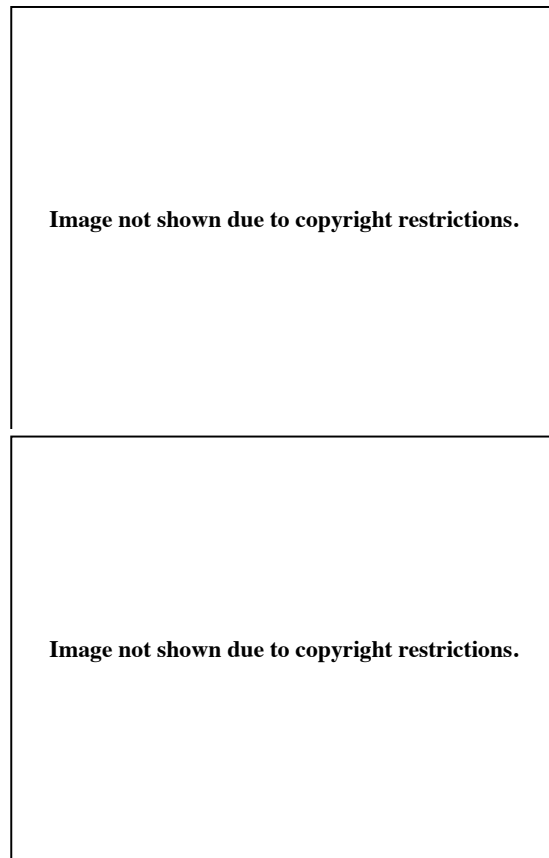


Figure 1.15: The distribution of kinematically selected nearby stars in the  $[\alpha/\text{Fe}]$ - $[\text{Fe}/\text{H}]$  space and velocity space. Note that the high- $\alpha$  population (blue) and low- $\alpha$  population (red), which are clearly separated in the  $[\text{Fe}/\text{H}]$ - $[\alpha/\text{Fe}]$  space, are also distributed in different regions in the velocity space. Taken from Figures 1 and 3 of *Nissen and Schuster [2010]*.

---

## 1.6 Some basic concepts relevant to this thesis

In this section, we briefly describe basic concepts in understanding the observation of stars, which are relevant to the topics in this thesis.

### 1.6.1 Metallicity

In the currently accepted Big Bang nucleosynthesis model, the essentially only elements in the early Universe are H and He. The first stars form out of this primordial gas, so that they are essentially metal-free – or to be more precise, they do not contain elements heavier than lithium. Heavy elements, such as iron (Fe), are produced in the explosive shock fronts of supernovae of first stars, and are dispersed into the interstellar medium (ISM). Second generation of stars are formed out of this polluted ISM, and thus contain small amount of metals. Supernovae and stellar winds of later generations of stars continuously pollute the ISM, so that the metal abundance of ISM monotonically increases as a function of time, if the system is a closed system. The situation is a little bit complicated if the system is not a closed system. In fact, in the course of hierarchical merger, there is a possibility that fresh primordial gas accrete onto already metal-enriched systems. However, there is a general trend that the metal abundance of ISM increase as a function of time, and therefore the metal abundance of later generations of stars are more likely to have higher metal abundance.

It has long been considered that the stellar atmospheric metal abundance of a given star is well conserved throughout its lifetime, except for the case when the stellar surface is exposed to active stellar wind of its binary companion, or when dredge-up processes convey synthesised heavy elements from core to the surface. In a general environment, stellar atmospheric metal abundance is assumed to be a good tracer of the metal abundance of the gas cloud from which it formed. (This conjecture of the constancy of stellar atmospheric metal abundance is a part of this thesis, as presented in Chapter 2.)

Observationally, stellar atmospheric abundance of an element X is often expressed by

$$[X/H] = \log(N_X/N_H)_* - \log(N_X/N_H)_\odot, \quad (1.6)$$

where  $N_H$  and  $N_X$  are the number of hydrogen and element X, respectively, and the subscripts ‘\*’ and ‘ $\odot$ ’ denote the value of the star in discussion and that of the Sun, respectively. In many cases, the iron abundance  $[Fe/H]$  is called metallicity, and we follow this convention throughout this thesis. By definition, the Solar metallicity is

---

$[\text{Fe}/\text{H}] = 0$ , and the first stars are expected to have  $[\text{Fe}/\text{H}] = -\infty$  if they survive until today and their appearance do not change.

### 1.6.2 Initial mass function

Initial mass function (IMF) is a probability density distribution function that determines the mass distribution of a given stellar population at their birth-time. In many cases, IMF  $\xi(m)$  is expressed as a function of the stellar mass  $m$ , so that  $\xi(m)dm$  corresponds to the number fraction of stars with initial mass between  $m$  and  $(m + dm)$ .

[Salpeter \[1955\]](#) determine the IMF of nearby disk stars to be of the form  $\xi(m) \propto m^{-2.35}$ . Although some sophistication have been suggested in more detailed studies, the overall behaviour of the derived IMF has been essentially unchanged so far. Some authors have recently claimed that there is a suggestive (not conclusive) observational evidence that IMF varies as a function of metallicity  $[\text{Fe}/\text{H}]$ , in such a way that the relative fraction of low-mass stars decreases with decreasing metallicity [[Kroupa et al., 2013](#)]. The suggested variation of IMF as a function of metallicity is in favor of theoretical prediction. In more metal-poor gas clouds, the metal cooling becomes less effective, so that both Jeans mass and the typical stellar mass are expected to be larger.

With this regard, primordial gas clouds ( $[\text{Fe}/\text{H}] = -\infty$ ) are the extreme environments in which more fraction of massive stars are expected to form. Recent numerical calculations predict that most of the first stars have more than  $\sim 10M_{\odot}$  [[Hirano et al., 2013](#)]. If this is the case in the real Universe, then we expect little probability of finding surviving first stars in the Milky Way, since first stars with  $M > M_{\odot}$  cannot survive until present. (This is a part of our topic presented in Chapter 2.)

## Chapter 2

# Evidence of Metal Accretion onto Main-Sequence Halo Stars

*Based on Hattori et al. 2014, The Astrophysical Journal, in press*

### 2.1 Abstract of this chapter

The entire evolution of the Milky Way, including its mass-assembly and star-formation history, is imprinted onto the chemo-dynamical distribution function of its member stars,  $f(x, v, [X/H])$ , in the multi-dimensional phase space spanned by position, velocity, and elemental abundance ratios. In particular, the chemo-dynamical distribution functions for low-mass stars (e.g., G- or K-type dwarfs) are precious tracers of the earliest stages of the Milky Way's formation, since their main-sequence lifetimes approach or exceed the age of the universe. A basic tenet of essentially all previous analyses is that the stellar metallicity, usually parametrized as  $[Fe/H]$ , is conserved over time for main-sequence stars (at least those that have not been polluted due to mass transfer from binary companions). If this holds true, any correlations between metallicity and kinematics for long-lived main-sequence stars of different masses, effective temperatures, or spectral types must strictly be the same, since they reflect the same mass-assembly and star-formation histories. By analyzing a sample of nearby metal-poor halo and thick-disk stars on the main sequence, taken from Data Release 8 of the Sloan Digital Sky Survey, we find that the median metallicity of G-type dwarfs is systematically higher (by about 0.2 dex) than that of K-type dwarfs having the same median rotational velocity about the Galactic center. If it can be confirmed, this finding may invalidate the long-accepted assumption that the atmospheric metallicities of long-lived stars are

---

conserved over time.

## 2.2 Introduction

Numerical calculations of the nuclear processes that take place in stellar interiors have established that the evolutionary track of a given star is determined primarily by two parameters – its mass and chemical composition (other parameters, such as stellar rotation and magnetic fields may play roles as well, but they are expected to be smaller). While main-sequence stars are believed to retain the initial values of their mass and composition from birth through the completion of core H burning, it has been conjectured previously that this may not necessarily be the case, depending on their surrounding environment. For example, Bondi [1952] demonstrated, from theoretical considerations, that a star can accrete gas onto its surface at a rate proportional to  $v_{\text{rel}}^{-3}$ , where  $v_{\text{rel}}$  is the relative velocity between the star and the gas with which it collides. In particular, if initially metal-poor stars accrete metal-rich gas, this would lead to an enhancement of the metallicity in their atmospheres, and thus confound a straightforward interpretation of the chemical evolution of the Galaxy.

Yoshii [1981] was the first to speculate that Bondi mass accretion onto halo stars may drastically alter their surface metal abundances in the course of formation of the Galactic halo, proposing that more metal-poor halo stars would suffer greater surface metal enhancements than metal-rich stars, due to their shallower surface convective envelopes. He argued that, early in the formation history of the Milky Way, before the emergence of the disk, gaseous material is primarily distributed throughout the halo. During this era, high-density gas clouds move more or less randomly throughout the halo. If halo stars formed from these clouds, it is possible for them to collide at small relative velocity with chemically processed dense gas from previous star-formation episodes in these same clouds, so that mass accretion as well as surface metal enhancement is likely to occur. After the halo gas has contracted to form the disk stellar populations, mass accretion onto halo stars becomes negligible, for two reasons. First, halo stars collide with dense gas only occasionally, when they pass through the disk. Secondly, such collisions occur near the pericenter of the stellar orbits, hence the relative velocity between halo stars and the disk gas is too large to enable efficient mass accretion.

According to the currently favored hierarchical galaxy formation paradigm in a  $\Lambda$ -CDM universe, the Galaxy is thought to form through mergers of sub-galactic systems for which the internal velocity dispersion is much smaller than that of the ensemble of

---

these systems that make up the entire halo (see, e.g., [Tissera et al. 2013](#), and references therein). Because the relative velocity between the stars and the gas within these systems is on the order of their internal velocity dispersions, this scenario implicitly involves conditions that are favorable for mass accretion, as suggested years ago by [Yoshii \[1981\]](#).

Several previous authors have attempted to evaluate the rate of mass accretion in a cosmological context, and reached similar conclusions, that the surface metal abundances of low-mass, initially metal-poor (or even near zero-metallicity stars) could indeed be enhanced significantly (e.g., [Komiya et al. 2010](#); [Shigeyama et al. 2003](#)). Other authors have argued against the notion that significant mass accretion onto halo stars could have occurred. For example, [Frebel et al. \[2009\]](#) calculated the orbits of individual halo stars in order to evaluate the amount of mass that might have been accreted as they penetrate the disk (several times over the age of the Galaxy), and concluded that their surface metal abundances are hardly enhanced. However, in this work, the amount of mass accreted by individual stars within their natal sub-galactic systems, which may be the dominant source, is not taken into account.

In order to break this stalemate, we propose an observational test to decide whether or not the accretion hypothesis may indeed be supported. Suppose that metal-poor halo G- and K-type dwarfs, with main-sequence lifetimes close to or exceeding the age of the universe, experience no mass accretion and associated surface metallicity enhancement, and that their kinematical properties are independent of spectral type, because they share the same star-formation and mass-assembly histories. Then, any observed correlation between metallicity and kinematics for G-type dwarfs must be identical to that observed for K-type dwarfs. However, if mass accretion and metallicity enhancement did occur, the situation is expected to be quite different. According to theoretical studies of the internal structures of stars, the mass of the surface convective envelope for dwarfs drastically decreases with increasing effective temperature,  $T_{\text{eff}}$ . This implies that the affect of surface metal enhancement on G-type dwarfs is expected to be much larger than for K-type dwarfs (due to the lack of dilution in their surface layers), even if they had the same initial metal abundance and the same amount of mass accreted. Thus, we can accept or reject the accretion hypothesis by examining whether a spectral-type dependent shift in metallicity for stars with otherwise identical kinematics exists or not.

Note that this test is possible only statistically, based on a large, kinematically unbiased sample of metal-poor main-sequence dwarfs. In this chapterchapter, we employ spectroscopic observations of G- and K-type dwarfs in a relatively local region of the



---

halo, taken from Data Release 8 of the Sloan Digital Sky Survey (SDSS DR8, [Aihara et al. 2011](#)), to derive the relation between the median rotational velocity,  $\langle V_\phi \rangle_{\text{med}}$ , and the surface metal abundance,  $[\text{Fe}/\text{H}]$ , for stars of different spectral types. If the above mentioned shift in metallicity with respect to kinematics is confirmed, it would be the first observational evidence of the importance of mass accretion onto halo stars. Given the implications of this, and the clear influence on the interpretation of future observations, it is crucial to seek confirmation (or refutation) based on additional studies.

This chapter is organized as follows. We describe our sample selection in Section 2.3, and present our analysis and results in Section 2.4. The plausibility of our results is discussed in Section 2.5. Our interpretation of these results is presented in Section 2.6. Finally, in Section 2.7 we summarize our results, and suggest future tests of this hypothesis.

## 2.3 Sample

In this section, we describe how we construct a kinematically unbiased sample of low-mass main-sequence stars based on SDSS DR8.

### 2.3.1 Target selection

The spectroscopic samples in SDSS, as well as in its stellar-specific sub-surveys, the Sloan Extension for Galactic Understanding and Exploration (SEGUE-1; [Yanny et al. 2009](#)) and SEGUE-2 (Rockosi et al., in preparation) are selected (targeted) based on a series of photometric (magnitude and color) and/or proper-motion cuts. In order to construct a kinematically unbiased sample, we avoid using stars whose target criteria includes any proper-motion cuts. Since the target criteria for stars in the different surveys are not identical, we first examined their detailed descriptions to determine which might be best used for our present purpose. After some consideration, from SDSS we include only those objects targeted as *BHB candidates* (a subset of these are used for a separate test below). From SEGUE-1, we select those objects whose target names are either *K-dwarf candidates*, *G-dwarf candidates*, or *low-metallicity candidates*. We do not select any objects from the SEGUE-2 sub-survey. The combined sample comprises the basis for our subsequent analysis. Note that our sample is based initially on the target criterion, not on how the star was classified after its spectrum was obtained.

---

### 2.3.2 Selection of G/K-type dwarfs with reliable stellar parameters and kinematics

In order to construct a sample of low-mass, main-sequence dwarfs with reliable estimates of atmospheric metallicity,  $[\text{Fe}/\text{H}]$ , 3-D positions, and space motions, we further restrict our selection to meet additional criteria. In this process, we make use of the stellar parameters derived from the most recent version of the SEGUE Stellar Parameter Pipeline (SSPP; see [Allende Prieto et al. 2008](#); [Lee et al. 2008a,b](#); [Smolinski et al. 2011](#)). Note that the SSPP metallicity estimate is optimized for low-mass dwarfs, in essentially the same way as in [Schlesinger et al. \[2012\]](#).

First, from the above-mentioned stellar sample, we select stars with  $S/N > 20$  per 1 Å pixel, colors in the range  $0.48 < (g - r)_0 < 0.75$ , derived surface gravity  $\log g > 4.1$ , and effective temperatures in the range  $4500 \text{ K} < T_{\text{eff}} < 6000 \text{ K}$ . Here,  $(g - r)_0$  is the reddening-corrected  $(g - r)$  color based on application of the prescription by [Schlegel et al. \[1998\]](#). The lower limit on the  $S/N$  ratio ensures that errors in  $[\text{Fe}/\text{H}]$  derived by the SSPP are not too large (typically smaller than 0.15 dex; [Allende Prieto et al. 2008](#)). The lower limit on  $\log g$  is set to reliably include dwarf stars. The upper and lower limits on effective temperature  $T_{\text{eff}}$  correspond to G0 and K4, respectively [[Habets and Heintze, 1981](#)]<sup>1</sup>. We then select those stars with one-sigma errors in line-of-sight velocity,  $v_{\text{los}}$ , smaller than  $20 \text{ km s}^{-1}$ , and with one-sigma proper-motion errors smaller than  $5 \text{ mas yr}^{-1}$ .

### 2.3.3 Construction of a volume-limited sample

The sample stars obtained in the previous subsection are widely distributed at  $14 \lesssim r_0 \lesssim 19$ , as can be seen in [Figure 2.1](#). Here,  $r_0$  is the absorption-corrected  $r$  magnitude. In this study, we select stars with  $15 < r_0 < 18.45$ , following the most conservative magnitude limit proposed by [Schlesinger et al. \[2012\]](#), in order to approximate a sample that reflects the nature of a volume-limited sample. Then, we select those stars with heliocentric distances,  $d$ , in the range  $0.84 \text{ kpc} < d < 1.64 \text{ kpc}$ , and with atmospheric metallicities in the range  $-2.0 < [\text{Fe}/\text{H}] < -0.5$ , as derived by the SSPP [[Beers et al., 2012](#)]. These distance and metallicity ranges are designed to ensure that the G- and K-dwarfs fairly explore the same volume (that is, we seek to avoid populating the volume differently for the two spectral types), based on the set of 10 Gyr model isochrones described in [An et al. \[2009\]](#) (see [Figure 2.2](#)). [Figure 2.3](#) shows the distribution of our

---

<sup>1</sup>Note that the MK system is defined for solar-metallicity stars, so these ranges on spectral type only loosely apply to low-metallicity stars.

---

sample stars in the color-magnitude diagram, along with the model isochrones of [An et al. \[2009\]](#). Finally, we divide our sample stars into G- and K-dwarf samples based on  $T_{\text{eff}}$ . Throughout this chapter, those dwarfs with  $5250 \text{ K} < T_{\text{eff}} < 6000 \text{ K}$  are referred to as G-type dwarfs, which (for solar-abundance stars) corresponds to G0-G9 [[Habets and Heintze, 1981](#)], while those with  $4500 \text{ K} < T_{\text{eff}} < 5250 \text{ K}$  are referred to as K-type dwarfs, which correspond to K0-K4 (for solar-abundance stars). Our final sample consists of 7124 G-type dwarfs and 3257 K-type dwarfs.

We do not observe a notable difference between the cumulative distributions of the heliocentric distance for the two samples (Figure 2.4). The mean distances of the two samples,  $1.263 \pm 0.003 \text{ kpc}$  (G-type dwarfs) and  $1.254 \pm 0.004 \text{ kpc}$  (K-type dwarfs) are quite close to one another. A two-sample Kolmogorov-Smirnov test of the distributions of heliocentric distance for the G- and K-dwarf samples is unable to reject the null hypothesis that they are drawn from the same parent distribution. The  $p$ -value of the test (0.081) is larger than the widely adopted threshold of 0.05; we conclude that the spatial distributions for these two samples do not significantly differ.

### 2.3.4 Caveats on a metallicity selection bias

We are aware that our sample is affected by a selection bias in which more metal-poor stars are preferentially observed (see section 4.7 of [Schlesinger et al. 2012](#)). Such a selection bias must be treated with care if we are concerned with extracting the metallicity distribution functions for stars in our sample. However, this metallicity-dependent selection bias should not impact our derivation of the median rotational velocity ( $V_\phi$  in a cylindrical system) for stars at a given *fixed* metallicity, since it does not depend on *how many* sample stars are used. In the following, we compare the relationship between  $\langle V_\phi \rangle_{\text{med}}$  – by which we indicate the median rotational velocity – and  $[\text{Fe}/\text{H}]$  for different stellar subsamples.

## 2.4 Median velocity as a function of metallicity

### 2.4.1 Kinematical information

In this chapter we assume that the Local Standard of Rest (LSR) is on a circular orbit with a rotation speed of  $220 \text{ km s}^{-1}$  [[Bovy et al., 2012](#); [Kerr and Lynden-Bell, 1986](#)], and that the Galactocentric distance of the Sun is  $R_\odot = 8.5 \text{ kpc}$  [[Ghez et al., 2008](#); [Koposov et al., 2010](#)]. We also assume that the peculiar motion of the Sun with respect to the LSR is  $(U_\odot, V_\odot, W_\odot) = (10.0, 5.3, 7.2) \text{ km s}^{-1}$  [[Dehnen and Binney, 1998](#)].

---

With these assumptions, and the available estimated distances, line-of-sight velocities, and proper motions, we calculate the 3-D positions and space motions of our sample stars. Noting that the fractional error in the SSPP distance is around 10-20%, and that the typical error in line-of-sight velocity and proper motion is around  $2 \text{ km s}^{-1}$  and  $3.5 \text{ mas yr}^{-1}$ , respectively, the associated error in each of the velocity components of our sample stars is typically around  $30\text{-}40 \text{ km s}^{-1}$ .

## 2.4.2 Median rotational velocity behavior with [Fe/H]

### 2.4.2.1 Use of full sample

Panels (a) and (b) of Figure 2.5 show the distribution of G and K-type dwarfs, respectively, in the  $V_\phi$ -[Fe/H] space. In each panel, a solid line indicates the running median  $\langle V_\phi \rangle_{\text{med}}$  as a function of [Fe/H], sweeping through the sample with overlapping bins of  $N$  stars sorted in [Fe/H] (with an overlap of  $0.9N$  stars per bin), using  $N = 250$  G-type dwarfs and  $N = 300$  K-type dwarfs. Panel (c) of Figure 1 compares the two distributions, with an associated error in  $\langle V_\phi \rangle_{\text{med}}$  estimated by assuming a Gaussian-like distribution of  $V_\phi$ . For both the G- and K-dwarf samples, we note a gradual transition from a nearly non-rotating, halo-dominated region at  $[\text{Fe}/\text{H}] < [\text{Fe}/\text{H}]_{\text{knee}} \simeq -1.5$  to a rapidly-rotating, thick-disk dominated region at  $[\text{Fe}/\text{H}] \gtrsim -1.0$ .<sup>1</sup> However, we also note that there appears to be a systematic offset in the  $\langle V_\phi \rangle_{\text{med}}$ -[Fe/H] relation between the G- and K-type dwarfs, such that the offset in [Fe/H] increases as  $\langle V_\phi \rangle_{\text{med}}$  decreases. The offset in [Fe/H] (when  $\langle V_\phi \rangle_{\text{med}}$  is fixed) increases as a function of  $\langle V_\phi \rangle_{\text{med}}$ , from  $\delta = 0.05$  dex at  $\langle V_\phi \rangle_{\text{med}} \simeq 150 \text{ km s}^{-1}$  to  $\delta = 0.20$  dex at  $\langle V_\phi \rangle_{\text{med}} \simeq 50 \text{ km s}^{-1}$ , below which the  $\langle V_\phi \rangle_{\text{med}}$ -[Fe/H] relation becomes flat. In other words, the offset becomes larger in the more metal-poor, and therefore more halo-dominated region.

It is also intriguing to note that the offset becomes milder at  $\langle V_\phi \rangle_{\text{med}} > 150 \text{ km s}^{-1}$ , where the contribution from the thick disk becomes larger, and that the offset becomes invisible at  $\langle V_\phi \rangle_{\text{med}} > 170 \text{ km s}^{-1}$  or  $[\text{Fe}/\text{H}] > -0.8$ , where the sample is dominated by thick-disk stars.

We note here the possibility that some perturbative mechanisms (such as close encounters with giant molecular clouds in the disk plane) could result in a mass segregation of disk stars, and produce a difference in the  $\langle V_\phi \rangle_{\text{med}}$ -[Fe/H] relation. We check this possibility using a simple mass distribution model for the Milky Way, and find that the difference in the stellar masses of G- and K-type dwarfs is too small to cause the

---

<sup>1</sup>Note that most of our sample stars are located more than 0.5 kpc away from the disk plane, while the scale heights of thin- and thick-disk components are around 0.25-0.35 kpc and 0.7-1.2 kpc, respectively [Gilmore and Reid, 1983; Yoshii, 1982, 2013].

---

observed offset of  $30\text{-}40 \text{ km s}^{-1}$  at  $[\text{Fe}/\text{H}] \simeq -1.4$ . Therefore, hereafter we interpret the detected offset in  $\langle V_\phi \rangle_{\text{med}}\text{-}[\text{Fe}/\text{H}]$  relation as an offset in  $[\text{Fe}/\text{H}]$ , not as one in  $\langle V_\phi \rangle_{\text{med}}$ .

#### 2.4.2.2 Use of $z_{\text{max}}$ -limited subsamples

Next, we derive the orbital parameters for each of the sample stars, assuming the Stäckel-type gravitational potential of the Milky Way adopted by [Chiba and Beers \[2001\]](#). We divide our G- and K-dwarf samples according to whether  $z_{\text{max}}$  is larger or smaller than 3 kpc ( $z_{\text{max}}$  denotes the largest orbital excursion perpendicular to the Galactic disk plane achieved by a given star during its orbit), and perform the same analysis as carried out above.

Panels (a) and (b) in Figure 2.6 show the median value of  $V_\phi$ , as a function of  $[\text{Fe}/\text{H}]$ , for our sample stars with  $z_{\text{max}} < 3$  kpc and  $z_{\text{max}} > 3$  kpc, respectively. The binning procedure is the same as used for Figure 2.5, with the  $N$  employed shown on each panel. Although the offset in  $\langle V_\phi \rangle_{\text{med}}\text{-}[\text{Fe}/\text{H}]$  relation is not clear in panel (a), it becomes very apparent in panel (b). The magnitude of the offset on panel (b) is  $\delta \simeq 0.20$  dex, which is as large as the maximum offset seen in Figure 2.5.

## 2.5 Plausibility of our results

In section 2.4, we find that G- and K-type dwarfs show different behaviour in the  $\langle V_\phi \rangle_{\text{med}}\text{-}[\text{Fe}/\text{H}]$  relation. Here we discuss how the selection bias in SDSS or observational errors may affect our results and investigate the plausibility of our results.

### 2.5.1 Selection bias in SDSS

[Schlesinger et al. \[2012\]](#) point out that, even if they take into account the metallicity-dependent selection bias inherent in SDSS/SEGUE, the fraction of metal-poor K-type dwarfs is larger than that of G-type dwarfs, especially in the high  $|z|$ -region ( $|z|$  is the distance from the Galactic disk plane). In order to investigate if this discrepancy is involved with producing the observed offset in the  $\langle V_\phi \rangle_{\text{med}}\text{-}[\text{Fe}/\text{H}]$  relation, we select those sample stars that appear also in the [Schlesinger et al. \[2012\]](#) sample, and check the  $|z|$ -dependence of the  $\langle V_\phi \rangle_{\text{med}}\text{-}[\text{Fe}/\text{H}]$  relation. We find that the offset can be confirmed independent of  $|z|$ , which suggests that the observed offset is not relevant to the discrepancy found in [Schlesinger et al. \[2012\]](#).

---

## 2.5.2 Observational errors

### 2.5.2.1 Systematic errors in SSPP metallicity estimates

The simplest explanation of our finding that G- and K-type dwarfs show different  $\langle V_\phi \rangle_{\text{med}}\text{-}[\text{Fe}/\text{H}]$  relations is that it is due to a temperature-related systematic error in the determination of  $[\text{Fe}/\text{H}]$  by the SSPP. If such a systematic error in  $[\text{Fe}/\text{H}]$  exists, we may detect a systematic difference between SSPP metallicity and the metallicity derived from high-resolution spectroscopy for G/K-type dwarfs. We check this possibility by using five G-type dwarfs and two K-type dwarfs taken from Table 4 of [Allende Prieto et al. \[2008\]](#), and find that G-type dwarfs tend to have  $\sim 0.2$  dex higher SSPP metallicity than the high-resolution metallicity, while the two estimates of metallicity more or less agree with each other for K-type dwarfs.<sup>1</sup> Although the sample size (in total seven) is insufficient to be confident, the uncertainty in SSPP metallicity might influence the observed offset in  $\langle V_\phi \rangle_{\text{med}}\text{-}[\text{Fe}/\text{H}]$  relations in Figure 2.5 or 2.6.

However, if the apparent offset in Figure 2.5 is due to a spectral-type dependent systematic error in the SSPP metallicity, we would also expect a similar offset in Figure 2.6(a). The fact that we see a clear offset only in Figure 2.5 and 2.6(b) and not in Figure 2.6(a), may indicate that the existence or non-existence of the offset in the  $\langle V_\phi \rangle_{\text{med}}\text{-}[\text{Fe}/\text{H}]$  relation in these figures is real. This notion is supported by the mock data analysis presented in section 2.5.2.4.

### 2.5.2.2 Random errors in proper motion

The largest contribution to the uncertainty in the measured velocity components of our sample stars arises from the observational errors in proper motion, which are typically as large as  $3.5 \text{ mas yr}^{-1}$ . However, the proper-motion error does not seem to affect the median value,  $\langle V_\phi \rangle_{\text{med}}$ , since it is a purely random error in most cases. In order to estimate the effect of proper-motion errors on our results, we first construct 100 error-added samples of G- and K-type dwarfs. To do this, we randomly add/subtract an error term to the observed proper motion that obeys a Gaussian distribution with standard deviation corresponding to the one-sigma observational error in the proper motion. Then, we perform the same analysis to these error-added samples, and compare

---

<sup>1</sup> According to [Allende Prieto et al. \[2008\]](#), possible systematic errors in  $[\text{Fe}/\text{H}]$  for SDSS/SEGUE spectra with  $S/N > 20$  are less than 0.15 dex. However, this value does not directly apply to our sample dwarfs, since their sample includes not only dwarfs but also more luminous giants. Indeed, their Table 4 indicates that the uncertainty in the SSPP metallicity for G/K-type dwarfs might be as large as 0.3 dex.

---

the results with that of the as-observed sample. After these calculations, we confirm that the proper-motion error scarcely affects our results shown in Figure 2.5 or 2.6.

### 2.5.2.3 Systematic errors in SSPP distance estimates

We next consider how systematic errors in the determination of distance could affect our result. In our analysis, we select stars with distances in the range  $0.84 \text{ kpc} < d < 1.64 \text{ kpc}$ . If the distances to K dwarfs are over-estimated by the SSPP, then more K-type dwarfs in our sample are expected to reside closer to the Galactic disk plane, and the fraction of K-type dwarfs that belong to the thick disk is over-estimated in our sample. In this case, we unintentionally compare the low- $|z|$  K dwarfs and high- $|z|$  G-type dwarfs, leading to a higher value of  $\langle V_\phi \rangle_{\text{med}}$  for K-type dwarfs at a fixed  $[\text{Fe}/\text{H}]$ . In order to test this bias, we construct two different samples of K-type dwarfs selected by the same criteria as in Section 2, but assigned distances that are 20% smaller or larger compared to the adopted distance. In both instances, we confirm that the difference between the resultant  $\langle V_\phi \rangle_{\text{med}}-[\text{Fe}/\text{H}]$  relation and the original one is less than  $20 \text{ km s}^{-1}$  at  $[\text{Fe}/\text{H}] > -1.5$ . We conclude that a systematic error of  $\sim 20\%$  in distance determination cannot explain the observed difference in the  $\langle V_\phi \rangle_{\text{med}}-[\text{Fe}/\text{H}]$  relationship between the G- and K-type dwarfs.

### 2.5.2.4 Mock data analysis

In order to check the validity of our results, we also examine how random and/or systematic errors in the observed quantities (such as distance and metallicity) could affect our results in Figures 2.5 and 2.6. For this purpose, we construct a set of realistic mock catalogs in which the information on effective temperature, surface gravity, metallicity, distance, Galactic latitude and longitude is identical to that of our real sample,<sup>1</sup> but the information on line-of-sight velocity and proper motion reflects a given distribution function model as well as assumed realistic errors in metallicity, distance, line-of-sight velocity and proper motion. Note that the effect of metal accretion is not taken into account in our mock catalogs. (See Appendix for the full description of our mock catalogs.)

We consider various models of random and/or systematic errors in the observed quantities, and prepare 100 mock catalogs for each error model. Then we perform the same analyses on our mock catalogs as applied to our real sample, and derive the

---

<sup>1</sup>Since the values of  $T_{\text{eff}}$ ,  $\log g$ ,  $[\text{Fe}/\text{H}]$ , and  $d$  are the same as those of the real sample, the spatial and metallicity distributions of G- and K-type dwarfs of any given mock catalog are identical to those of our real sample.

---

$\langle V_\phi \rangle_{\text{med}}\text{-}[\text{Fe}/\text{H}]$  relations which correspond to Figures 2.5 (full sample) and 2.6 ( $z_{\text{max}}$ -limited subsamples).

First, we find that the  $\langle V_\phi \rangle_{\text{med}}\text{-}[\text{Fe}/\text{H}]$  relations for G- and K-type dwarfs in our mock catalogs are statistically identical, if we do not introduce any spectral-type dependence in the observational errors. Noting that the spatial distributions of the mock G- and K-type dwarfs are identical to those of the real G- and K-type dwarfs, this result justifies our starting point that the spatial distributions of our G- and K-type dwarfs are essentially identical (section 2.3.3).

Secondly, we find that the offset in the  $\langle V_\phi \rangle_{\text{med}}\text{-}[\text{Fe}/\text{H}]$  relation similar to that in Figure 2.5 is seen only when the random or systematic errors in  $[\text{Fe}/\text{H}]$  depend on the spectral type. In addition, we find that when such an offset is seen in the full sample, a similar offset is also seen in the low- $z_{\text{max}}$  subsample, and vice versa. In other words, random or systematic errors in  $[\text{Fe}/\text{H}]$  either produce an offset for *both* Figures 2.5(c) and 2.6(a), or produce no offset for *both* of these figures. This finding is in sharp contrast with our results for the real sample, in which a clear offset is seen only in Figure 2.5(c) and not in Figure 2.6(a). Moreover, we also find that the offset in the  $\langle V_\phi \rangle_{\text{med}}\text{-}[\text{Fe}/\text{H}]$  relation for the high- $z_{\text{max}}$  subsample is, if anything, less clear than that for the low- $z_{\text{max}}$  subsample. Presumably, this result is due to the smaller number of stars in the high- $z_{\text{max}}$  subsample. This finding is also opposite to our results for the real sample, in which a clearer offset is seen in Figure 2.6(b) than in Figures 2.6(a).

These results suggest that the observed offset in the  $\langle V_\phi \rangle_{\text{med}}\text{-}[\text{Fe}/\text{H}]$  relation cannot be explained by observational errors that may or may not depend on the spectral type. Therefore, we conclude that the observed offset in Figures 2.5 and 2.6(b), as well as apparent non-existence of the offset in Figure 2.6(a), are all real.

## 2.6 Discussion

In this chapter we have derived the relation of  $\langle V_\phi \rangle_{\text{med}}$  (median value of  $V_\phi$ ) as a function of  $[\text{Fe}/\text{H}]$  for halo G- and K-type dwarfs from SDSS DR8. We find that the run of  $\langle V_\phi \rangle_{\text{med}}$  vs.  $[\text{Fe}/\text{H}]$  can be characterized by a boundary metallicity,  $[\text{Fe}/\text{H}]_{\text{knee}}$ , below which the nearly non-rotating halo stars dominate, and that  $[\text{Fe}/\text{H}]_{\text{knee}}$  for G-type dwarfs occurs at a higher abundance than that for K-type dwarfs by an offset of  $\delta \simeq 0.20$  dex. This offset is also seen for those sample stars that have large vertical motion. Below we consider the implications of this result.



---

### 2.6.1 Evidence of metal accretion onto main-sequence halo stars

We interpret this non-zero value of  $\delta \simeq 0.20$  dex between the characteristic metallicities of halo G- and K-type dwarfs to be the first tentative evidence that halo stars have been *externally* polluted by the accretion of metal-enriched gas from their natal clouds. The effect is more noticeable for G-type dwarfs, whose convective envelopes are shallower than those of K-type dwarfs, since they will not have diluted accreted material as fully.

If this interpretation is correct, we expect an even larger offset in metallicity for red giants (e.g., K giants), which possess deeper surface convective envelopes than K-type dwarfs [Yoshii, 1981]. That is, the knee of the  $\langle V_\phi \rangle_{\text{med}}\text{-}[\text{Fe}/\text{H}]$  relation for K giants, if plotted as in Figure 2.5, should be located to the left of that for K dwarfs. Although there is no large publicly available database of nearby K giants, other types of post-main-sequence stars might serve as alternatives, since the surface heavy element abundance is expected to remain unchanged when red giants evolve into either horizontal-branch stars or RR Lyrae stars. During the course of this evolution, red giants lose mass from their surface convective envelopes. The total amount of mass loss is expected to be  $\simeq 0.2 M_\odot$  for a red giant of initially  $0.8 M_\odot$  (see Yoshii 1981, and references therein), which is smaller than the total mass of the surface convective envelope ( $\simeq 0.3 M_\odot$ ) in the red-giant stage [Sweigart and Gross, 1978].

Thus, instead of red giants, we have explored the  $\langle V_\phi \rangle_{\text{med}}\text{-}[\text{Fe}/\text{H}]$  relation for 290 blue horizontal-branch (BHB) stars with  $T_{\text{eff}} > 7500$  K,  $\log g < 3.8$ , located at  $2 \text{ kpc} < |z| < 5 \text{ kpc}$ ,  $5 \text{ kpc} < R < 20 \text{ kpc}$ , taken from Xue et al. [2011]. Here,  $R$  and  $|z|$  are the Galactocentric distance projected onto the Galactic disk plane and the distance above or below the disk plane, respectively. The cuts in  $T_{\text{eff}}$  and  $\log g$  are adopted following the selection criteria proposed by R. Santucci et al. (in preparation).

In Figure 2.7, we show the distribution of BHB stars in the  $V_\phi\text{-}[\text{Fe}/\text{H}]$  space, along with the median value  $\langle V_\phi \rangle_{\text{med}}$  for the binned sample. From inspection of this figure, the  $\langle V_\phi \rangle_{\text{med}}$  of BHB stars is nearly constant (consistent with  $0 \text{ km s}^{-1}$ ) at  $[\text{Fe}/\text{H}] < [\text{Fe}/\text{H}]_{\text{knee}} \simeq -1.7$ .<sup>1</sup> This suggests that inner-halo BHB stars dominate over metal-weak thick-disk BHB stars below  $[\text{Fe}/\text{H}] = [\text{Fe}/\text{H}]_{\text{knee}}$  at  $2 \text{ kpc} < |z| < 5 \text{ kpc}$ . Noting that a lower value of  $[\text{Fe}/\text{H}]_{\text{knee}}$  is expected for a sample of stars with lower  $|z|$  (due to the larger fraction of thick-disk stars in the sample), we expect that  $[\text{Fe}/\text{H}]_{\text{knee}}$  for BHB stars would be even lower than  $-1.7$  if we could obtain a BHB sample with distances

---

<sup>1</sup> The plateau value of  $\langle V_\phi \rangle_{\text{med}}$  at  $[\text{Fe}/\text{H}] < [\text{Fe}/\text{H}]_{\text{knee}}$  for the BHB sample ( $\simeq 0 \text{ km s}^{-1}$ ) is lower than that for G/K-type dwarfs ( $\simeq 50 \text{ km s}^{-1}$ ; see Figure 2.5). This discrepancy seems to arise from the different spatial regions covered by these samples. In fact, Chiba and Beers [2000] find that the mean rotational velocity  $\langle V_\phi \rangle$  for nearby metal-poor stars with  $[\text{Fe}/\text{H}] < -1.5$  is higher for those sample stars with smaller  $|z|$  [see their Figure 3(a)], which is consistent with our discrepancy.

---

in the range  $0.84 \text{ kpc} < d < 1.64 \text{ kpc}$ , as was used above for the G- and K-dwarf samples. Since the positions of  $[\text{Fe}/\text{H}]_{\text{knee}}$  for the G and K-type dwarfs are  $-1.4$  and  $-1.6$ , respectively, in this distance range (see Figure 2.5), it follows that  $[\text{Fe}/\text{H}]_{\text{knee}}$  for BHB stars should be lower, by *at least* 0.3 dex and 0.1 dex, respectively, if these samples could be fairly compared. This may indicate that the BHB stars are even less affected by surface metal pollution than K-type dwarfs. The sample of 290 BHB stars is not sufficiently large to be certain of this effect, but the present result does serve to support the accretion hypothesis for halo stars. Surveys such as LAMOST and Gaia will provide larger kinematically unbiased samples of low-mass dwarfs and red giants. At that stage, we will be able to compare the chemo-dynamical correlations of these stars more rigorously, and test the metal accretion hypothesis thoroughly.

### 2.6.2 Where did the metal accretion take place?

As mentioned in the Introduction, the efficiency of metal accretion in halo stars is proportional to  $v_{\text{rel}}^{-3}$ , where  $v_{\text{rel}}$  is the relative velocity of the star and the colliding gas. Therefore, metal accretion onto halo stars may or may not be important, depending on the nature of the environments in which it could take place. Recent observations [Beers et al., 2012; Carollo et al., 2007, 2010] and numerical simulations [Font et al., 2011; McCarthy et al., 2012; Tissera et al., 2013] suggest that the stellar halo of the Milky Way comprises two distinct components with different origins, which are often referred to as the inner- and outer-halo populations. In this picture, inner-halo stars formed from relatively more massive sub-galactic systems ( $10^{9-10} M_{\odot}$ ) in the main progenitors of the Milky Way, while much smaller sub-galactic systems ( $10^{7-8} M_{\odot}$  or less), similar to lower-mass dwarf-like galaxies, were disrupted to contribute the bulk of the low-metallicity outer-halo stars. In the progenitor systems of the inner-halo stars, the internal velocity dispersion is expected to be  $\sim 30 \text{ km s}^{-1}$  [Tissera et al., 2013], so that the above-mentioned  $v_{\text{rel}}$  may have been too large for inner-halo stars to experience efficient metal accretion. On the other hand, the internal velocity dispersion of ultra-faint dwarf galaxies – whose constituent stars are typically as metal-poor as  $[\text{Fe}/\text{H}] \lesssim -2.0$ , similar to nearby outer-halo stars – is  $\sim 5 \text{ km s}^{-1}$  (Simon and Geha 2007; Walker et al. 2009; see also Yoshii and Arimoto 1987), so that  $v_{\text{rel}}$  may have been small enough to enable efficient metal accretion onto constituent stars. Therefore, in this inner/outer halo picture, the outer-halo stars are much more likely to have experienced metal accretion. In other words, if the dual halo picture is correct, we expect that inner-halo dominated sample of G- and K-type dwarfs would exhibit little or no offset

---

in the  $\langle V_\phi \rangle_{\text{med-}}[\text{Fe}/\text{H}]$  relation, while the outer-halo dominated sample of G- and K-type dwarfs would show noticeable offsets.

Observationally, it is suggested that the fraction of outer-halo stars increases as  $z_{\text{max}}$  increases [Carollo et al., 2010]. Thus, if we divide each of our G- and K-dwarf samples into two subsamples with respect to  $z_{\text{max}}$ , the fraction of outer-halo stars is expected to be larger in the higher- $z_{\text{max}}$  subsample than in the lower- $z_{\text{max}}$  one. It follows that we expect a clearer offset in the  $\langle V_\phi \rangle_{\text{med-}}[\text{Fe}/\text{H}]$  relation for the higher- $z_{\text{max}}$  subsample. This expectation is indeed consistent with the results in Figure 2.6, in which we observe a clearer offset in the  $\langle V_\phi \rangle_{\text{med-}}[\text{Fe}/\text{H}]$  relation for our sample stars with  $z_{\text{max}} > 3$  kpc, and not for those stars with  $z_{\text{max}} < 3$  kpc.<sup>1</sup> These results can be understood if a dual inner/outer halo applies to the Milky Way, as originally suggested by Carollo et al. [2007], and metal accretion is efficient only for stars associated with the progenitors of the outer halo.

We note here that typical halo stars with  $z_{\text{max}} > 3$  kpc would penetrate through the Galactic disk with a velocity of  $v_{\text{rel}} > 100 \text{ km s}^{-1}$  relative to the gas clouds in the disk. Therefore, metal accretion when the halo stars penetrate the Galactic disk plane accounts for only a negligible fraction of the total amount of metals accreted onto halo stars, supporting the view of Frebel et al. [2009]. However, the fact that we see a clear offset in panel (b) of Figure 3 suggests that the outer-halo stars are likely to have experienced metal accretion within their progenitor systems, which were *later* disrupted.

### 2.6.3 Impact on the metallicity distribution function in the stellar halo system

One obvious impact of our results is that the metallicity distribution function (MDF) of halo main-sequence stars may need to be re-examined. In the hierarchical galaxy formation scenario, halo stars form in sub-galactic systems that are later disrupted by tidal interaction with the Galaxy, hence halo stars originating from these disrupted systems are likely to have experienced metal accretion within these systems [Komiya et al., 2010; Shigeyama et al., 2003; Suda et al., 2004]. As a consequence, the shape of the MDF of halo stars is expected to be skewed toward higher  $[\text{Fe}/\text{H}]$  when compared to their original MDF, because the surface metallicity is enhanced for stars with lower

---

<sup>1</sup> Our boundary at  $z_{\text{max}} = 3$  kpc is smaller than that adopted in Carollo et al. [2010], so that we have a sufficient number of stars in the higher- $z_{\text{max}}$  subsample. However, this difference is not crucially important, since our aim is to examine two subsamples with different fractions of inner/outer-halo stars. Our higher- $z_{\text{max}}$  subsample includes numerous stars with  $z_{\text{max}}$  as large as 10-50 kpc.

---

[Fe/H] due to their shallow surface convective envelopes, while it is less enhanced for stars with higher [Fe/H] due to their deeper surface convective envelopes [Mengel et al., 1979].

In this respect, it is intriguing to note the apparent discrepancy between the MDFs of main-sequence turn-off (MSTO) stars and BHB stars in the outer halo region of the Milky Way. Sesar et al. [2011] show that the median metallicity of MSTO stars at Galactocentric distances in the range of  $10 \text{ kpc} < r < 30 \text{ kpc}$  is  $[\text{Fe}/\text{H}] \simeq -1.5$ , almost independent of  $r$ .<sup>1</sup> On the other hand, Beers et al. [2012] show that the median metallicity of BHB stars at  $10 \text{ kpc} < r < 40 \text{ kpc}$  is  $[\text{Fe}/\text{H}] \simeq -2.0$ , almost independent of  $r$ .<sup>2</sup> This discrepancy can be well explained by the accretion hypothesis. MSTO and BHB stars are of similar age, yielding no systematic difference in the mass accreted in their main-sequence stage. Thus, the surface metallicity of BHB stars is much less enhanced than that of MSTO stars, because the red giants that were progenitors of the stars presently on the BHB had very deep surface convective envelopes compared to MSTO stars (see section 2.6.1).

Furthermore, noting that the surface convective envelopes of MSTO stars are shallower than those of G-type dwarfs, it is also interesting to note that the apparent offset in the median metallicity of the MDF for MSTO and BHB stars ( $[\text{Fe}/\text{H}]_{\text{median,MSTO}} - [\text{Fe}/\text{H}]_{\text{median,BHB}} \simeq 0.5 \text{ dex}$ ) is consistent with the offset in the break metallicity ( $[\text{Fe}/\text{H}]_{\text{knee,G}} - [\text{Fe}/\text{H}]_{\text{knee,BHB}} \gtrsim 0.3 \text{ dex}$ ) of the  $\langle V_\phi \rangle_{\text{med}} - [\text{Fe}/\text{H}]$  relation for G-type dwarfs and BHB stars (see section 2.6.1). Our interpretation of this consistency in terms of the accretion hypothesis may be tested based on a much larger sample of BHB stars or red giants that should be available in the near future.

Another intriguing aspect of the observed halo MDF is the possible existence of a cutoff metallicity at  $[\text{Fe}/\text{H}]_{\text{cutoff}} \simeq -4$ , below which the MDF shows a sharp decline (Li et al. 2010; Schörck et al. 2009; see also Yong et al. 2013). There are not yet a sufficient number of stars known with  $[\text{Fe}/\text{H}] < -3.5$ , let alone with  $[\text{Fe}/\text{H}] < -4.0$ , to evaluate whether the cutoff is real, or simply the result of small number statistics in the ultra metal-poor regime. Future observations of G/K-type dwarfs might well detect a spectral-type dependence of this cutoff metallicity, in the sense that  $[\text{Fe}/\text{H}]_{\text{cutoff,K}} < [\text{Fe}/\text{H}]_{\text{cutoff,G}}$ , if metal accretion and subsequent surface metal enhancement does indeed take place among metal-poor halo stars.

---

<sup>1</sup>See panels W3 and W4 in Figure 2.8, taken from Sesar et al. [2011], in which the influence from known substructures in the halo is not significant.

<sup>2</sup>See the right-hand panels in Figure 2.9, taken from Beers et al. [2012], in which the contamination from the Sagittarius dwarf galaxy is minimized, and Figure 4 of Carollo et al. [2007].

---

#### 2.6.4 On the case of $\omega$ Centauri

Some globular clusters appear to be ideal places to test the metal accretion hypothesis, if they are regarded as closed systems and the constituent stars are coeval, or nearly so. [Stanford et al. \[2007\]](#) investigate the metallicities of stars in the globular cluster  $\omega$  Cen, and find that the peak metallicity of near-turn-off stars is systematically higher than that of red giant branch (RGB) stars, by 0.01-0.05 dex (see [Figure 2.10](#)). This offset is smaller than the uncertainty in the derived  $[\text{Fe}/\text{H}]$  for their sample (0.15-0.20 dex). However, taking into account that the surface convective envelope is deeper for RGB stars than near-turn-off stars, the sense of the reported gap is in agreement with the prediction from the metal accretion hypothesis.

If the reported gap (0.01-0.05 dex) between near-turn-off stars and RGB stars is due to metal accretion, we expect that the typical metallicities of G- and K-type dwarfs in  $\omega$  Cen are different from each other by less than 0.05 dex, because of the milder difference in the depth of surface convective envelope between G- and K-type dwarfs. If we take into account the observed offset of  $\simeq 0.20$  dex in [Figure 2.6\(b\)](#), the metal accretion in typical progenitor systems of the Milky Way outer halo is more significant than that in  $\omega$  Cen. Noting that the efficiency of metal accretion is proportional to  $v_{\text{rel}}^{-3}$ , the seemingly low efficiency within  $\omega$  Cen indicates that typical progenitor systems of the outer halo must have smaller internal velocity dispersions than that of  $\omega$  Cen. It is suggested that such progenitor systems are similar to the currently observed ultra-faint dwarf galaxies (with central velocity dispersion  $\sim 5 \text{ km s}^{-1}$ ), and that the contribution from large and compact globular clusters (such as  $\omega$  Cen, with central velocity dispersion  $\simeq 17 \text{ km s}^{-1}$ ; [Sollima et al. 2009](#)) to the outer halo is not significant.

#### 2.6.5 Implication for the first stars

If primordial (zero-metal) stars from the very first generation (with main-sequence masses below  $0.8M_{\odot}$ ) were able to form, they could survive until today, and possibly be observed. Here we consider this possibility from the perspective of the accretion hypothesis.

The mass range of the first stars has been long debated, but some nucleosynthesis constraints have recently been placed by the discovery of four hyper metal-poor (HMP; technically, Fe-poor) stars with  $[\text{Fe}/\text{H}] \lesssim -5$  (HE 01072-5240: [Christlieb et al. 2002](#); HE 1327-2326: [Frebel et al. 2005](#); HE 0557-4840: [Norris et al. 2007](#); SDSS J102915+172927: [Caffau et al. 2012](#)). Three of the four stars (excluding SDSS J102915+172927) exhibit elemental abundance patterns that are significantly enhanced

---

with carbon (C) and nitrogen (N), and can be well-explained if they are second-generation stars, formed out of an interstellar medium that was chemically enriched by supernova ejecta from  $25M_{\odot}$  primordial stars [Iwamoto et al., 2005; Nomoto et al., 2013; Umeda and Nomoto, 2003].

However, if we allow for the metal accretion hypothesis, as suggested to apply in this chapter, it is possible to regard the above-mentioned HMP stars as surviving primordial stars whose surfaces were polluted by the accretion of the supernova ejecta of  $25M_{\odot}$  primordial stars [Shigeeyama et al., 2003]. Since the mass of these stars is as small as  $0.8M_{\odot}$ , our interpretation has an implicit requirement for the mass of primordial stars to range from less than  $1M_{\odot}$  up to more than a few tens of  $M_{\odot}$ , as predicted by some authors [Nakamura and Umemura, 2001; Yoshii and Saio, 1986]. In this respect, it is worth mentioning that SDSS J102915+172927 is an  $0.7M_{\odot}$  star with no significant C and N enhancement. The mass fraction of heavy elements derived for this star,  $Z < 7.4 \times 10^{-7}$ , is the lowest known to date, and heavy-element cooling in metal-poor gas with  $Z < Z_{\text{crit}} = 10^{-5} - 10^{-6}$  is superseded by purely atomic or molecular hydrogen or zero-metal cooling [Bromm et al., 2001; Safranek-Shrader et al., 2010; Silk, 1977; Smith et al., 2009; Yoshii and Sabano, 1980]. Therefore, the discovery of a  $0.7M_{\odot}$  star with  $Z < Z_{\text{crit}}$  indicates that this star could indeed have formed by zero-metal cooling. In other words, the zero-metal cooling process turns out to be able to produce primordial stars with the masses below  $1M_{\odot}$ .

We propose that at least some of the HMP stars could be surviving primordial stars that have experienced surface metal pollution after they formed. Given that the environments in which such pollution can occur is limited, we expect that even more HMP metal-poor stars similar to SDSS J102915+172927, with  $Z \ll Z_{\text{crit}}$ , may well be discovered.

## 2.7 Summary

In this chapter we have described possible observational evidence for the surface metal pollution of halo stars due to the accretion of metal-enriched material onto stellar surfaces, as theoretically predicted by Yoshii [1981]. If we take at face value our analysis of an additional sample of BHB stars, it might be the case that the initial metallicities of halo G-type dwarfs and halo K-type dwarfs are at least  $\sim 0.3$  dex and  $\sim 0.1$  dex *lower* than their observed atmospheric metallicities, respectively. We also suggest this interpretation, along with extant observations of HMP stars, may provide confirmation that the lower mass limit of the primordial initial stellar mass function extends to below

---

$1M_{\odot}$ .

In our current analysis, we could only compare the  $\langle V_{\phi} \rangle_{\text{med}}\text{-}[\text{Fe}/\text{H}]$  correlation for different types of stars, due to the large extant errors in proper motion. However, the situation will be greatly improved in the near future, when the Gaia satellite and large ground-based telescopes provide truly enormous samples of disk and halo stars with much more accurate kinematic and chemical information. Such datasets will enable analyses of other chemo-dynamical correlations – e.g., correlations between the full velocity dispersion tensors and surface metal abundances – as well as more rigorous analyses of the  $\langle V_{\phi} \rangle_{\text{med}}\text{-}[\text{Fe}/\text{H}]$  relation.

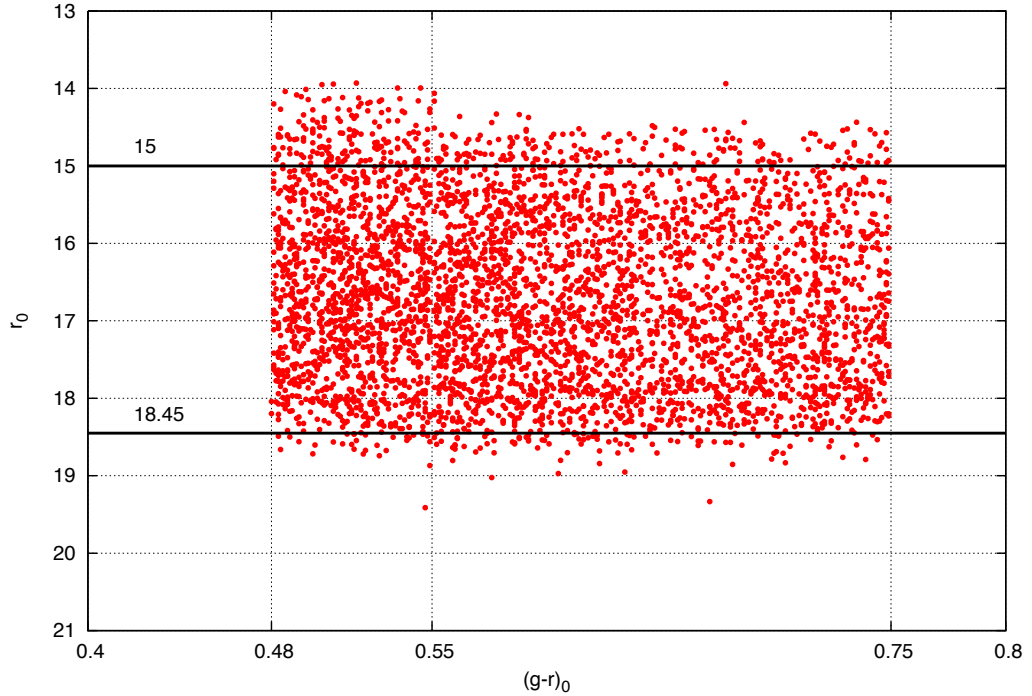


Figure 2.1: The distribution of sample stars with  $S/N > 20$ ,  $0.48 < (g - r) < 0.75$ , and without any cut on heliocentric distance  $d$  or metallicity  $[Fe/H]$ . Also shown are the adopted completeness limit of  $r_0 = 15$  and  $18.45$ , following the most conservative magnitude limits proposed by [Schlesinger et al. \[2012\]](#). For clarity, randomly selected 4 % and 20 % of the total sample is shown at  $0.48 < (g - r) < 0.55$  and  $0.55 < (g - r) < 0.75$ , respectively, so that the density of the sample stars in this diagram is nearly homogenous at  $15 < r_0 < 18.45$ .



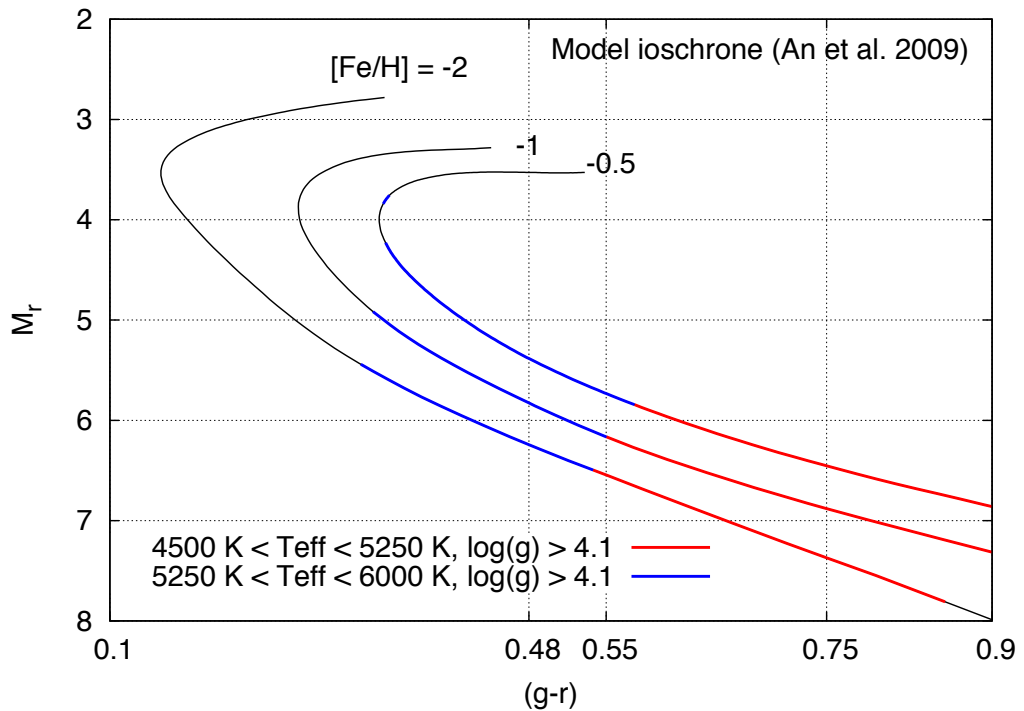


Figure 2.2: Published 10 Gyr isochrone models of [An et al. \[2009\]](#) in the SDSS  $(g-r)$  color versus SDSS  $M_r$  absolute magnitude space with different metallicity  $[\text{Fe}/\text{H}]$ . We see that the absolute magnitude  $M_r$  for main-sequence stars ( $\log g > 4.1$ ) with  $0.48 < (g-r) < 0.75$  lies at  $5.38 < M_r < 7.37$ . The bright limit of  $M_r = 5.38$  combined with the bright limit of our sample,  $r_0 = 15$ , corresponds to  $d = 0.84$  kpc, while the faint limit of  $M_r = 7.37$  combined with the faint limit of  $r_0 = 18.45$  corresponds to  $d = 1.64$  kpc.

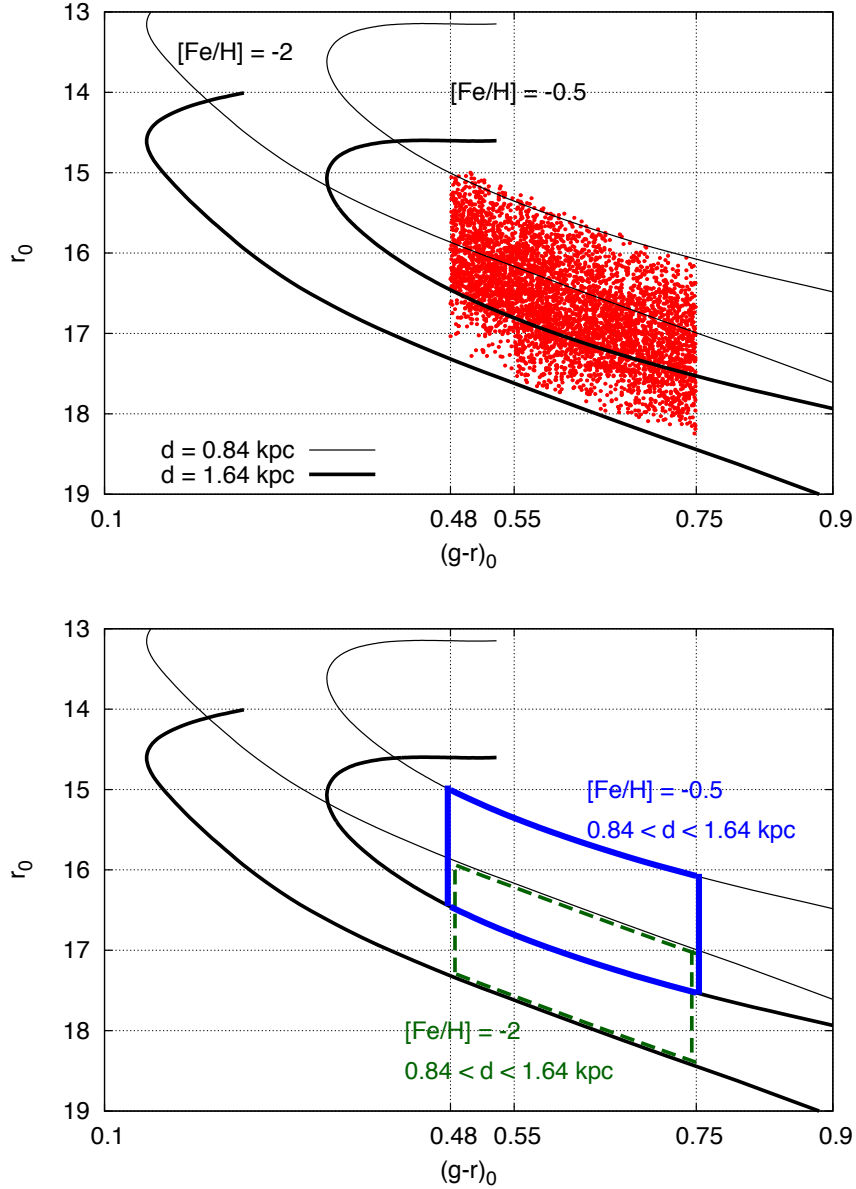


Figure 2.3: (Top) Red points represent the distribution of our sample stars in the  $(g-r)_0 - r_0$  space (red points). The black, thin lines represent the 10 Gyr isochrones [An et al., 2009] with  $[\text{Fe}/\text{H}] = -0.5$  (to the right) and  $[\text{Fe}/\text{H}] = -2.0$  (to the left), assuming a heliocentric distance  $d = 0.84$  kpc. The black, thick lines represent the same isochrones, but assuming  $d = 1.64$  kpc instead. (Bottom) The areas in which stars with  $0.84 \text{ kpc} < d < 1.64 \text{ kpc}$  are expected to be distributed. The expected areas for stars with  $[\text{Fe}/\text{H}] = -0.5$  and  $-2.0$  are shown by the blue (upper) and green (lower) areas, respectively. For a given  $[\text{Fe}/\text{H}]$  between  $-2.0$  and  $-0.5$ , the corresponding area lies somewhere in between. Note that some fraction of our sample stars are distributed *above* the blue area (see top panel). This is due to the slight ( $\lesssim 5\%$ ) difference between the adopted SSPP distance and the distance expected from An et al. [2009] isochrone.

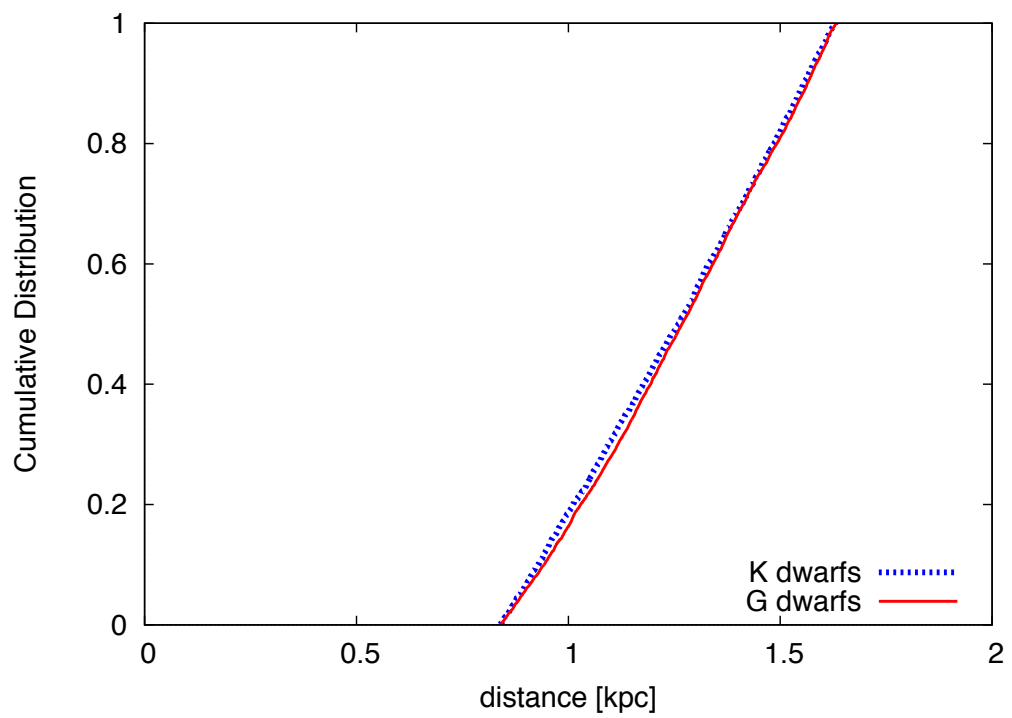


Figure 2.4: Cumulative distributions of the heliocentric distance for our G- and K-dwarf samples. The two distributions are very similar to each other, supporting the result of Kolmogorov-Smirnov test.

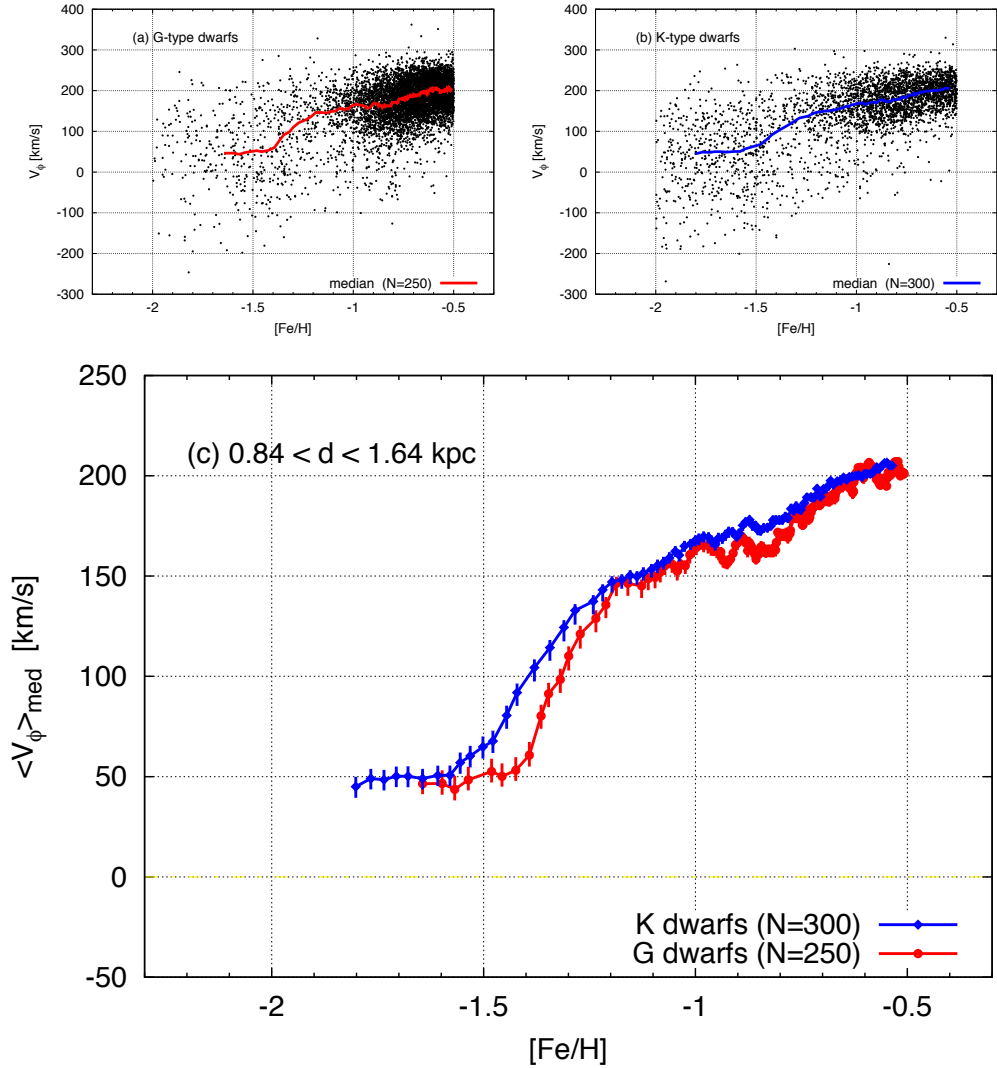


Figure 2.5: Distribution of our sample stars in the  $V_\phi$ -[Fe/H] space and the median value of  $V_\phi$  for binned samples in the metallicity range  $-2.0 \leq [\text{Fe}/\text{H}] \leq -0.5$ . (a) Results for G-type dwarfs. We bin  $N = 250$  stars sorted in [Fe/H], moving through the sample in steps of  $N/10$  stars, and show the median value of  $V_\phi$  (or  $\langle V_\phi \rangle_{\text{med}}$ ) at the median value of [Fe/H]. (b) Results for K-type dwarfs. The analysis is the same as in (a), but adopting  $N = 300$  instead. (c) Comparison of the median values  $\langle V_\phi \rangle_{\text{med}}$  for G- and K-type dwarfs. Error bars in  $\langle V_\phi \rangle_{\text{med}}$  are estimated by assuming a Gaussian-like distribution of  $V_\phi$ .

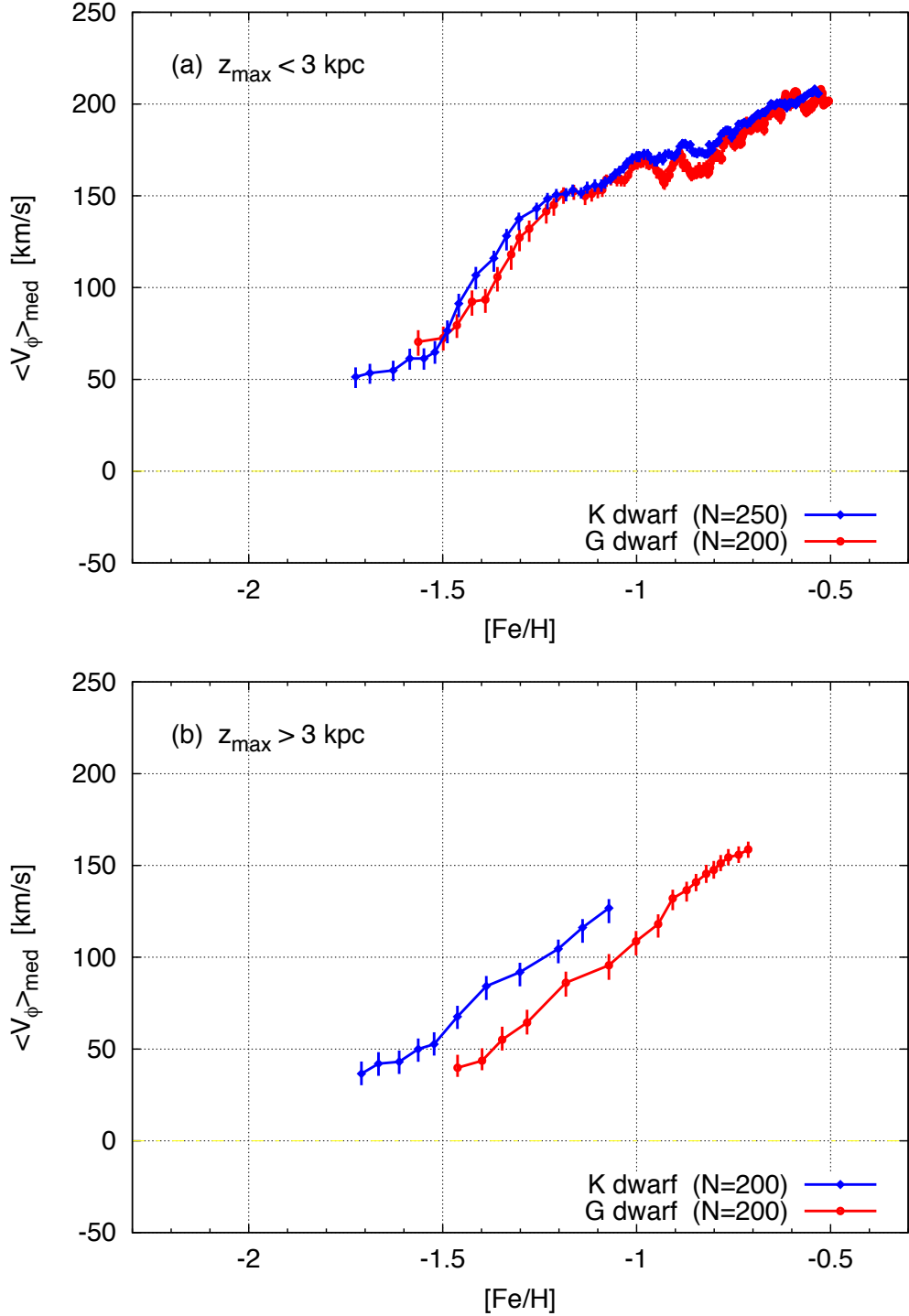


Figure 2.6: Median value of  $V_\phi$  as a function of  $[\text{Fe}/\text{H}]$  for G-dwarf (red) and K-dwarf (blue) sub-samples having different ranges of  $z_{\text{max}}$  (maximum orbital excursion perpendicular to the Galactic disk plane). The results for sample stars with  $z_{\text{max}} < 3$  kpc and  $z_{\text{max}} > 3$  kpc are shown in panels (a) and (b), respectively. The binning procedure is the same as in Figure 2.5, and the adopted value of bin size  $N$  for each subsample is shown on the panel.

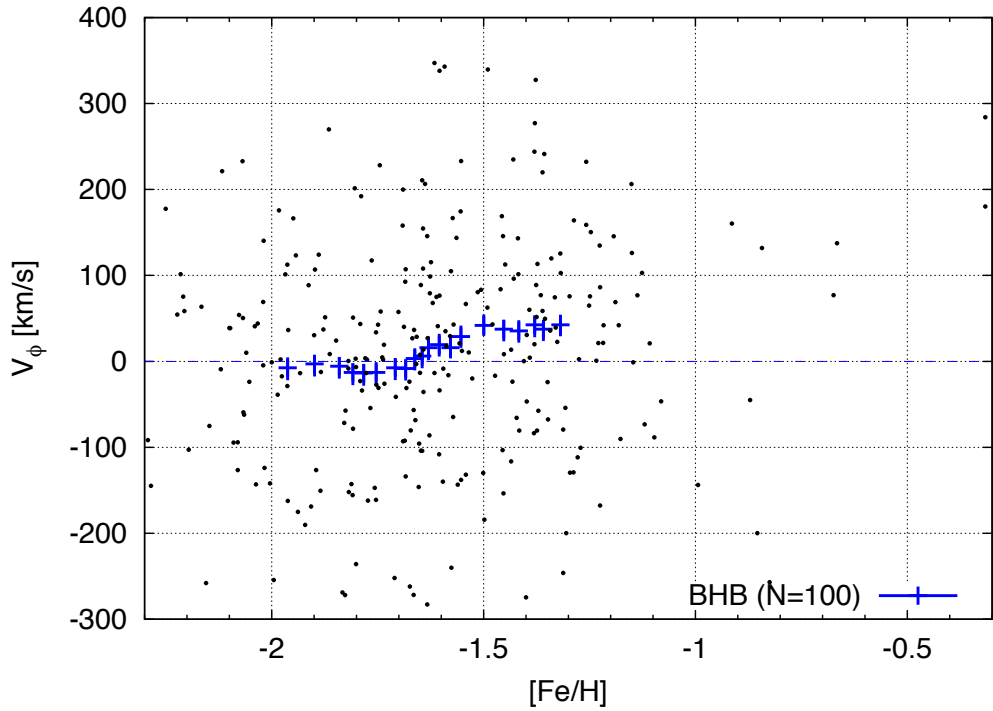
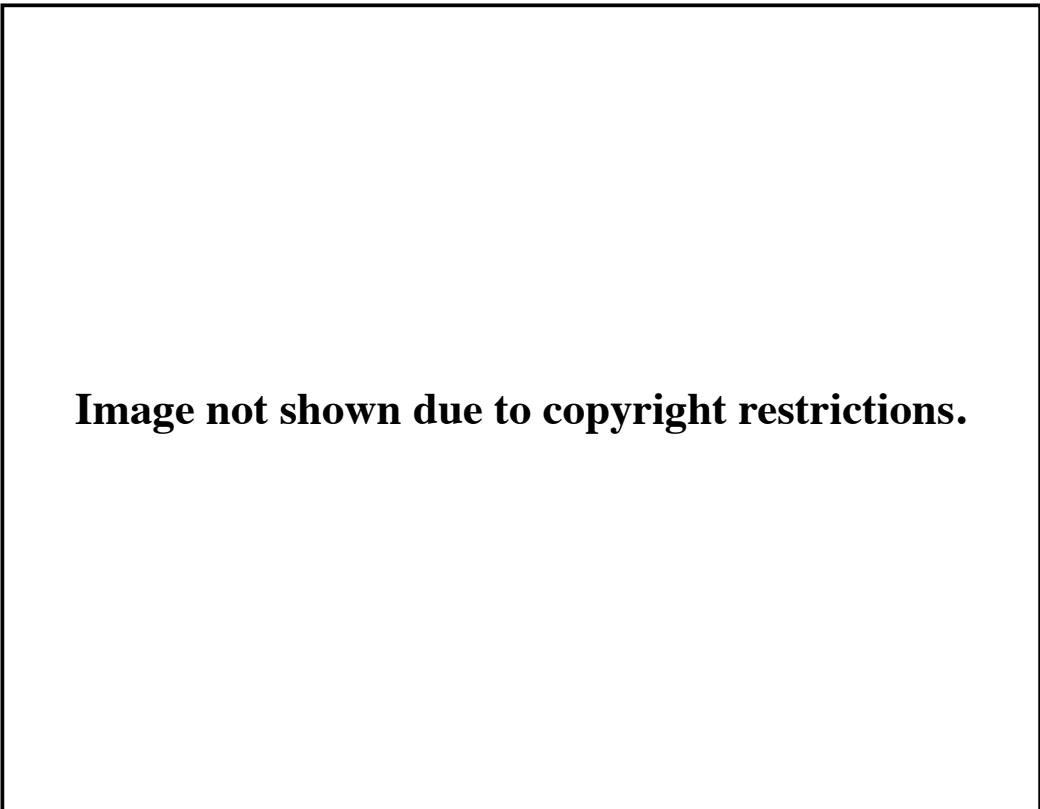


Figure 2.7: The distribution in the  $V_\phi$ - $[\text{Fe}/\text{H}]$  space of BHB stars with  $5 \text{ kpc} < R < 20 \text{ kpc}$  and  $2 \text{ kpc} < |z| < 5 \text{ kpc}$ . Also shown is the median value,  $\langle V_\phi \rangle_{\text{med}}$ , for the binned sample. The binning procedure is the same analysis as in Figure 2.5, but by binning  $N = 100$  stars and moving through each sample in steps of  $N/10$  stars. The associated error bar on  $\langle V_\phi \rangle_{\text{med}}$  represents the uncertainty estimated by assuming a Gaussian-like distribution of  $V_\phi$ .

---



**Image not shown due to copyright restrictions.**

Figure 2.8: Median photometric metallicity measured in four CFHTLS wide survey beams as a function Galactocentric distance  $R_{gal}$ . The W3 and W4 beams are not affected by significant contamination from known substructure. Within  $R_{gal} \sim 30$  kpc, the median metallicity is independent of distance and ranges from  $-1.4 < [\text{Fe}/\text{H}] < -1.6$ . The change in metallicity at  $R_{gal} \sim 15$  kpc, reported by [Carollo et al. \[2007\]](#) is not evident. Taken from Figure 12 of [Sesar et al. \[2011\]](#).

---

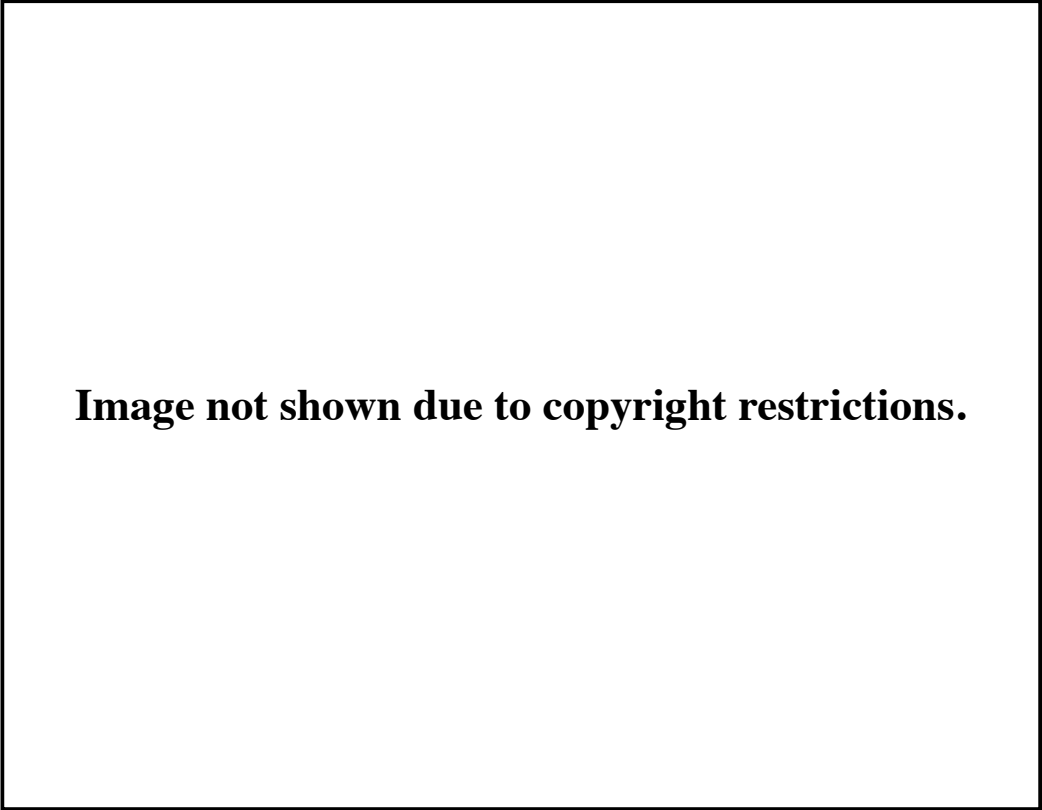


**Image not shown due to copyright restrictions.**

Figure 2.9: As-observed metallicity distribution function (MDF) for the Xue et al. (2011) BHB stars for various cuts on the distance from the Galactic center,  $r$ . Stars with  $|z| < 4$  kpc have been removed from the sample. *Right Panels:* Similar, but for the case where BHB stars from plug-plates in the direction of the two most prominent wraps of the Sagittarius tidal stream have been removed. In both cases, the nature of the MDF appears to shift from the top panels, which exhibit distributions that we associate with the inner-halo population, over to distributions in the lower three panels that are dominated by the outer-halo population. The dashed blue line provides a reference at  $[\text{Fe}/\text{H}] = -2.0$ . Taken from Figure 15 of *Beers et al. [2012]*.



---

**Image not shown due to copyright restrictions.**

Figure 2.10: Smoothed metallicity distribution functions (MDFs) of near-turnoff stars (solid line) and RGB stars (dashed line; taken from [Norris et al. 1996](#)) in  $\omega$  Centauri. The results for MSTO stars and subgiant branch stars are shown with solid line on panels (a) and (b), respectively. Note that the peak metallicity of RGB stars is more metal-poor than those of near-turnoff stars (MSTO or subgiant branch stars), although the offset (0.01-0.05 dex) is smaller than the uncertainty in  $[\text{Fe}/\text{H}]$  (0.15-0.20 dex) of sample stars. Taken from Figure 2 of [Stanford et al. \[2007\]](#).

## Chapter 3

# Negative Beta Problem

*Based on [Hattori et al. 2013](#), *The Astrophysical Journal Letters*, **763**, L17*

### 3.1 Abstract of this chapter

The orbital motions of halo stars in the Milky Way reflect the orbital motions of the progenitor systems in which they formed, making it possible to trace the mass-assembly history of the Galaxy. Direct measurement of three-dimensional velocities, based on accurate proper motions and line-of-sight velocities, has revealed that the majority of halo stars in the inner-halo region move on eccentric orbits. However, our understanding of the motions of distant, in-situ halo-star samples is still limited, due to the lack of accurate proper motions for these stars. Here we explore a model-independent analysis of the line-of-sight velocities and spatial distribution of a recent sample of 1865 carefully selected halo blue horizontal-branch (BHB) stars within 30 kpc of the Galactic center. We find that the mean rotational velocity of the very metal-poor ( $[\text{Fe}/\text{H}] < -2.0$ ) BHB stars significantly lags behind that of the relatively more metal-rich ( $[\text{Fe}/\text{H}] > -2.0$ ) BHB stars. We also find that the relatively more metal-rich BHB stars are dominated by stars with eccentric orbits, as previously observed for other stellar samples in the inner-halo region. By contrast, the very metal-poor BHB stars are dominated by stars on rounder, lower-eccentricity orbits. Our results indicate that the motion of the progenitor systems of the Galaxy that contributed to the stellar populations found within 30 kpc correlates directly with their metal abundance, which may be related to their physical properties such as gas fractions. These results are consistent with the existence of an inner/outer halo structure for the halo system, as advocated by [Carollo et al. \[2010\]](#).

---

## 3.2 Introduction

The luminosity of the Milky Way is dominated by its disk, where the great majority of stars ( $> 90\%$ ) are found. By comparison, out of  $\sim 10^{11}$  stars in the Milky Way, the stellar halo comprises only a tiny fraction ( $\sim 1\%$ ), but this component is a precious source of information on the formation history of the Galaxy. First, halo stars are very old ( $\sim 10 - 13$  Gyrs), and their chemical compositions provide information on the ancient environments in which these stars formed. Typically, the metal abundances of halo stars are less than 1/10th of the Solar value [Carollo et al., 2007, 2010; Chiba and Beers, 2000], which immediately suggests that the metal enrichment due to supernova explosions in the Universe had not progressed very far when halo stars were formed. Secondly, the stellar halo is a collisionless system, hence two-body relaxation is expected to be unable to fully erase the initial orbital properties of halo stars. It follows that the present motions of halo stars reflects their motions in the early Universe, which can be used to explore the kinematics of their progenitor systems, such as the gas clouds or dwarf galaxies in which these halo stars formed.

To date, detailed analyses of the chemical and dynamical properties of halo stars has been confined to stars up to  $\sim 10 - 15$  kpc from the Sun (centered at the Galactocentric distance of the Sun,  $\sim 8.5$  kpc), although the spatial distribution of the stellar halo extends to  $\sim 100$  kpc or more. This is mainly because we do not possess sufficiently accurate measurements of proper motions for more distant halo stars. In order to avoid this limitation, many authors have studied the line-of-sight velocities and spatial distribution of halo stars, making use of various kinematic models – such as distribution function models of the stellar halo, or gravitational potential models of the Milky Way. However, the conclusions of previous studies on the orbital distribution of halo stars well outside the local region are divergent. Some suggest tangentially-anisotropic orbital distributions [Kafle et al., 2012; Sommer-Larsen et al., 1997], others suggest radially-anisotropic distributions [Deason et al., 2012], and still others suggest nearly isotropic distributions [Sirko et al., 2004; Thom et al., 2005]. This might imply that the stellar halo is not a simple entity which can be described by a single distribution function model. Indeed, based on observations of relative nearby ( $d \leq 4$  kpc) halo stars, [Carollo et al., 2007, 2010] suggest that a dual-halo model is more appropriate, in which the stellar halo consists of a relatively metal-rich inner-halo component with a net zero to slightly prograde rotation, and a very metal-poor outer-halo component with a net retrograde rotation. Recent observations of retrograde outer-halo RR Lyrae stars by Kinman et al. [2012], and a model-fitting analysis for distant halo stars by Deason et al.

---

[2011] supports this idea, as do recent numerical simulations of the formation of Milky Way-like galaxies (e.g., [McCarthy et al. 2012](#)). Here we introduce a new analysis of the halo system, which requires only a minimum of assumptions, and does not require any kinematic models.

This chapter is outlined as follows. In Section 3.3 we describe our sample selection and expected errors in distance, line-of-sight velocities, and metallicities. Section 3.4 describes our analysis approach. In Section 3.5, we examine the application of this technique to our sample of halo BHB stars, segregated on metallicity. Section 3.6 presents a brief discussion and conclusions.

### 3.3 Sample selection

Our sample comprises 1865 blue horizontal-branch (BHB) stars from Data Release 8 of the Sloan Digital Sky Survey [[Aihara et al., 2011](#)], with Galactocentric distances in the range  $6 < r/\text{kpc} < 30$ , as originally selected and carefully validated by [Xue et al. \[2011\]](#). This sample is free from significant contamination by the Sagittarius stream and the thick disk, as we apply a spatial masking scheme in their selection. Distances from the Sun are accurate to  $\sim 5 - 10\%$ , and the line-of-sight velocity errors are  $5 - 20 \text{ km s}^{-1}$  (see [Xue et al. 2011](#)). Stellar metallicities,  $[\text{Fe}/\text{H}]$ , for this sample are also available. Following [Xue et al. \[2011\]](#), we use the metallicities obtained by the [Wilhelm et al.](#) methodology in the SEGUE Stellar Parameter Pipeline (SSPP; see [Lee et al. 2008a](#) for details), which are likely to be the most reliable for stars with effective temperatures of BHB stars (on the order of 0.3 dex). We then divide this sample on metallicity – 994 of our stars are relatively metal-rich ( $[\text{Fe}/\text{H}] > -2.0$ ), while 871 stars are very metal-poor ( $[\text{Fe}/\text{H}] < -2.0$ ).<sup>1</sup>

### 3.4 Analysis method

#### 3.4.1 Derivation of rotational velocity

Let us denote by  $S$  an imaginary observer located at the Sun who is at rest with respect to the Galactic rest frame, and by  $O$  an observer located at the Sun who moves with the Sun. Here, we assume that the velocity of  $O$  with respect to  $S$ ,  $\mathbf{v}_{\odot}$ , and the three-dimensional (3-D) position of the Sun with respect to the Galactic center are known.

---

<sup>1</sup> Our boundary metallicity ( $[\text{Fe}/\text{H}] = -2.0$ ) lies between the peak metallicities of the inner-halo ( $[\text{Fe}/\text{H}]_{\text{peak}} \simeq -1.6$ ) and outer-halo ( $[\text{Fe}/\text{H}]_{\text{peak}} \simeq -2.2$ ) components [[Carollo et al., 2007](#)].

---

Now, suppose that the  $k$ -th star ( $k = 1, \dots, n$ ) is observed in the direction of  $\mathbf{x}_k^{los}$  by  $S$  and  $O$ . Then, the line-of-sight velocity with respect to  $S$  can be expressed as:

$$v_k^{los} \equiv \mathbf{v}_k \cdot \mathbf{x}_k^{los}, \quad (3.1)$$

where  $\mathbf{v}_k$  is the velocity of this star with respect to  $S$ . Since the line-of-sight velocity of this star with respect to  $O$  is:

$$v_k^{los, hel} \equiv (\mathbf{v}_k - \mathbf{v}_\odot) \cdot \mathbf{x}_k^{los} = v_k^{los} - \mathbf{v}_\odot \cdot \mathbf{x}_k^{los}, \quad (3.2)$$

we can calculate  $v_k^{los}$  from  $(\mathbf{v}_\odot, v_k^{los, hel}, \mathbf{x}_k^{los})$ .

On the other hand, if we decompose  $\mathbf{v}_k$  as:

$$\mathbf{v}_k = v_{r,k} \mathbf{e}_{r,k} + v_{\theta,k} \mathbf{e}_{\theta,k} + v_{\phi,k} \mathbf{e}_{\phi,k}, \quad (3.3)$$

we obtain

$$v_k^{los} = v_{r,k} Q_{r,k} + v_{\theta,k} Q_{\theta,k} + v_{\phi,k} Q_{\phi,k}, \quad (3.4)$$

where

$$Q_{i,k} \equiv \mathbf{x}_k^{los} \cdot \mathbf{e}_{i,k} \quad (i = r, \theta, \phi). \quad (3.5)$$

Here,  $v_{i,k}$  and  $\mathbf{e}_{i,k}$  ( $i = r, \theta, \phi$ ) are the  $i$ -th velocity component of the  $k$ -th star, and the basis unit vectors of the spherical coordinate system at the position of the  $k$ -th star, respectively.

Given the assumptions:

- (A1) There is no correlation between the velocity and position of a star
- (A2) The distributions of  $v_r$ ,  $v_\theta$ , and  $v_\phi$  are symmetric around  $v_r = 0$ ,  $v_\theta = 0$ , and  $v_\phi = V_{\text{rot}}$ , respectively

then the data points  $\{(Q_{\phi,k}, v_k^{los})\}$  are likely to be distributed around a linear function of form:

$$v^{los} = V_{\text{rot}} Q_\phi \quad (3.6)$$

Thus, by performing a linear fit to the data in the  $Q_\phi - v^{los}$  plane, we can obtain  $\hat{V}_{\text{rot}}$  – by which we denote the estimated value of  $V_{\text{rot}}$  – by measuring the slope of the best-fit linear function. This approach is similar to that of [Frenk and White \[1980\]](#).

---

### 3.4.2 Derivation of 3-D velocity dispersion

In estimating the velocity dispersion, we use a modified version of the approach used by Woolley [1978].

In addition to (A1) and (A2) above, let us further assume that the velocity distribution of the sample stars satisfies the following:

- (A3) The velocity ellipsoid is aligned with a spherical coordinate system
- (A4) The dispersions in the distributions of  $v_r$ ,  $v_\theta$ , and  $v_\phi$  around their centers are  $\sigma_r$ ,  $\sigma_\theta$ , and  $\sigma_\phi$ , respectively

Then, it can be shown, for  $i = r, \theta, \phi$  (see Morrison et al. 1990 for the case of  $i = \phi$ ), that

$$\begin{aligned} \mathbb{E} \left[ \text{var} \left[ v^{los} Q_i \right] \right] &= \sigma_r^2 \frac{1}{n} \sum_{k=1}^n Q_{i,k}^2 Q_{r,k}^2 + \sigma_\theta^2 \frac{1}{n} \sum_{k=1}^n Q_{i,k}^2 Q_{\theta,k}^2 + \sigma_\phi^2 \frac{1}{n} \sum_{k=1}^n Q_{i,k}^2 Q_{\phi,k}^2 \\ &\quad + \frac{V_{\text{rot}}^2}{n-1} \left\{ \sum_{k=1}^n Q_{i,k}^2 Q_{\phi,k}^2 - \frac{1}{n} \left( \sum_{k=1}^n Q_{i,k} Q_{\phi,k} \right)^2 \right\}, \quad (3.7) \end{aligned}$$

where we denote the expectation and variance of  $X$  by  $\mathbb{E}[X]$  and  $\text{var}[X]$ , respectively.

Thus, by substituting the observed ( $\text{var} [v^{los} Q_i]$ ) for  $\mathbb{E} [\text{var} [v^{los} Q_i]]$ , and the already estimated  $\hat{V}_{\text{rot}}$  for  $V_{\text{rot}}$ , we obtain:

$$\begin{aligned} \begin{bmatrix} \text{var} [v^{los} Q_r] \\ \text{var} [v^{los} Q_\theta] \\ \text{var} [v^{los} Q_\phi] \end{bmatrix} &- \frac{\hat{V}_{\text{rot}}^2}{n-1} \begin{bmatrix} \sum_k Q_{r,k}^2 Q_{\phi,k}^2 - \frac{1}{n} (\sum_k Q_{r,k} Q_{\phi,k})^2 \\ \sum_k Q_{\theta,k}^2 Q_{\phi,k}^2 - \frac{1}{n} (\sum_k Q_{\theta,k} Q_{\phi,k})^2 \\ \sum_k Q_{\phi,k}^4 - \frac{1}{n} (\sum_k Q_{\phi,k}^2)^2 \end{bmatrix} \\ &= \frac{1}{n} \begin{bmatrix} \sum_k Q_{r,k}^4 & \sum_k Q_{r,k}^2 Q_{\theta,k}^2 & \sum_k Q_{r,k}^2 Q_{\phi,k}^2 \\ \sum_k Q_{r,k}^2 Q_{\theta,k}^2 & \sum_k Q_{\theta,k}^4 & \sum_k Q_{\theta,k}^2 Q_{\phi,k}^2 \\ \sum_k Q_{r,k}^2 Q_{\phi,k}^2 & \sum_k Q_{\theta,k}^2 Q_{\phi,k}^2 & \sum_k Q_{\phi,k}^4 \end{bmatrix} \begin{bmatrix} \hat{\sigma}_r^2 \\ \hat{\sigma}_\theta^2 \\ \hat{\sigma}_\phi^2 \end{bmatrix}. \quad (3.8) \end{aligned}$$

The solutions  $(\hat{\sigma}_r^2, \hat{\sigma}_\theta^2, \hat{\sigma}_\phi^2)$  for this equation are the unbiased estimates for  $(\sigma_r^2, \sigma_\theta^2, \sigma_\phi^2)$ .

### 3.4.3 Testing the reliability of our method

In order to estimate the error that accompanies our estimate of the three-dimensional velocity dispersion, we construct mock catalogs, and perform simulated observation

---

of mock stars drawn from these catalogs. In this Monte Carlo simulation, each mock catalog is designed so that the distribution of  $r$  for the relatively metal-rich (or very metal-poor) mock stars resemble those of the observed relatively metal-rich (or very metal-poor) BHB stars, and that the velocity of the mock stars obey a given anisotropic Gaussian velocity distribution (with or without net rotation). We vary the velocity anisotropy parameter,  $\beta = 1 - (\sigma_\theta^2 + \sigma_\phi^2)/(2\sigma_r^2)$ , and produce 1000 mock catalogs for each case. We find that the derived  $\sigma_\theta$  and  $\sigma_\phi$  is only reliable for  $r < 16.3$  kpc and  $r < 18$  kpc for the relatively metal-rich and very metal-poor sample, respectively, while estimates of  $\sigma_r$  are reliable at any  $r$ .

### 3.5 Application of our methodology – derivation of rotation velocities, velocity dispersions, and velocity anisotropy parameters

Throughout this chapter, we assume that the Local Standard of Rest (LSR) is on a circular orbit with a rotation speed of  $220 \text{ km s}^{-1}$  [Kerr and Lynden-Bell, 1986]. It is worth noting that our assumed values for the Galactocentric distance of the Sun,  $R_\odot = 8.5$  kpc, and the circular velocity of the LSR are both consistent with two recent independent determinations of these quantities by Ghez et al. [2008] and Koposov et al. [2010]. Bovy et al. [2012] have recently determined, on the basis of accurate line-of-sight velocities for stars in the APOGEE sub-survey of SDSS-III, that the circular velocity of the LSR is close to  $220 \text{ km s}^{-1}$ . We also assume that the peculiar motion of the Sun with respect to the LSR is  $(U_\odot, V_\odot, W_\odot) = (10.0, 5.3, 7.2) \text{ km s}^{-1}$  [Dehnen and Binney, 1998].

Figure 3.1 shows the determination of mean rotational velocity,  $V_{\text{rot}}$ , for the relatively metal-rich (red) and very metal-poor (blue) BHB samples, as a function of Galactocentric distance,  $r$ . The shaded regions indicate the uncertainties in each result, estimated from a bootstrap approach (sampling with replacement). Inspection of this figure suggests that  $V_{\text{rot}}$  at  $13 - 23$  kpc is a slightly decreasing function of  $r$  for the relatively metal-rich sample, while that for the very metal-poor sample is more or less flat. The relatively more metal-rich sample is in modest prograde rotation, with  $V_{\text{rot}} \sim 0 - 20 \text{ km s}^{-1}$ , while the very metal-poor sample is in retrograde motion, with  $V_{\text{rot}} \sim -20$  to  $-50 \text{ km s}^{-1}$ , and lags that of the relatively metal-rich sample by  $\sim 20 - 50 \text{ km s}^{-1}$ , similar to previous observations of stars in a much more local sample by Carollo et al. [2007, 2010], the outer-halo analysis based on distribution-function

---

fitting [Deason et al., 2011], and some recently simulated stellar haloes (e.g., Tissera et al. 2012). It is also intriguing to see that the rotational shear between two samples seems to shrink at  $r \sim 20$  kpc. We confirm that varying the LSR velocity only changes the absolute value of  $V_{\text{rot}}$ , and that the very metal-poor sample *always* lags behind the relatively metal-rich sample, independent of the assumed LSR velocity.

Figure 3.2 shows determinations of the radial velocity dispersion,  $\sigma_r$ , and the two components of the tangential velocity dispersion,  $\sigma_\theta$  and  $\sigma_\phi$ , for the relatively metal-rich and very metal-poor samples, as a function of  $r$ . As seen in the figure,  $\sigma_r$  is about  $100 \text{ km s}^{-1}$ , and exhibits a declining behavior over  $12.5 < r < 20$  kpc for both samples, supporting most previous studies (e.g., Brown et al. 2010; Xue et al. 2008). In addition, this figure suggests that  $\sigma_\theta \simeq \sigma_\phi$  holds for the very metal-poor sample. Noting that the gravitational potential is nearly spherical well above the disk plane, and that  $V_{\text{rot}}$  of the very metal-poor stars is small compared with its velocity dispersion, it follows that they obey a distribution function that depends mainly on the orbital energy and angular momentum [Binney and Tremaine, 2008], and thus their spatial distribution is nearly spherical. The different behavior of the 3-D velocity dispersions for the two samples implies that both the functional form of the distribution function and spatial distribution for these samples are different.

Figure 3.3 shows the velocity anisotropy parameter,  $\beta = 1 - (\sigma_\theta^2 + \sigma_\phi^2)/(2\sigma_r^2)$ . This parameter quantifies the relative dominance of the radial and tangential velocity dispersions, and provides a simple diagnostic of the orbital properties of our sample stars. If  $\beta$  takes on values  $\beta < 0$ , we can infer that the halo stars are dominated by round orbits, while if  $0 < \beta < 1$ , we can infer that the halo stars are dominated by radial orbits. When  $\beta$  is (nearly) zero, we can infer that the velocity distribution is (nearly) isotropic. Figure 3.3 suggests that relatively metal-rich BHB stars are dominated by radial orbits at  $12 < r/\text{kpc} < 15$  ( $\beta = 0.3 \pm 0.3$ ), while the very metal-poor BHB stars are dominated by circular orbits over  $13 < r/\text{kpc} < 18$  ( $\beta = -0.9 \pm 0.7$ ). A similar trend in the eccentricity distribution is also confirmed in the more local sample of halo stars reported by Carollo et al. [2010], in which very metal-poor halo stars possess a higher fraction of low-eccentricity orbits (see Figure 1.12).

### 3.6 Discussion and conclusions

The observed systematic differences in the orbital motions of the relatively metal-rich and very metal-poor BHB stars suggest that the orbital motion of the progenitor systems of the stellar halo depends on their metal abundances. Noting that dwarf



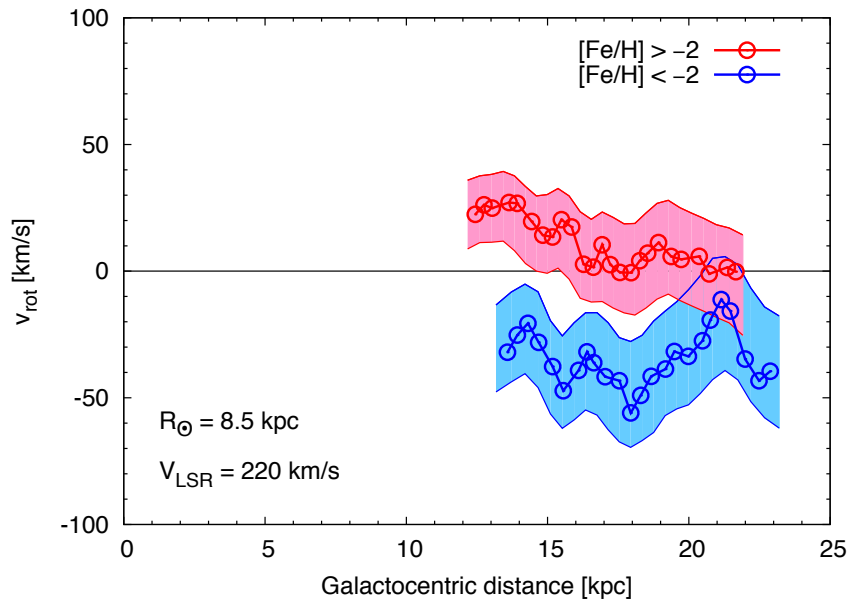


Figure 3.1: The mean rotational velocity,  $V_{\text{rot}}$ , for the relatively metal-rich BHB sample (red) and very metal-poor BHB samples (blue), as a function of Galactocentric distance  $r$ . Open circles show the result for our BHB samples. In this plot, we bin the relatively metal-rich (and very metal-poor) BHB stars in  $r$  by binning 500 stars (400 stars), sorted in  $r$ , and moving through the sample in steps of 20 stars. Each bin contains stars with a typical standard deviation in  $r$  of  $\sim 3$  kpc, and the resultant  $V_{\text{rot}}$  is presented at the median value of  $r$ . The associated shaded regions represent the uncertainties of our results, estimated from the bootstrap method, and denote the range covered by the 16% and 84% percentiles.

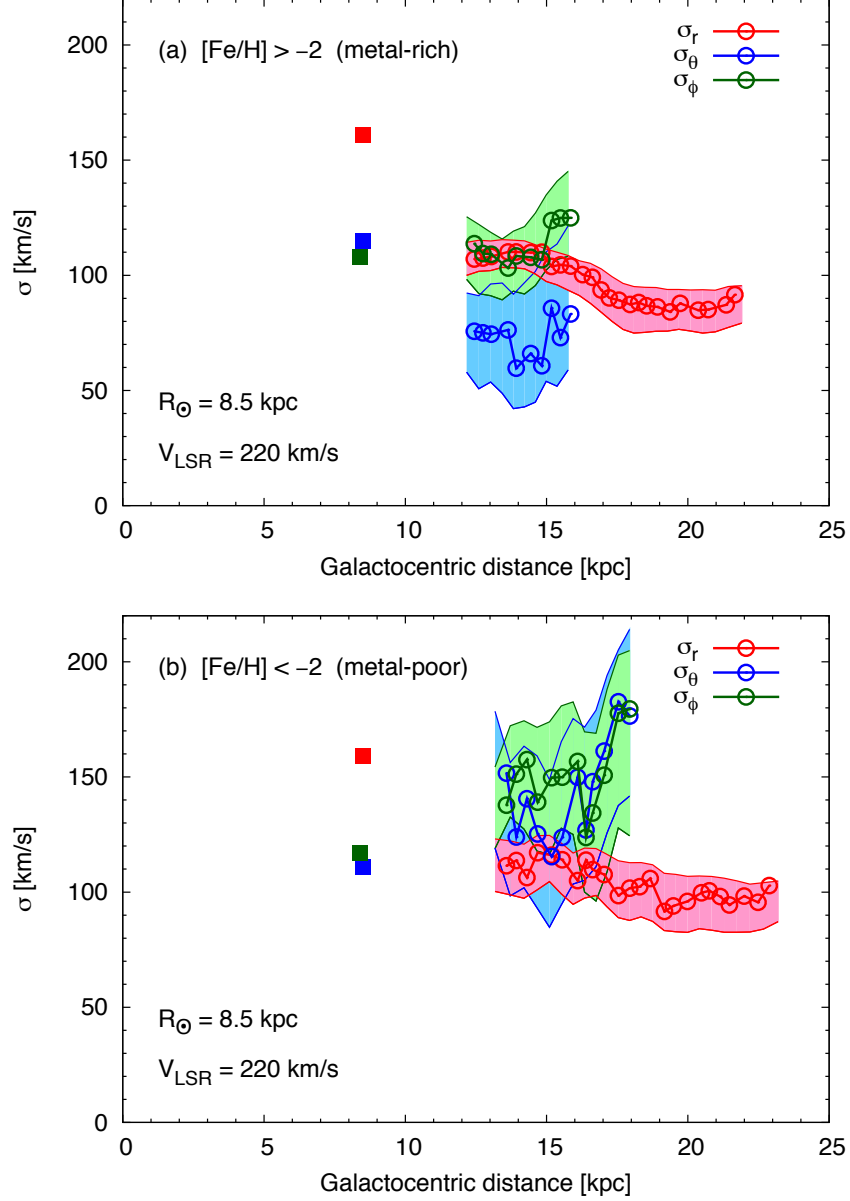


Figure 3.2: Three-dimensional velocity dispersions  $\sigma_r$  (red),  $\sigma_\theta$  (blue), and  $\sigma_\phi$  (green), as a function of Galactocentric distance. Open circles show the result for our BHB samples. The same binning procedure as in Figure 3.1 is adopted. For the tangential velocity dispersions, some of the bins with large Galactocentric distance are excluded, because of a large systematic error indicated from Monte Carlo simulations. The associated shaded regions represent the uncertainties of our results, estimated from the bootstrap method. Results for the relatively metal-rich BHB sample and very metal-poor BHB sample are shown in panel (a) and (b), respectively. Filled squares at  $r = 8.5$  kpc in panel (a) and (b) represent the Solar-neighborhood observations of halo stars with  $-2 < [\text{Fe}/\text{H}] < -1.6$  and  $[\text{Fe}/\text{H}] < -2$ , respectively, taken from Chiba and Yoshii [1998].

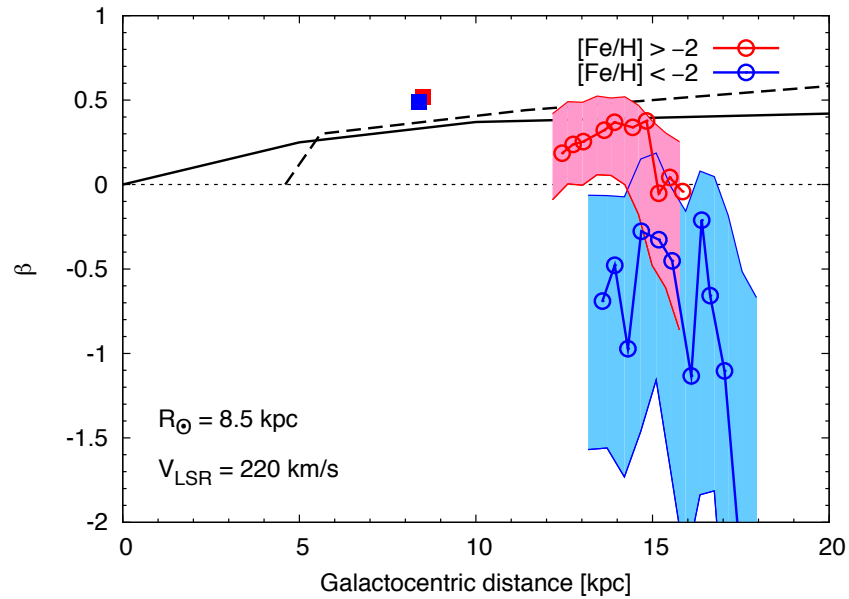


Figure 3.3: The velocity anisotropy parameter,  $\beta = 1 - (\sigma_\theta^2 + \sigma_\phi^2)/(2\sigma_r^2)$ , for the relatively metal-rich (red) and very metal-poor (blue) BHB samples, as a function of Galactocentric distance. Open circles show the result for our BHB samples, and correspond to those bins presented in Figure 3.2. The associated shaded regions represent the uncertainties of our results, estimated from the bootstrap method. Filled squares at  $r = 8.5$  kpc represent the Solar-neighborhood observations of halo stars with  $-2 < [\text{Fe}/\text{H}] < -1.6$  (red) and  $[\text{Fe}/\text{H}] < -2$  (blue), taken from Chiba and Yoshii [1998]. The black solid and black dashed line represent the  $\beta$  profiles of simulated stellar haloes from Diemand et al. [2005] and Sales et al. [2007], respectively. The dotted horizontal line at  $\beta = 0$  is added to guide the eye.

---

galaxies with smaller total stellar masses tend to have lower metal abundances (Kirby et al. 2008, and references therein), which can be understood as a result of a smaller rate of metal-enrichment events such as supernova explosions, our findings suggest that low-gas-fraction (‘star-rich’) systems tend to move in radial orbits, while high-gas-fraction (‘gas-rich’) systems tend to move in round orbits when they convert their gas to stars.

In the hierarchical galaxy formation scenario, the Milky Way (and other large systems) attains its mass as a result of the mergers of infalling smaller systems [Blumenthal et al., 1984; White and Rees, 1978]. Due to the deep gravitational potential well of the Milky Way, these infalling systems tend to have radial orbits [Sales et al., 2007]. At this stage, we expect that the orbital properties of infalling systems is independent of whether they are star-rich or gas-rich. However, the situation may be different when such radially infalling systems pass near the Galactic center. In such a region, star-rich systems (e.g., massive dwarf galaxies with low gas fractions) are expected to be disrupted by tidal interactions, which give rise to field halo stars with radial orbits [Sales et al., 2007]. On the other hand, gas-rich systems are expected to interact with other gas-rich systems, and lose some orbital energy via dissipational processes [Sharma et al., 2012; Sommer-Larsen and Christensen, 1989; Theis, 1996]. If the angular momentum of such a gas-rich system is approximately conserved, the orbit is circularized, and the pericentric distance (distance of closest approach to the Galactic center) increases. Once its pericentric distance become sufficiently large to avoid the central region of the Milky Way, further orbital change becomes less likely, since encounters with other gas-rich systems becomes less probable. Therefore, gas-rich systems tend to move in round orbits. When the Galactic disk forms, some gas-rich systems with similar orbital motions to disk gas may be absorbed into the disk, due to their small relative velocities, while others remain moving on orbits across the halo, and eventually form field halo stars with round orbits. If the total orbital angular momentum of gaseous systems is initially near zero, these halo stars would exhibit a net retrograde rotation with respect to disk stars. Some gas-rich systems in the Milky Way that have not yet formed many stars might be associated with the observed high-velocity clouds [Blitz et al., 1999; Putman et al., 2012].

In the Solar neighborhood, observations suggest that  $\beta \simeq 0.5$  for halo stars, almost independent of metal abundance (Chiba and Yoshii 1998; see also Yoshii and Saio 1979), as overplotted in Figure 3.3. Combined with our result, we see that the motion of the relatively metal-rich BHB stars move on radial orbits at  $8.5 < r/\text{kpc} < 15$ . This behavior is consistent with recent cosmological simulations in which most halo stars originate from accreted dwarf galaxies [Diemand et al., 2005; Sales et al., 2007], as

---

also overplotted in Figure 3.3. However, our very metal-poor halo BHB stars suggest a transition from radially-anisotropic to tangentially-anisotropic velocity distributions. The existence of very metal-poor outer-halo stars with round orbits,<sup>1</sup> which is not confirmed in simulated stellar haloes, suggests that current simulations of disk galaxy formation may lack some important mechanisms, such as those proposed in the previous paragraph. We here note that many authors have pointed out that the simulated dwarf galaxies show an over-production of stars, when compared with observed dwarf galaxies [Sawala et al., 2011]. This phenomenon is often called the “overcooling problem”, and this might result in underestimation of the gas-rich progenitors in simulated haloes, which in turn underestimate the numbers of metal-poor halo stars with round orbits.

We find that the kinematics of outer-halo stars exhibit a marked dependence on stellar metal abundance, which provides information about the physical properties of their progenitor systems (such as the gas fraction). Both of our main results, that the relatively metal-rich and very metal-poor stars are dominated by radial and round orbits, respectively, and that the mean rotational velocity of very metal-poor halo stars lags that of relatively metal-rich halo stars, can be explained if very metal-poor stars originate from gas-rich systems and metal-rich stars from star-rich systems. Our findings cast a new light on the formation mechanism of the Milky Way and similar disk galaxies.

---

<sup>1</sup> This may be termed ‘**negative  $\beta$  problem**’.

## Chapter 4

# Summary and conclusions

Beginning with the seminal paper of [Eggen et al. \[1962\]](#), kinematics and chemical abundances of halo stars have long been studied to infer the formation history of the Milky Way. In this avenue of studies, there are two, widely-accepted assumptions, namely,

- (1) the motion of halo stars observed today reflect the motion of the progenitor systems in which they formed; and
- (2) the chemical abundance of heavy elements of halo stars observed today reflect the chemical abundance of the gas from which they formed.

The assumption (1) is validated not only by theoretical argument of collisions nature of the stellar halo but also by recent numerical simulations of galaxy formations [[Helmi, 2008](#)]. On the other hand, the assumption (2) of constancy of stellar surface metal abundances has not been fully validated yet, although there is a possibility that accretion of metal-enriched material onto its surface enhances the surface metal content [[Yoshii, 1981](#)].

In the first half of this thesis (Chapter 2), we propose a purely observational test on the validity of assumption (2). The underlying idea of our method is that if both assumptions (1) and (2) are valid, we expect identical chemo-dynamical correlations for G- and K-type main-sequence stars, since these long-lived stars reflect the same mass-assembly and star-formation histories. We make use of the kinematical information and surface metallicity data of G/K-type dwarfs taken from data release 8 of Sloan Digital Sky Survey (SDSS DR8) and calculate the correlation between rotational velocity  $V_\phi$  and stellar surface metallicity  $[\text{Fe}/\text{H}]$ .

---

As a result, we find a statistically significant offset in  $[\text{Fe}/\text{H}]$  between the correlations of GK dwarfs in such a way that G-type dwarfs have systematically higher  $[\text{Fe}/\text{H}]$  than K-type dwarfs do at a fixed rotational velocity (see Figure 2.5). This result is consistent with the prediction from metal accretion, since G-type dwarfs are more sensitive to metal accretion due to their shallower surface convective envelope.

We also find that similar offset can be seen for those stars with  $z_{\text{max}} > 3$  kpc, while a subsample of stars with  $z_{\text{max}} < 3$  kpc does not show such an offset, where  $z_{\text{max}}$  is the maximum vertical excursion above the disk plane (see Figure 2.6). According to [Carollo et al. \[2010\]](#), those halo stars with larger  $z_{\text{max}}$  are more likely to be outer-halo stars (those originate from small systems – such as dwarf galaxies – which have accreted and been disrupted), while those halo stars with smaller  $z_{\text{max}}$  are more likely to be inner-halo stars (those formed in the main progenitor of the Milky Way). Therefore, our results indicate that metal accretion is effective only in small progenitor systems and that metal accretion is not effective in the main progenitor of the Milky Way. This indication is favoured by metal accretion scenario, if we take into account that metal accretion is more effective in those environments where relative velocity of the accreting gas with respect to the star is smaller, since internal velocity dispersion is smaller for smaller systems.

As a complementary analysis, we also check for the correlation for blue horizontal-branch (BHB) stars. The result for BHB stars suggests that BHB stars are less affected by metal accretion, which is consistent with the prediction from metal accretion scenario (see Figure 2.7).

Based on these results (as well as a set of Monte Carlo simulations that validate these results; see Appendix A), we conclude that the metal accretion is likely to have occurred in the formation process of the Milky Way, especially in small progenitor systems like ultra-faint dwarf galaxies.

One important impact of our conclusion is that it might affect the formation scenario of Population III stars. At this moment, no metal-free stars have ever been observed. The simplest interpretation for this observational fact is that all the Population III stars have high enough mass ( $M > M_{\odot}$ ) so that they have already died out. However, if metal accretion cannot be neglected, then there is a possibility that some fraction of Population III stars are low-mass enough to survive until today, disguising themselves as ordinary Population II stars due to metal accretion. Therefore, our findings leave some room for the existence of low-mass Population III stars.

Another important impact of our conclusion is that our current understanding of the formation history of the Milky Way might require modification. A large portion

---

of observable halo stars in the Solar neighborhood are low mass main-sequence stars, albeit their low-luminosities. If metal accretion plays an important role, then observed surface metal abundances of these dwarfs mean only upper limits of the original ones. Therefore, the shapes of metallicity distribution function (MDF) of halo dwarfs (especially G dwarfs with shallow surface convective envelopes) may be biased. For example, [An et al. \[2013\]](#) use high-Galactic latitude ( $b > 35$  deg) main-sequence stars at the heliocentric distance range of  $5 \text{ kpc} < d < 8 \text{ kpc}$  and claim that the fraction of outer halo component is  $\sim 20 - 35\%$  in this region, but this figure might need modification if the sample stars are affected by metal accretion. Also, since stellar metallicities of dwarfs are used in estimating their photometric distances, inaccurate estimate of stellar metallicity brings some systematic error in the derived photometric distance (and tangential velocity when photometric distance is used). Thus, observational studies of the spatial distribution and/or kinematics of nearby dwarfs based on photometric distances might require reconsideration of the results. For example, [Carollo et al. \[2010\]](#) investigate a nearby sample of  $\sim 10000$  stars and claim that the difference in the mean metallicity between inner and outer halo components is  $\sim 0.6$  dex. However, this figure might be only a lower limit, since their sample include a significant number of low-mass main-sequence stars and some of which might be affected by metal accretion, especially those belong to outer halo (more metal-poor component). A good news is that our results suggest that metal accretion does not have significant impact on those stars with  $[\text{Fe}/\text{H}] > -1$ , which may be due to deeper surface convective envelope for metal-rich stars. Thus observational studies on disk stars may require minor modifications if any.

In near future, Gaia and JASMINE will provide rich astrometric data, while Gaia-ESO survey will provide much accurate stellar metallicity than SSPP metallicity. These forthcoming data will be helpful in quantifying the significance of metal accretion onto halo stars. For example, by applying similar analysis to these accurate data, we can not only test whether our results presented here are real or not, but also quantify the typical amount of mass which have accreted onto halo stars. If we can determine how the reliability of the observed metallicity depends on the stellar type, we can discuss the star formation history of the Milky Way or distant dwarf galaxies more rigorously, by using the most reliable metallicity tracers (which are presumably those stars with deep surface convective envelopes). Also, if we can estimate the typical total mass accreted onto halo stars, we can infer the environments of the progenitor systems of typical halo stars. This kind of information is beyond our reach at this moment, but might be helpful in understanding the mass assembly history of the Milky Way.



---

In the last half of this thesis (Chapter 3), we derive the kinematical properties of distant BHB stars and investigate their [Fe/H]-dependence. Since evolved, post-main-sequence stars are expected to be less affected by metal accretion, we assume both of the above-mentioned assumptions (1) and (2) throughout Chapter 3. There, we present a model-independent analysis of the line-of-sight velocities and spatial distribution of 1865 halo BHB stars within 30 kpc of the Galactic center taken from SDSS DR8.

First, we make use of [Frenk and White \[1980\]](#) method to estimate the mean rotational velocity of BHB stars as a function of Galactocentric distance  $r$ . We find that the mean rotational velocity of the very metal-poor ([Fe/H] < -2.0) BHB stars significantly lags behind that of the relatively more metal-rich ([Fe/H] > -2.0) BHB stars in the Galactocentric distance range of  $13 \text{ kpc} < r < 23 \text{ kpc}$  (see [Figure 3.1](#)). Secondly, we derive the 3-dimensional velocity dispersion of BHB stars as a function of  $r$  by making use of a new method (generalized [Woolley \[1978\]](#) method). We find that the relatively more metal-rich BHB stars are dominated by stars with eccentric orbits at  $12 \text{ kpc} < r < 15 \text{ kpc}$ , while the very metal-poor BHB stars are dominated by stars on round, low-eccentricity orbits at  $13 \text{ kpc} < r < 18 \text{ kpc}$  (see [Figures 3.2](#) and [3.3](#)).

The derived ‘mean rotational velocity curve’ of halo stars above and below [Fe/H] = -2 is the first observational evidence for the existence of the rotational shear of halo stars outside the Solar neighborhood. Our result is in favor of the interpretation by [Carollo et al. \[2007, 2010\]](#) that the asymmetric  $V_\phi$ -distribution of nearby halo stars is reflecting the dual nature of the stellar halo, not the artefact arising from inadequate tangential velocity estimate as criticised by [Schönrich et al. \[2011\]](#).

Our finding that distant, very metal-poor BHB stars are dominated by round orbits poses a challenge to numerical simulations of galaxy formation, since it contradicts their prediction. All the recent simulations (as far as the author knows) predict that the orbits of halo stars in Milky Way-like galaxies are dominated by radial orbits at any Galactocentric distance  $r$ . Our result suggests that numerical simulations lack in some physical processes in which metal-poor halo stars form. As a possible explanation, we propose a scenario that these metal-poor outer halo stars with round orbits formed in gas-rich systems (similar to high-velocity clouds) whose orbits had been circularised due to inelastic interaction with other gas-rich systems.

Although our findings provide some new insights into the formation history of the stellar halo, our results have to be confirmed by future direct measurements of velocity distribution, since we do not make use of proper motion data. With this regard, next generation astrometric satellites such as Gaia and JASMINE will provide the best opportunity to unravel the structure and history of the Milky Way.

# Appendix A

## A Mock catalogs of G/K-type dwarfs

### A.1 Construction of mock catalogs

In section 2.5.2.4, we used a set of mock catalogs of G/K-type dwarfs in order to investigate the reality of the observed offset in the  $\langle V_\phi \rangle_{\text{med}} - [\text{Fe}/\text{H}]$ . Here we present some additional information on these mock catalogs.

The observed (real) catalog of G/K-type dwarfs can be mathematically expressed as

$$\left\{ \left( T_{\text{eff},i}, \log g_i, [\text{Fe}/\text{H}]_i, d_i, \ell_i, b_i, v_{\text{los},i}^{\text{hel}}, PM_i^\ell, PM_i^b \right) \mid i = 1, \dots, N \right\}, \quad (\text{observed sample}), \quad (1)$$

where  $N$  is the total number of G/K-type dwarfs and the nine quantities for the  $i$ -th entry denote the effective temperature ( $T_{\text{eff},i}$ ), surface gravity ( $\log g_i$ ), atmospheric metallicity ( $[\text{Fe}/\text{H}]_i$ ), SSPP distance ( $d_i$ ), Galactic longitude ( $\ell_i$ ), Galactic latitude ( $b_i$ ), heliocentric line-of-sight velocity ( $v_{\text{los},i}^{\text{hel}}$ ), proper motion in the  $\ell$ - and  $b$ -directions ( $PM_i^\ell, PM_i^b$ ) of the  $i$ -th star. We generate each of our mock catalogs so that the  $i$ -th star in the mock catalog ( $i = 1, \dots, N$ ) has the same information on effective temperature, surface gravity, metallicity and 3-D position as those of the  $i$ -th star in our real (observed) catalog, while its 3-D velocity is assigned according to a given realistic Galactic model, as well as to the assumed error models. Namely, the  $j$ -th mock catalog ( $j = 1, \dots, M$ ) can be expressed as

$$\left\{ \left( T_{\text{eff},i}, \log g_i, [\text{Fe}/\text{H}]_i, d_i, \ell_i, b_i, v_{\text{los},i,j}^{\text{mock-obs,hel}}, PM_{i,j}^{\text{mock-obs},\ell}, PM_{i,j}^{\text{mock-obs},b} \right) \mid i = 1, \dots, N \right\}, \quad (j\text{-th mock catalog}). \quad (2)$$

---

In assigning the 3-D velocity information to the  $i$ -th star of a given mock catalog, we follow four steps:

- **Step 1** Assign the ‘true’  $[\text{Fe}/\text{H}]$  and the ‘true’ 3-D position to the mock star;
- **Step 2** Determine whether the  $i$ -th mock star belongs to halo or thick disk with a certain probability based on the ‘true’  $[\text{Fe}/\text{H}]$  and the ‘true’ 3-D position;
- **Step 3** Assign the ‘true’ 3-D velocity according to the distribution function model of the halo and thick disk;
- **Step 4** Decompose the ‘true’ 3-D velocity into the line-of-sight velocity and proper motion and add realistic observational errors.

Note that the ‘true’  $[\text{Fe}/\text{H}]$  and the ‘true’ distance are only used as internal variables, and do not appear explicitly in the mock catalogs. In the following, we describe each step in more detail.

In **Step 1**, we assign the ‘true’ metallicity

$$[\text{Fe}/\text{H}]_{i,j}^{true} = [\text{Fe}/\text{H}]_i + E_r([\text{Fe}/\text{H}]_i) \quad (3)$$

to the  $i$ -th star in the  $j$ -th mock catalog. Here,  $E_r$  is the error-correcting term. Also, we assign the ‘true’ distance

$$d_{i,j}^{true} = d_i \times \mathcal{N}(\mu_{dist}, 0.2) \quad (4)$$

to the  $i$ -th star. Here,  $\mathcal{N}(\mu, \sigma)$  is a random number generator that generate random numbers obeying a Gaussian distribution function with the mean of  $\mu$  and the dispersion of  $\sigma$ . When there is no systematic error, we set  $\mu_{dist} = 1$ . The choice of  $\sigma = 0.2$  is motivated by the  $\sim 20\%$  random error in the distance estimation. We note that there is a tiny probability for the random number generator  $\mathcal{N}$  to generate negative numbers. In that case, we set  $d_{i,j}^{true} = 0.1$  kpc.

In **Step 2**, we randomly assign a flag of  $H$  (halo) or  $TD$  (thick disk) to the  $i$ -th star with a probability of  $p$  or  $(1 - p)$ , respectively, where  $p$  is defined by

$$p = \frac{f_H([\text{Fe}/\text{H}]_{i,j}^{true})}{f_H([\text{Fe}/\text{H}]_{i,j}^{true}) + f_{TD}([\text{Fe}/\text{H}]_{i,j}^{true}) \times D(d_{i,j}^{true} \cdot \sin b_i)}. \quad (5)$$

---

Here,  $D(z)$  describes the density profile of the thick disk as a function of the vertical distance from the Galactic disk plane  $|z|$ ; and  $f_H$  and  $f_{TD}$  denote the MDFs at the Galactic plane ( $z = 0$  kpc) of halo and thick disk stars, respectively. We assume the following models for these functions:

$$f_k([\text{Fe}/\text{H}]) = F_k \times \frac{1}{\sqrt{2\pi}\sigma_k} \exp\left[-\frac{1}{2}\left(\frac{[\text{Fe}/\text{H}] - \mu_k}{\sigma_k}\right)^2\right], \quad (k = H, TD), \quad (6)$$

$$D(z) = \exp\left[-\frac{|z|}{h_z}\right], \quad h_z = 1.0 \text{ kpc}, \quad (7)$$

and we set  $(F_H, \mu_H, \sigma_H) = (0.001, -1.5, 0.3)$ ,  $(F_{TD}, \mu_{TD}, \sigma_{TD}) = (0.040, -0.6, 0.2)$ . We note here that we do not expect significant contribution from the thin disk, because of our metallicity cut of  $[\text{Fe}/\text{H}] < -0.5$ .

In **Step 3**, we assign the ‘true’ 3-D velocity of the  $i$ -th star in the usual Galactic cylindrical coordinate system by

$$(V_{R,i,j}^{true}, V_{\phi,i,j}^{true}, V_{z,i,j}^{true}) = \begin{cases} (\mathcal{N}(0, 80), \mathcal{N}(50, 150), \mathcal{N}(0, 70)) \text{ km s}^{-1} & (flag = H), \\ (\mathcal{N}(0, 30), \mathcal{N}(180, 30), \mathcal{N}(0, 30)) \text{ km s}^{-1} & (flag = TD). \end{cases} \quad (8)$$

Here, it is assumed that the mean rotational velocities of halo and thick disk are  $50 \text{ km s}^{-1}$  and  $180 \text{ km s}^{-1}$ , respectively.

In **Step 4**, we calculate the ‘true’ heliocentric line-of-sight velocity  $v_{los,i,j}^{true,hel}$  and the ‘true’ proper motion  $PM_{i,j}^{true,\ell}$ ,  $PM_{i,j}^{true,b}$  of the  $i$ -th mock star in  $j$ -th mock catalog, by using the ‘true’ distance  $d_{i,j}^{true}$  and by assuming the same LSR and peculiar solar velocity as those described in section 2.4.1. Then we calculate the ‘mock-observed’ values for these quantities by using

$$v_{los,i,j}^{mock-obs,hel} = v_{los,i,j}^{true,hel} + \mathcal{N}(0, 2) \text{ km s}^{-1}, \quad (9)$$

$$PM_{i,j}^{mock-obs,\ell} = PM_{i,j}^{true,\ell} + \mathcal{N}(0, 3.5) \text{ mas yr}^{-1}, \quad (10)$$

$$PM_{i,j}^{mock-obs,b} = PM_{i,j}^{true,b} + \mathcal{N}(0, 3.5) \text{ mas yr}^{-1}. \quad (11)$$

We note that the adopted errors in the line-of-sight velocity ( $2 \text{ km s}^{-1}$ ) and in proper motion ( $3.5 \text{ mas yr}^{-1}$ ) are typical values in our real sample.

Table 1: Metallicity error models in the mock catalogs

Model	$E_r([\text{Fe}/\text{H}])$ for G-type dwarfs	$E_r([\text{Fe}/\text{H}])$ for K-type dwarfs
Model A	$\mathcal{N}(0, 0.2)$	$\mathcal{N}(0, 0.2)$
Model B	$\mathcal{N}(0, 0.2)$	$\mathcal{N}(0, 0.3)$
Model C	$\begin{cases} \mathcal{N}(0, 0.2) & ([\text{Fe}/\text{H}] \geq -1) \\ \mathcal{N}(0, 0.2) + 0.2 \times ([\text{Fe}/\text{H}] + 1.0) & ([\text{Fe}/\text{H}] < -1) \end{cases}$	$\begin{cases} \mathcal{N}(0, 0.2) & ([\text{Fe}/\text{H}] \geq -1) \\ \mathcal{N}(0, 0.2) - 0.2 \times ([\text{Fe}/\text{H}] + 1.0) & ([\text{Fe}/\text{H}] < -1) \end{cases}$

---

## A.2 Mock observations of mock catalogs

Observational errors in  $[\text{Fe}/\text{H}]$  and distance are the most important factors that affect the derived  $\langle V_\phi \rangle_{\text{med}}\text{-}[\text{Fe}/\text{H}]$  relations. In order to evaluate how observational errors in  $[\text{Fe}/\text{H}]$  affect our analyses, we consider three models of the error-correcting term  $E_r([\text{Fe}/\text{H}])$ , as presented in Table 1. Among these models, Model A does not carry a spectral-type dependence in the  $[\text{Fe}/\text{H}]$  error, while Models B and C are designed to carry this spectral-type dependence. We also consider three types of systematic errors in distance, by adopting  $\mu_{\text{dist}} = 0.8, 1.0$ , or  $1.2$ . For each of the nine combinations of the error models (three for the  $[\text{Fe}/\text{H}]$  error and three for the distance error), we generate 100 mock catalogs and derive the  $\langle V_\phi \rangle_{\text{med}}\text{-}[\text{Fe}/\text{H}]$  relations.

In Figures A.1, A.2, and A.3, we show the results for Models A, B, and C, respectively, with  $\mu_{\text{dist}}$  fixed to be 1.0. In these figures, we show the median curve of 100  $\langle V_\phi \rangle_{\text{med}}\text{-}[\text{Fe}/\text{H}]$  relations derived from the mock catalogs. The panels (a), (b), and (c) correspond to Figures 2.5(c), 2.6(a), and 2.6(b), respectively.

Figure A.1 suggests that, if the observational errors in  $[\text{Fe}/\text{H}]$  do not possess a spectral-type dependence (Model A), the resultant  $\langle V_\phi \rangle_{\text{med}}\text{-}[\text{Fe}/\text{H}]$  relations are statistically identical for G- and K-type dwarfs. On the other hand, Figures A.2 and A.3 suggest that we expect an offset in the  $\langle V_\phi \rangle_{\text{med}}\text{-}[\text{Fe}/\text{H}]$  relation for the full sample and the low- $z_{\text{max}}$  subsample, if there is a spectral-type dependence in the observational errors in  $[\text{Fe}/\text{H}]$  (Model B or C), although the offset is not very clear for the high- $z_{\text{max}}$  subsample (due to the small sample size).

By comparing the panels (a) and (b) in Figures A.1, A.2, and A.3, it is suggested that, whenever we see an offset in the full sample [panel (a)], we should also see a similar offset in the low- $z_{\text{max}}$  subsample [panel (b)]. In other words, if the observed offset in Figure 2.5(c) is due to the observational errors in  $[\text{Fe}/\text{H}]$ , then a similar offset is also expected in Figure 2.6(a) as well. Thus, it seems that the detected offset in Figures 2.5(c) and 2.6(b), as well as the non-existence of the offset in Figure 2.6(a), are due to neither an observational error in  $[\text{Fe}/\text{H}]$  nor its spectral-type dependence.

If we further vary the value of  $\mu_{\text{dist}}$  for G- and/or K-type dwarfs, the results are essentially the same as in the case of  $\mu_{\text{dist}} = 1.0$ . The only difference is in the overall location of the  $\langle V_\phi \rangle_{\text{med}}\text{-}[\text{Fe}/\text{H}]$  curves. If  $\mu_{\text{dist}}$  is set to be 0.8 and the SSPP distance is overestimated, the resultant curve of the  $\langle V_\phi \rangle_{\text{med}}\text{-}[\text{Fe}/\text{H}]$  relation is shifted downwards (toward lower  $\langle V_\phi \rangle_{\text{med}}$ ), due to the overestimate of the relative velocities of the sample stars with respect to the Sun. On the other hand, if  $\mu_{\text{dist}}$  is set to be 1.2 and the SSPP distance is underestimated, the resultant curve of  $\langle V_\phi \rangle_{\text{med}}\text{-}[\text{Fe}/\text{H}]$  relation is shifted

---

upwards. The effect of  $\mu_{dist}$  is most prominently seen at the low-metallicity tail of the  $\langle V_\phi \rangle_{med}$ -[Fe/H] relation. For example, if we adopt Model A, the plateau value of  $\langle V_\phi \rangle_{med}$  in the low-metallicity tail becomes  $\simeq 20 \text{ km s}^{-1}$  when  $\mu_{dist} = 0.8$ , while this value becomes  $\simeq 70 \text{ km s}^{-1}$  when  $\mu_{dist} = 1.2$  (see Figure A.4). The fact that both the G- and K-type dwarfs exhibit  $\langle V_\phi \rangle_{med} \simeq 50 \text{ km s}^{-1}$  at the low-metallicity tail in Figure 2.5(c) suggests that there is no spectral-type dependence in  $\mu_{dist}$  in our sample. Therefore, we conclude that the observed offset in the  $\langle V_\phi \rangle_{med}$ -[Fe/H] relation [Figures 2.5(c) and 2.6(b)], or the non-existence of it [Figure 2.6(a)], are not due to observational errors in [Fe/H] or distance.

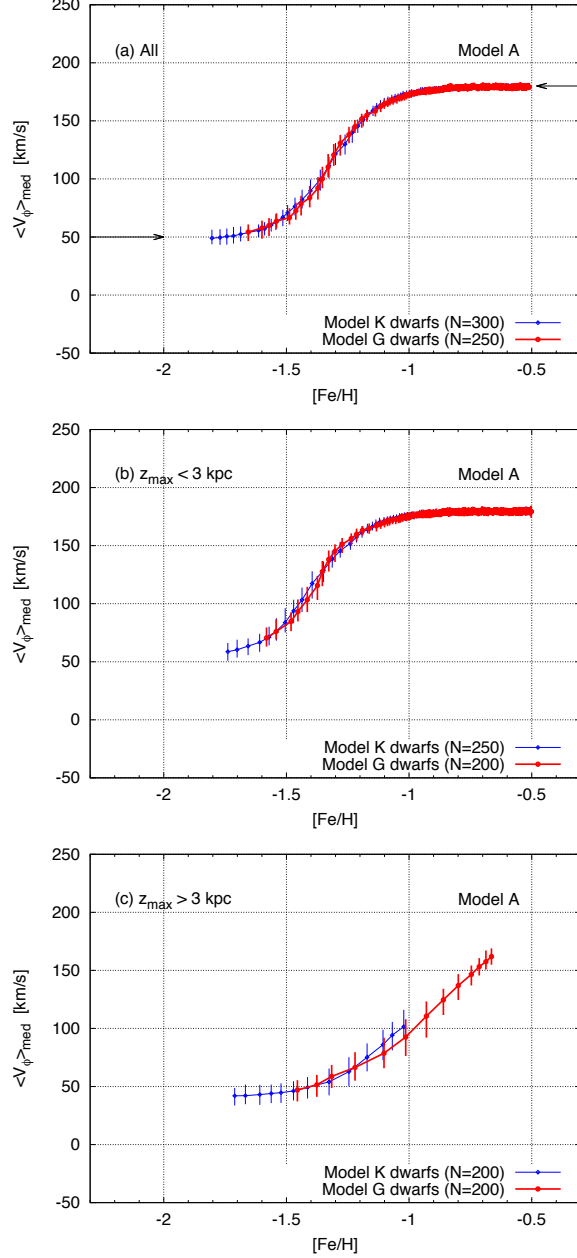


Figure A.1: The  $\langle V_\phi \rangle_{\text{med}}$ -[Fe/H] relations for 100 mock catalogs with  $\mu_{\text{dist}} = 1.0$ . The implemented error in [Fe/H] is described by Model A for these mock catalogs. The red and blue lines indicate the median curve of 100  $\langle V_\phi \rangle_{\text{med}}$ -[Fe/H] relations for G- and K-type dwarfs, respectively. (a) The result for the full sample without  $z_{\text{max}}$  cut applied, which corresponds to Figure 2.5(c). The horizontal arrows at  $50 \text{ km s}^{-1}$  and  $180 \text{ km s}^{-1}$  indicate the mean velocities of halo and thick-disk stars, respectively, expected from the input distribution function model [see equation (8)]. (b) The result for the subsample of stars with  $z_{\text{max}} < 3$  kpc, which corresponds to Figure 2.6(a). (c) The result for the subsample of stars with  $z_{\text{max}} > 3$  kpc, which corresponds to Figure 2.6(b).



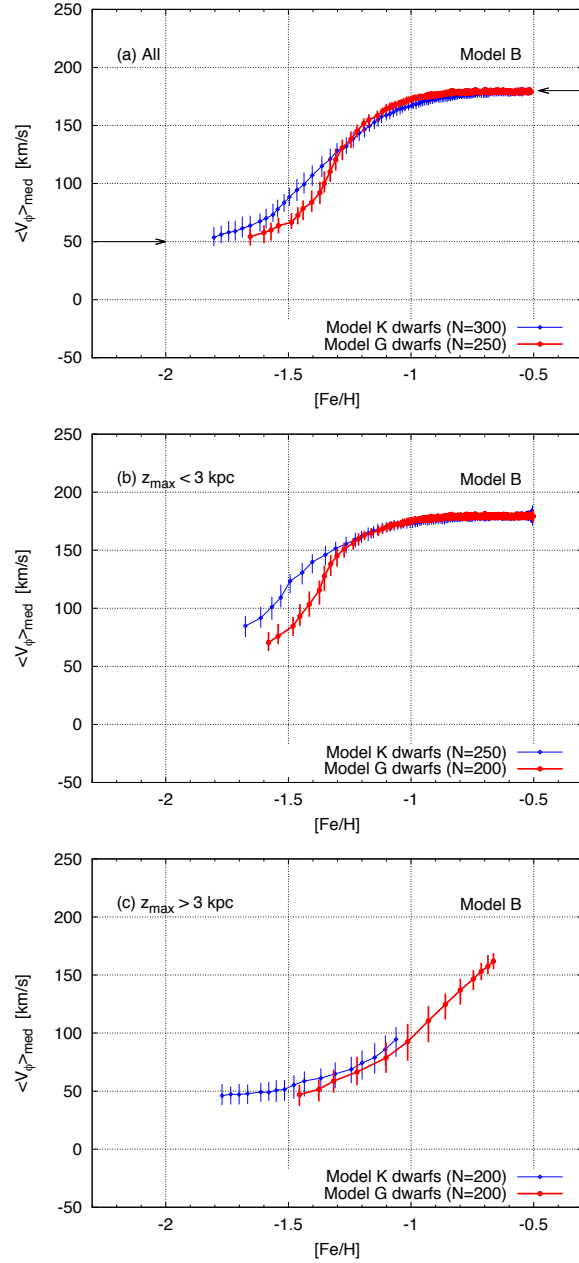


Figure A.2: The same as in Figure A.1, but for 100 mock catalogs in which the error in  $[\text{Fe}/\text{H}]$  is described by Model B.

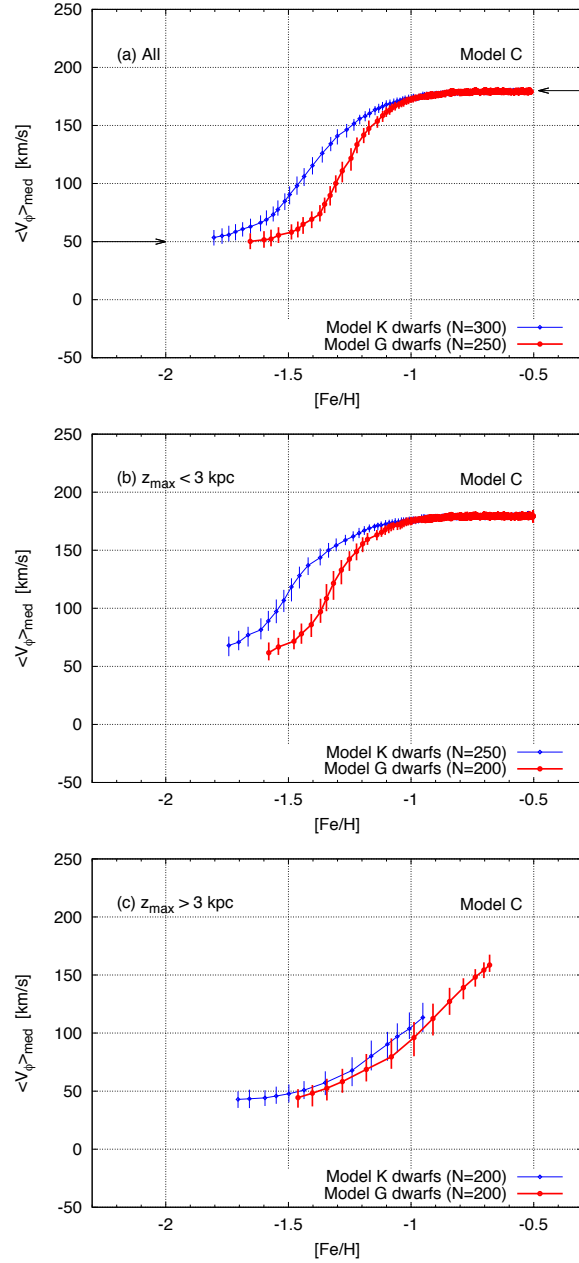


Figure A.3: The same as in Figure A.1, but for 100 mock catalogs in which the error in [Fe/H] is described by Model C.

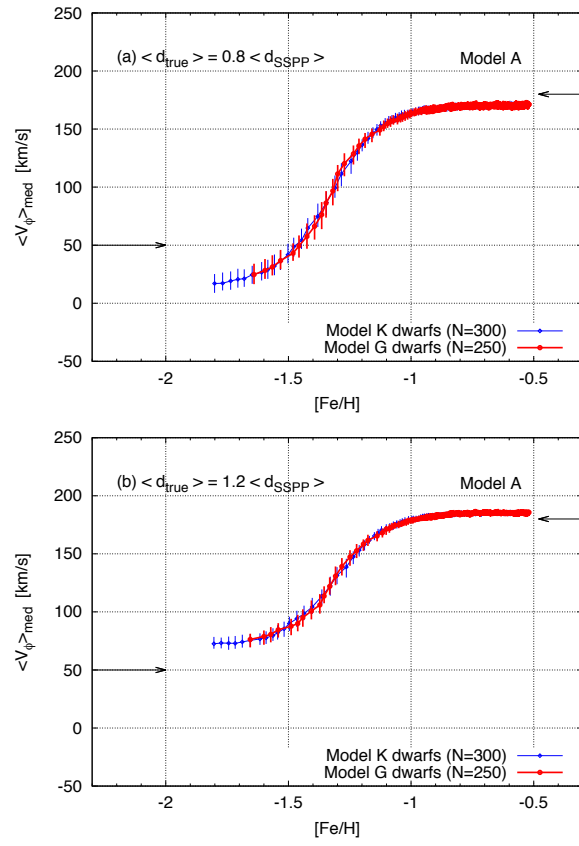


Figure A.4: The same as in Figure A.1(a), but for  $\mu_{\text{dist}} = 0.8$  (top) and  $\mu_{\text{dist}} = 1.2$  (bottom).

# References

H. Aihara, C. Allende Prieto, D. An, S. F. Anderson, É. Aubourg, E. Balbinot, T. C. Beers, A. A. Berlind, S. J. Bickerton, D. Bizyaev, M. R. Blanton, J. J. Bochanski, A. S. Bolton, J. Bovy, W. N. Brandt, J. Brinkmann, P. J. Brown, J. R. Brownstein, N. G. Busca, H. Campbell, M. A. Carr, Y. Chen, C. Chiappini, J. Comparat, N. Connolly, M. Cortes, R. A. C. Croft, A. J. Cuesta, L. N. da Costa, J. R. A. Davenport, K. Dawson, S. Dhital, A. Ealet, G. L. Ebelke, E. M. Edmondson, D. J. Eisenstein, S. Escoffier, M. Esposito, M. L. Evans, X. Fan, B. Femenía Castellá, A. Font-Ribera, P. M. Frinchaboy, J. Ge, B. A. Gillespie, G. Gilmore, J. I. González Hernández, J. R. Gott, A. Gould, E. K. Grebel, J. E. Gunn, J.-C. Hamilton, P. Harding, D. W. Harris, S. L. Hawley, F. R. Hearty, S. Ho, D. W. Hogg, J. A. Holtzman, K. Honscheid, N. Inada, I. I. Ivans, L. Jiang, J. A. Johnson, C. Jordan, W. P. Jordan, E. A. Kazin, D. Kirkby, M. A. Klaene, G. R. Knapp, J.-P. Kneib, C. S. Kochanek, L. Koesterke, J. A. Kollmeier, R. G. Kron, H. Lampeitl, D. Lang, J.-M. Le Goff, Y. S. Lee, Y.-T. Lin, D. C. Long, C. P. Loomis, S. Lucatello, B. Lundgren, R. H. Lupton, Z. Ma, N. MacDonald, S. Mahadevan, M. A. G. Maia, M. Makler, E. Malanushenko, V. Malanushenko, R. Mandelbaum, C. Maraston, D. Margala, K. L. Masters, C. K. McBride, P. M. McGehee, I. D. McGreer, B. Ménard, J. Miralda-Escudé, H. L. Morrison, F. Mullally, D. Muna, J. A. Munn, H. Murayama, A. D. Myers, T. Naugle, A. F. Neto, D. C. Nguyen, R. C. Nichol, R. W. O'Connell, R. L. C. Ogando, M. D. Olmstead, D. J. Oravetz, N. Padmanabhan, N. Palanque-Delabrouille, K. Pan, P. Pandey, I. Pâris, W. J. Percival, P. Petitjean, R. Pfaffenberger, J. Pforr, S. Phleps, C. Pichon, M. M. Pieri, F. Prada, A. M. Price-Whelan, M. J. Raddick, B. H. F. Ramos, C. Reylé, J. Rich, G. T. Richards, H.-W. Rix, A. C. Robin, H. J. Rocha-Pinto, C. M. Rockosi, N. A. Roe, E. Rollinde, A. J. Ross, N. P. Ross, B. M. Rossetto, A. G. Sánchez, C. Sayres, D. J. Schlegel, K. J. Schlesinger, S. J. Schmidt, D. P. Schneider, E. Sheldon, Y. Shu, J. Simmerer, A. E. Simmons, T. Sivarani, S. A. Snedden,

- J. S. Sobek, M. Steinmetz, M. A. Strauss, A. S. Szalay, M. Tanaka, A. R. Thakar, D. Thomas, J. L. Tinker, B. M. Tofflemire, R. Tojeiro, C. A. Tremonti, J. Vandenberg, M. Vargas Magaña, L. Verde, N. P. Vogt, D. A. Wake, J. Wang, B. A. Weaver, D. H. Weinberg, M. White, S. D. M. White, B. Yanny, N. Yasuda, C. Yèche, and I. Zehavi. The Eighth Data Release of the Sloan Digital Sky Survey: First Data from SDSS-III. *ApJS*, 193:29, April 2011. doi: 10.1088/0067-0049/193/2/29. 30, 57
- C. Allende Prieto, T. Sivarani, T. C. Beers, Y. S. Lee, L. Koesterke, M. Shetrone, C. Sneden, D. L. Lambert, R. Wilhelm, C. M. Rockosi, D. K. Lai, B. Yanny, I. I. Ivans, J. A. Johnson, W. Aoki, C. A. L. Bailer-Jones, and P. Re Fiorentin. The SEGUE Stellar Parameter Pipeline. III. Comparison with High-Resolution Spectroscopy of SDSS/SEGUE Field Stars. *AJ*, 136:2070–2082, November 2008. doi: 10.1088/0004-6256/136/5/2070. 31, 35
- D. An, M. H. Pinsonneault, T. Masseron, F. Delahaye, J. A. Johnson, D. M. Terndrup, T. C. Beers, I. I. Ivans, and Ž. Ivezić. Galactic Globular and Open Clusters in the Sloan Digital Sky Survey. II. Test of Theoretical Stellar Isochrones. *ApJ*, 700:523–544, July 2009. doi: 10.1088/0004-637X/700/1/523. 31, 32, 46, 47
- D. An, T. C. Beers, J. A. Johnson, M. H. Pinsonneault, Y. S. Lee, J. Bovy, Ž. Ivezić, D. Carollo, and M. Newby. The Stellar Metallicity Distribution Function of the Galactic Halo from SDSS Photometry. *ApJ*, 763:65, January 2013. doi: 10.1088/0004-637X/763/1/65. 69
- T. C. Beers, D. Carollo, Ž. Ivezić, D. An, M. Chiba, J. E. Norris, K. C. Freeman, Y. S. Lee, J. A. Munn, P. Re Fiorentin, T. Sivarani, R. Wilhelm, B. Yanny, and D. G. York. The Case for the Dual Halo of the Milky Way. *ApJ*, 746:34, February 2012. doi: 10.1088/0004-637X/746/1/34. 17, 18, 31, 39, 41, 53
- J. Binney and S. Tremaine. *Galactic Dynamics: Second Edition*. Princeton University Press, 2008. 4, 61
- L. Blitz, D. N. Spergel, P. J. Teuben, D. Hartmann, and W. B. Burton. High-Velocity Clouds: Building Blocks of the Local Group. *ApJ*, 514:818–843, April 1999. doi: 10.1086/306963. 65
- G. R. Blumenthal, S. M. Faber, J. R. Primack, and M. J. Rees. Formation of galaxies and large-scale structure with cold dark matter. *Nature*, 311:517–525, October 1984. doi: 10.1038/311517a0. 65

- H. Bondi. On spherically symmetrical accretion. *MNRAS*, 112:195, 1952. [28](#)
- J. Bovy, C. Allende Prieto, T. C. Beers, D. Bizyaev, L. N. da Costa, K. Cunha, G. L. Ebelke, D. J. Eisenstein, P. M. Frinchaboy, A. E. García Pérez, L. Girardi, F. R. Hearty, D. W. Hogg, J. Holtzman, M. A. G. Maia, S. R. Majewski, E. Malanushenko, V. Malanushenko, S. Mészáros, D. L. Nidever, R. W. O’Connell, C. O’Donnell, A. Oravetz, K. Pan, H. J. Rocha-Pinto, R. P. Schiavon, D. P. Schneider, M. Schultheis, M. Skrutskie, V. V. Smith, D. H. Weinberg, J. C. Wilson, and G. Zasowski. The Milky Way’s Circular-velocity Curve between 4 and 14 kpc from APOGEE data. *ApJ*, 759:131, November 2012. doi: 10.1088/0004-637X/759/2/131. [32](#), [60](#)
- V. Bromm, A. Ferrara, P. S. Coppi, and R. B. Larson. The fragmentation of pre-enriched primordial objects. *MNRAS*, 328:969–976, December 2001. doi: 10.1046/j.1365-8711.2001.04915.x. [43](#)
- W. R. Brown, M. J. Geller, S. J. Kenyon, and A. Diaferio. Velocity Dispersion Profile of the Milky Way Halo. *AJ*, 139:59–67, January 2010. doi: 10.1088/0004-6256/139/1/59. [61](#)
- E. Caffau, P. Bonifacio, P. François, M. Spite, F. Spite, S. Zaggia, H.-G. Ludwig, M. Steffen, L. Mashonkina, L. Monaco, L. Sbordone, P. Molaro, R. Cayrel, B. Plez, V. Hill, F. Hammer, and S. Randich. A primordial star in the heart of the Lion. *A&A*, 542:A51, June 2012. doi: 10.1051/0004-6361/201118744. [42](#)
- D. Carollo, T. C. Beers, Y. S. Lee, M. Chiba, J. E. Norris, R. Wilhelm, T. Sivarani, B. Marsteller, J. A. Munn, C. A. L. Bailer-Jones, P. R. Fiorentin, and D. G. York. Two stellar components in the halo of the Milky Way. *Nature*, 450:1020–1025, December 2007. doi: 10.1038/nature06460. [15](#), [16](#), [17](#), [18](#), [19](#), [20](#), [39](#), [40](#), [41](#), [52](#), [56](#), [57](#), [60](#), [70](#)
- D. Carollo, T. C. Beers, M. Chiba, J. E. Norris, K. C. Freeman, Y. S. Lee, Ž. Ivezić, C. M. Rockosi, and B. Yanny. Structure and Kinematics of the Stellar Halos and Thick Disks of the Milky Way Based on Calibration Stars from Sloan Digital Sky Survey DR7. *ApJ*, 712:692–727, March 2010. doi: 10.1088/0004-637X/712/1/692. [15](#), [16](#), [17](#), [18](#), [21](#), [22](#), [23](#), [39](#), [40](#), [55](#), [56](#), [60](#), [61](#), [68](#), [69](#), [70](#)
- M. Chiba and T. C. Beers. Kinematics of Metal-poor Stars in the Galaxy. III. Formation of the Stellar Halo and Thick Disk as Revealed from a Large Sample of Nonkinemat-

- ically Selected Stars. *AJ*, 119:2843–2865, June 2000. doi: 10.1086/301409. [6](#), [7](#), [9](#), [10](#), [11](#), [38](#), [56](#)
- M. Chiba and T. C. Beers. Structure of the Galactic Stellar Halo Prior to Disk Formation. *ApJ*, 549:325–336, March 2001. doi: 10.1086/319068. [34](#)
- M. Chiba and Y. Yoshii. Early evolution of the Galactic halo revealed from Hipparcos observations of metal-poor stars. *AJ*, 115:168, January 1998. doi: 10.1086/300177. [6](#), [8](#), [9](#), [63](#), [64](#), [65](#)
- N. Christlieb, M. S. Bessell, T. C. Beers, B. Gustafsson, A. Korn, P. S. Barklem, T. Karlsson, M. Mizuno-Wiedner, and S. Rossi. A stellar relic from the early Milky Way. *Nature*, 419:904–906, October 2002. doi: 10.1038/nature01142. [42](#)
- A. J. Deason, V. Belokurov, and N. W. Evans. Rotation of halo populations in the Milky Way and M31. *MNRAS*, 411:1480–1494, March 2011. doi: 10.1111/j.1365-2966.2010.17785.x. [56](#), [61](#)
- A. J. Deason, V. Belokurov, N. W. Evans, and J. An. Broken degeneracies: the rotation curve and velocity anisotropy of the Milky Way halo. *MNRAS*, 424:L44–L48, July 2012. doi: 10.1111/j.1745-3933.2012.01283.x. [56](#)
- W. Dehnen and J. J. Binney. Local stellar kinematics from HIPPARCOS data. *MNRAS*, 298:387–394, August 1998. doi: 10.1046/j.1365-8711.1998.01600.x. [4](#), [32](#), [60](#)
- J. Diemand, P. Madau, and B. Moore. The distribution and kinematics of early high- $\sigma$  peaks in present-day haloes: implications for rare objects and old stellar populations. *MNRAS*, 364:367–383, December 2005. doi: 10.1111/j.1365-2966.2005.09604.x. [64](#), [65](#)
- O. J. Eggen, D. Lynden-Bell, and A. R. Sandage. Evidence from the motions of old stars that the Galaxy collapsed. *ApJ*, 136:748, November 1962. doi: 10.1086/147433. [5](#), [6](#), [7](#), [67](#)
- A. S. Font, A. J. Benson, R. G. Bower, C. S. Frenk, A. Cooper, G. De Lucia, J. C. Helly, A. Helmi, Y.-S. Li, I. G. McCarthy, J. F. Navarro, V. Springel, E. Starkeburg, J. Wang, and S. D. M. White. The population of Milky Way satellites in the  $\Lambda$  cold dark matter cosmology. *MNRAS*, 417:1260–1279, October 2011. doi: 10.1111/j.1365-2966.2011.19339.x. [16](#), [39](#)

- 
- A. Frebel, W. Aoki, N. Christlieb, H. Ando, M. Asplund, P. S. Barklem, T. C. Beers, K. Eriksson, C. Fechner, M. Y. Fujimoto, S. Honda, T. Kajino, T. Minezaki, K. Nomoto, J. E. Norris, S. G. Ryan, M. Takada-Hidai, S. Tsangarides, and Y. Yoshii. Nucleosynthetic signatures of the first stars. *Nature*, 434:871–873, April 2005. doi: 10.1038/nature03455. [42](#)
- A. Frebel, J. L. Johnson, and V. Bromm. The minimum stellar metallicity observable in the Galaxy. *MNRAS*, 392:L50–L54, January 2009. doi: 10.1111/j.1745-3933.2008.00587.x. [29](#), [40](#)
- C. S. Frenk and S. D. M. White. The kinematics and dynamics of the galactic globular cluster system. *MNRAS*, 193:295–311, October 1980. [58](#), [70](#)
- A. M. Ghez, S. Salim, N. N. Weinberg, J. R. Lu, T. Do, J. K. Dunn, K. Matthews, M. R. Morris, S. Yelda, E. E. Becklin, T. Kremenek, M. Milosavljevic, and J. Naiman. Measuring Distance and Properties of the Milky Way’s Central Supermassive Black Hole with Stellar Orbits. *ApJ*, 689:1044–1062, December 2008. doi: 10.1086/592738. [32](#), [60](#)
- G. Gilmore and N. Reid. New light on faint stars. III - Galactic structure towards the South Pole and the Galactic thick disc. *MNRAS*, 202:1025–1047, March 1983. [33](#)
- G. M. H. J. Habets and J. R. W. Heintze. Empirical bolometric corrections for the main-sequence. *A&AS*, 46:193–237, November 1981. [31](#), [32](#)
- K. Hattori, Y. Yoshii, T. C. Beers, D. Carollo, and Y. S. Lee. Very Metal-poor Outer-halo Stars with Round Orbits. *ApJ*, 763:L17, January 2013. doi: 10.1088/2041-8205/763/1/L17. [55](#)
- K. Hattori, Y. Yoshii, T. C. Beers, D. Carollo, and Y. S. Lee. Possible Evidence for Metal Accretion onto the Surfaces of Metal-Poor Main-Sequence Stars. *ArXiv e-prints*, February 2014. [27](#)
- A. Helmi. The stellar halo of the Galaxy. *A&A Rev.*, 15:145–188, June 2008. doi: 10.1007/s00159-008-0009-6. [67](#)
- A. Helmi and P. T. de Zeeuw. Mapping the substructure in the Galactic halo with the next generation of astrometric satellites. *MNRAS*, 319:657–665, December 2000. doi: 10.1046/j.1365-8711.2000.03895.x. [10](#), [12](#)



- A. Helmi, S. D. M. White, P. T. de Zeeuw, and H. Zhao. Debris streams in the solar neighbourhood as relicts from the formation of the Milky Way. *Nature*, 402:53–55, November 1999. doi: 10.1038/46980. 8, 10, 11
- S. Hirano, T. Hosokawa, N. Yoshida, H. Umeda, K. Omukai, G. Chiaki, and H. W. Yorke. One Hundred First Stars : Protostellar Evolution and the Final Masses. *ArXiv e-prints*, August 2013. 26
- R. A. Ibata, G. Gilmore, and M. J. Irwin. Sagittarius: the nearest dwarf galaxy. *MNRAS*, 277:781–800, December 1995. 10
- M. N. Ishigaki, M. Chiba, and W. Aoki. Chemical Abundances of the Milky Way Thick Disk and Stellar Halo. I. Implications of  $[\alpha/\text{Fe}]$  for Star Formation Histories in Their Progenitors. *ApJ*, 753:64, July 2012. doi: 10.1088/0004-637X/753/1/64. 17
- N. Iwamoto, H. Umeda, N. Tominaga, K. Nomoto, and K. Maeda. The First Chemical Enrichment in the Universe and the Formation of Hyper Metal-Poor Stars. *Science*, 309:451–453, July 2005. doi: 10.1126/science.1112997. 43
- P. R. Kafle, S. Sharma, G. F. Lewis, and J. Bland-Hawthorn. Kinematics of the Stellar Halo and the Mass Distribution of the Milky Way Using Blue Horizontal Branch Stars. *ApJ*, 761:98, December 2012. doi: 10.1088/0004-637X/761/2/98. 56
- F. J. Kerr and D. Lynden-Bell. Review of galactic constants. *MNRAS*, 221:1023–1038, August 1986. 4, 32, 60
- T. D. Kinman, C. Cacciari, A. Bragaglia, R. Smart, and A. Spagna. The kinematic properties of BHB and RR Lyrae stars towards the Anticentre and the North Galactic Pole: the transition between the inner and the outer halo. *MNRAS*, 422:2116–2144, May 2012. doi: 10.1111/j.1365-2966.2012.20747.x. 56
- E. N. Kirby, J. D. Simon, M. Geha, P. Guhathakurta, and A. Frebel. Uncovering Extremely Metal-Poor Stars in the Milky Way’s Ultrafaint Dwarf Spheroidal Satellite Galaxies. *ApJ*, 685:L43–L46, September 2008. doi: 10.1086/592432. 11, 14, 65
- Y. Komiya, A. Habe, T. Suda, and M. Y. Fujimoto. Formation History of Metal-poor Halo Stars with the Hierarchical Model and the Effect of Interstellar Matter Accretion on the Most Metal-poor Stars. *ApJ*, 717:542–561, July 2010. doi: 10.1088/0004-637X/717/1/542. 29, 40

- S. E. Koposov, H.-W. Rix, and D. W. Hogg. Constraining the Milky Way Potential with a Six-Dimensional Phase-Space Map of the GD-1 Stellar Stream. *ApJ*, 712: 260–273, March 2010. doi: 10.1088/0004-637X/712/1/260. [32](#), [60](#)
- P. Kroupa, C. Weidner, J. Pflamm-Altenburg, I. Thies, J. Dabringhausen, M. Marks, and T. Maschberger. *The Stellar and Sub-Stellar Initial Mass Function of Simple and Composite Populations*, page 115. 2013. doi: 10.1007/978-94-007-5612-0\_4. [26](#)
- Y. S. Lee, T. C. Beers, T. Sivarani, C. Allende Prieto, L. Koesterke, R. Wilhelm, P. Re Fiorentin, C. A. L. Bailer-Jones, J. E. Norris, C. M. Rockosi, B. Yanny, H. J. Newberg, K. R. Covey, H.-T. Zhang, and A.-L. Luo. The SEGUE Stellar Parameter Pipeline. I. Description and Comparison of Individual Methods. *AJ*, 136:2022–2049, November 2008a. doi: 10.1088/0004-6256/136/5/2022. [31](#), [57](#)
- Y. S. Lee, T. C. Beers, T. Sivarani, J. A. Johnson, D. An, R. Wilhelm, C. Allende Prieto, L. Koesterke, P. Re Fiorentin, C. A. L. Bailer-Jones, J. E. Norris, B. Yanny, C. Rockosi, H. J. Newberg, K. M. Cudworth, and K. Pan. The SEGUE Stellar Parameter Pipeline. II. Validation with Galactic Globular and Open Clusters. *AJ*, 136:2050–2069, November 2008b. doi: 10.1088/0004-6256/136/5/2050. [31](#)
- H. N. Li, N. Christlieb, T. Schörck, J. E. Norris, M. S. Bessell, D. Yong, T. C. Beers, Y. S. Lee, A. Frebel, and G. Zhao. The stellar content of the Hamburg/ESO survey. VI. Metallicity distribution of main-sequence turnoff stars in the Galactic halo. *A&A*, 521:A10, October 2010. doi: 10.1051/0004-6361/201014797. [41](#)
- I. G. McCarthy, A. S. Font, R. A. Crain, A. J. Deason, J. Schaye, and T. Theuns. Global structure and kinematics of stellar haloes in cosmological hydrodynamic simulations. *MNRAS*, 420:2245–2262, March 2012. doi: 10.1111/j.1365-2966.2011.20189.x. [39](#), [57](#)
- J. G. Mengel, P. Demarque, A. V. Sweigart, and P. G. Gross. Stellar evolution from the zero-age main sequence. *ApJS*, 40:733–791, August 1979. doi: 10.1086/190603. [41](#)
- H. L. Morrison, C. Flynn, and K. C. Freeman. Where does the disk stop and the halo begin? Kinematics in a rotation field. *AJ*, 100:1191–1222, October 1990. doi: 10.1086/115587. [59](#)
- F. Nakamura and M. Umemura. On the Initial Mass Function of Population III Stars. *ApJ*, 548:19–32, February 2001. doi: 10.1086/318663. [43](#)

- 
- P. E. Nissen and W. J. Schuster. Two distinct halo populations in the solar neighborhood. Evidence from stellar abundance ratios and kinematics. *A&A*, 511:L10, February 2010. doi: 10.1051/0004-6361/200913877. [17](#), [24](#)
- K. Nomoto, C. Kobayashi, and N. Tominaga. Nucleosynthesis in Stars and the Chemical Enrichment of Galaxies. *ARA&A*, 51:457–509, August 2013. doi: 10.1146/annurev-astro-082812-140956. [43](#)
- J. E. Norris, K. C. Freeman, and K. J. Mighell. The Giant Branch of omega Centauri. V. The Calcium Abundance Distribution. *ApJ*, 462:241, May 1996. doi: 10.1086/177145. [54](#)
- J. E. Norris, N. Christlieb, A. J. Korn, K. Eriksson, M. S. Bessell, T. C. Beers, L. Wisotzki, and D. Reimers. HE 0557-4840: Ultra-Metal-Poor and Carbon-Rich. *ApJ*, 670:774–788, November 2007. doi: 10.1086/521919. [42](#)
- J. H. Oort. Some peculiarities in the motion of stars of high velocity. *Bull. Astron. Inst. Netherlands*, 1:133, September 1922. [5](#)
- M. E. Putman, J. E. G. Peek, and M. R. Joung. Gaseous Galaxy Halos. *ARA&A*, 50: 491–529, September 2012. doi: 10.1146/annurev-astro-081811-125612. [65](#)
- N. G. Roman. A Catalogue of High-Velocity Stars. *ApJS*, 2:195, December 1955. doi: 10.1086/190021. [5](#)
- C. Safranek-Shrader, V. Bromm, and M. Milosavljević. Fragmentation in the First Galaxies. *ApJ*, 723:1568–1582, November 2010. doi: 10.1088/0004-637X/723/2/1568. [43](#)
- L. V. Sales, J. F. Navarro, M. G. Abadi, and M. Steinmetz. Satellites of simulated galaxies: survival, merging and their relation to the dark and stellar haloes. *MNRAS*, 379:1464–1474, August 2007. doi: 10.1111/j.1365-2966.2007.12024.x. [64](#), [65](#)
- E. E. Salpeter. The Luminosity Function and Stellar Evolution. *ApJ*, 121:161, January 1955. doi: 10.1086/145971. [26](#)
- T. Sawala, Q. Guo, C. Scannapieco, A. Jenkins, and S. White. What is the (dark) matter with dwarf galaxies? *MNRAS*, 413:659–668, May 2011. doi: 10.1111/j.1365-2966.2010.18163.x. [66](#)

- D. J. Schlegel, D. P. Finkbeiner, and M. Davis. Maps of Dust Infrared Emission for Use in Estimation of Reddening and Cosmic Microwave Background Radiation Foregrounds. *ApJ*, 500:525, June 1998. doi: 10.1086/305772. [31](#)
- K. J. Schlesinger, J. A. Johnson, C. M. Rockosi, Y. S. Lee, H. L. Morrison, R. Schönrich, C. Allende Prieto, T. C. Beers, B. Yanny, P. Harding, D. P. Schneider, C. Chiappini, L. N. da Costa, M. A. G. Maia, I. Minchev, H. Rocha-Pinto, and B. X. Santiago. The Metallicity Distribution Functions of SEGUE G and K Dwarfs: Constraints for Disk Chemical Evolution and Formation. *ApJ*, 761:160, December 2012. doi: 10.1088/0004-637X/761/2/160. [31](#), [32](#), [34](#), [45](#)
- R. Schönrich, M. Asplund, and L. Casagrande. On the alleged duality of the Galactic halo. *MNRAS*, 415:3807–3823, August 2011. doi: 10.1111/j.1365-2966.2011.19003.x. [16](#), [17](#), [18](#), [70](#)
- T. Schörck, N. Christlieb, J. G. Cohen, T. C. Beers, S. Shectman, I. Thompson, A. McWilliam, M. S. Bessell, J. E. Norris, J. Meléndez, S. Ramírez, D. Haynes, P. Cass, M. Hartley, K. Russell, F. Watson, F.-J. Zickgraf, B. Behnke, C. Fechner, B. Fuhrmeister, P. S. Barklem, B. Edvardsson, A. Frebel, L. Wisotzki, and D. Reimers. The stellar content of the Hamburg/ESO survey. V. The metallicity distribution function of the Galactic halo. *A&A*, 507:817–832, November 2009. doi: 10.1051/0004-6361/200810925. [41](#)
- L. Searle and R. Zinn. Compositions of halo clusters and the formation of the galactic halo. *ApJ*, 225:357–379, October 1978. doi: 10.1086/156499. [6](#), [10](#)
- B. Sesar, M. Jurić, and Ž. Ivezić. The Shape and Profile of the Milky Way Halo as Seen by the Canada-France-Hawaii Telescope Legacy Survey. *ApJ*, 731:4, April 2011. doi: 10.1088/0004-637X/731/1/4. [41](#), [52](#)
- S. Sharma, M. Steinmetz, and J. Bland-Hawthorn. On the Origin of the Angular Momentum Properties of Gas and Dark Matter in Galactic Halos and Its Implications. *ApJ*, 750:107, May 2012. doi: 10.1088/0004-637X/750/2/107. [65](#)
- T. Shige-yama, T. Tsujimoto, and Y. Yoshii. Excavation of the First Stars. *ApJ*, 586:L57–L60, March 2003. doi: 10.1086/374635. [29](#), [40](#), [43](#)
- J. Silk. On the fragmentation of cosmic gas clouds. I - The formation of galaxies and the first generation of stars. *ApJ*, 211:638–648, February 1977. doi: 10.1086/154972. [43](#)

- J. D. Simon and M. Geha. The Kinematics of the Ultra-faint Milky Way Satellites: Solving the Missing Satellite Problem. *ApJ*, 670:313–331, November 2007. doi: 10.1086/521816. [39](#)
- E. Sirko, J. Goodman, G. R. Knapp, J. Brinkmann, Ž. Ivezić, E. J. Knerr, D. Schlegel, D. P. Schneider, and D. G. York. Blue Horizontal-Branch Stars in the Sloan Digital Sky Survey. II. Kinematics of the Galactic Halo. *AJ*, 127:914–924, February 2004. doi: 10.1086/381486. [56](#)
- B. D. Smith, M. J. Turk, S. Sigurdsson, B. W. O’Shea, and M. L. Norman. Three Modes of Metal-Enriched Star Formation in the Early Universe. *ApJ*, 691:441–451, January 2009. doi: 10.1088/0004-637X/691/1/441. [43](#)
- J. P. Smolinski, Y. S. Lee, T. C. Beers, D. An, S. J. Bickerton, J. A. Johnson, C. P. Loomis, C. M. Rockosi, T. Sivarani, and B. Yanny. The SEGUE Stellar Parameter Pipeline. IV. Validation with an Extended Sample of Galactic Globular and Open Clusters. *AJ*, 141:89, March 2011. doi: 10.1088/0004-6256/141/3/89. [31](#)
- A. Sollima, M. Bellazzini, R. L. Smart, M. Correnti, E. Pancino, F. R. Ferraro, and D. Romano. The non-peculiar velocity dispersion profile of the stellar system  $\omega$  Centauri. *MNRAS*, 396:2183–2193, July 2009. doi: 10.1111/j.1365-2966.2009.14864.x. [42](#)
- J. Sommer-Larsen and P. R. Christensen. Blue horizontal branch field stars in the galactic halo - Observations versus kinematic models. *MNRAS*, 239:441–457, July 1989. [65](#)
- J. Sommer-Larsen and C. Zhen. Armchair cartography - A map of the Galactic halo based on observations of local, metal-poor stars. *MNRAS*, 242:10–24, January 1990. [15](#)
- J. Sommer-Larsen, T. C. Beers, C. Flynn, R. Wilhelm, and P. R. Christensen. A Dynamical and Kinematical Model of the Galactic Stellar Halo and Possible Implications for Galaxy Formation Scenarios. *ApJ*, 481:775, May 1997. doi: 10.1086/304081. [56](#)
- L. M. Stanford, G. S. Da Costa, J. E. Norris, and R. D. Cannon. Abundances on the Main Sequence of  $\omega$  Centauri. *ApJ*, 667:911–929, October 2007. doi: 10.1086/520794. [42](#), [54](#)

- T. Suda, M. Aikawa, M. N. Machida, M. Y. Fujimoto, and I. Iben, Jr. Is HE 0107-5240 A Primordial Star? The Characteristics of Extremely Metal-Poor Carbon-Rich Stars. *ApJ*, 611:476–493, August 2004. doi: 10.1086/422135. [40](#)
- A. V. Sweigart and P. G. Gross. Evolutionary sequences for red giant stars. *ApJS*, 36:405–437, March 1978. doi: 10.1086/190506. [38](#)
- C. Theis. Evolution of Anisotropy in Collapsing Systems. In A. Burkert, D. H. Hartmann, and S. A. Majewski, editors, *The History of the Milky Way and Its Satellite System*, volume 112 of *Astronomical Society of the Pacific Conference Series*, page 35, 1996. [65](#)
- C. Thom, C. Flynn, M. S. Bessell, J. Hänninen, T. C. Beers, N. Christlieb, D. James, J. Holmberg, and B. K. Gibson. Kinematics of the Galactic halo from horizontal branch stars in the Hamburg/ESO survey. *MNRAS*, 360:354–359, June 2005. doi: 10.1111/j.1365-2966.2005.09038.x. [56](#)
- P. B. Tissera, S. D. M. White, and C. Scannapieco. Chemical signatures of formation processes in the stellar populations of simulated galaxies. *MNRAS*, 420:255–270, February 2012. doi: 10.1111/j.1365-2966.2011.20028.x. [61](#)
- P. B. Tissera, C. Scannapieco, T. C. Beers, and D. Carollo. Stellar haloes of simulated Milky-Way-like galaxies: chemical and kinematic properties. *MNRAS*, 432:3391–3400, July 2013. doi: 10.1093/mnras/stt691. [16](#), [29](#), [39](#)
- E. Tolstoy, V. Hill, and M. Tosi. Star-Formation Histories, Abundances, and Kinematics of Dwarf Galaxies in the Local Group. *ARA&A*, 47:371–425, September 2009. doi: 10.1146/annurev-astro-082708-101650. [14](#)
- H. Umeda and K. Nomoto. First-generation black-hole-forming supernovae and the metal abundance pattern of a very iron-poor star. *Nature*, 422:871–873, April 2003. [43](#)
- M. G. Walker, M. Mateo, E. W. Olszewski, J. Peñarrubia, N. Wyn Evans, and G. Gilmore. A Universal Mass Profile for Dwarf Spheroidal Galaxies? *ApJ*, 704:1274–1287, October 2009. doi: 10.1088/0004-637X/704/2/1274. [39](#)
- S. D. M. White and M. J. Rees. Core condensation in heavy halos - A two-stage theory for galaxy formation and clustering. *MNRAS*, 183:341–358, May 1978. [65](#)

- R. Wilhelm, T. C. Beers, and R. O. Gray. Spectroscopy of Hot Stars in the Galactic Halo. II. The Identification and Classification of Horizontal-Branch and Other A-Type Stars. *AJ*, 117:2308–2328, May 1999. doi: 10.1086/300824. 57
- R. Woolley. The velocity ellipsoid of RR Lyrae variable stars. *MNRAS*, 184:311–317, August 1978. 59, 70
- X. X. Xue, H. W. Rix, G. Zhao, P. Re Fiorentin, T. Naab, M. Steinmetz, F. C. van den Bosch, T. C. Beers, Y. S. Lee, E. F. Bell, C. Rockosi, B. Yanny, H. Newberg, R. Wilhelm, X. Kang, M. C. Smith, and D. P. Schneider. The Milky Way’s Circular Velocity Curve to 60 kpc and an Estimate of the Dark Matter Halo Mass from the Kinematics of  $\sim 2400$  SDSS Blue Horizontal-Branch Stars. *ApJ*, 684:1143–1158, September 2008. doi: 10.1086/589500. 61
- X.-X. Xue, H.-W. Rix, B. Yanny, T. C. Beers, E. F. Bell, G. Zhao, J. S. Bullock, K. V. Johnston, H. Morrison, C. Rockosi, S. E. Koposov, X. Kang, C. Liu, A. Luo, Y. S. Lee, and B. A. Weaver. Quantifying Kinematic Substructure in the Milky Way’s Stellar Halo. *ApJ*, 738:79, September 2011. doi: 10.1088/0004-637X/738/1/79. 38, 57
- B. Yanny, C. Rockosi, H. J. Newberg, G. R. Knapp, J. K. Adelman-McCarthy, B. Alcorn, S. Allam, C. Allende Prieto, D. An, K. S. J. Anderson, S. Anderson, C. A. L. Bailer-Jones, S. Bastian, T. C. Beers, E. Bell, V. Belokurov, D. Bizyaev, N. Blythe, J. J. Bochanski, W. N. Boroski, J. Brinchmann, J. Brinkmann, H. Brewington, L. Carey, K. M. Cudworth, M. Evans, N. W. Evans, E. Gates, B. T. Gänsicke, B. Gillespie, G. Gilmore, A. Nebot Gomez-Moran, E. K. Grebel, J. Greenwell, J. E. Gunn, C. Jordan, W. Jordan, P. Harding, H. Harris, J. S. Hendry, D. Holder, I. I. Ivans, Ž. Ivezić, S. Jester, J. A. Johnson, S. M. Kent, S. Kleinman, A. Kniazev, J. Krzesinski, R. Kron, N. Kuropatkin, S. Lebedeva, Y. S. Lee, R. French Leger, S. Lépine, S. Levine, H. Lin, D. C. Long, C. Loomis, R. Lupton, O. Malanushenko, V. Malanushenko, B. Margon, D. Martinez-Delgado, P. McGehee, D. Monet, H. L. Morrison, J. A. Munn, E. H. Neilsen, Jr., A. Nitta, J. E. Norris, D. Oravetz, R. Owen, N. Padmanabhan, K. Pan, R. S. Peterson, J. R. Pier, J. Platson, P. Re Fiorentin, G. T. Richards, H.-W. Rix, D. J. Schlegel, D. P. Schneider, M. R. Schreiber, A. Schwobe, V. Sibley, A. Simmons, S. A. Snedden, J. Allyn Smith, L. Stark, F. Stauffer, M. Steinmetz, C. Stoughton, M. SubbaRao, A. Szalay, P. Szkody, A. R. Thakar, T. Sivarani, D. Tucker, A. Uomoto, D. Vanden Berk, S. Vidrih, Y. Wadadekar, S. Watters, R. Wilhelm, R. F. G. Wyse, J. Yarger, and D. Zucker. SEGUE: A Spec-

- 
- trosopic Survey of 240,000 Stars with  $g = 14-20$ . *AJ*, 137:4377, May 2009. doi: 10.1088/0004-6256/137/5/4377. [30](#)
- D. Yong, J. E. Norris, M. S. Bessell, N. Christlieb, M. Asplund, T. C. Beers, P. S. Barklem, A. Frebel, and S. G. Ryan. The Most Metal-poor Stars. III. The Metallicity Distribution Function and Carbon-enhanced Metal-poor Fraction. *ApJ*, 762:27, January 2013. doi: 10.1088/0004-637X/762/1/27. [41](#)
- Y. Yoshii. Metal enrichment in the atmospheres of extremely metal-deficient dwarf stars by accretion of interstellar matter. *A&A*, 97:280–290, April 1981. [18](#), [28](#), [29](#), [38](#), [43](#), [67](#)
- Y. Yoshii. Density Distribution of Faint Stars in the Direction of the North Galactic Pole. *PASJ*, 34:365, 1982. [33](#)
- Y. Yoshii. *Star Counts and Nature of the Galactic Thick Disk*, page 393. 2013. doi: 10.1007/978-94-007-5612-0\_8. [33](#)
- Y. Yoshii and N. Arimoto. Spheroidal systems as a one-parameter family of mass at their birth. *A&A*, 188:13–23, December 1987. [39](#)
- Y. Yoshii and Y. Sabano. Fragmentation of Cosmic Gas Clouds due to Thermal Instabilities. *PASJ*, 32:229, 1980. [43](#)
- Y. Yoshii and H. Saio. Kinematics of the Old Stars and Initial Contraction of the Galaxy. *PASJ*, 31:339–368, 1979. [5](#), [6](#), [7](#), [65](#)
- Y. Yoshii and H. Saio. Initial mass function for zero-metal stars. *ApJ*, 301:587–600, February 1986. doi: 10.1086/163925. [43](#)